Damage Accumulation in Graphite/Epoxy Laminates due to Cyclic Gradient Stress Fields

by

KENNETH JOHN BONELLO

B.S.M.E. GMI Engineering & Management Institute
(1988)

SUBMITTED IN PARTIAL FULFILLMENT OF THE
REQUIREMENTS FOR THE DEGREE OF

MASTER OF SCIENCE

IN

AERONAUTICS AND ASTRONAUTICS

AT THE

MASSACHUSETTS INSTITUTE OF TECHNOLOGY

May, 1990

Signature of Author _____
Department of Aeronautics and Astronautics
May 11, 1990

Certified by _____
Prof. Paul A. Lagace
Thesis Supervisor, Department of Aeronautics and Astronautics

Accepted by _____
Prof. Harold Y. Wachman
Chairman, Department Graduate Committee

Damage Accumulation in Graphite/Epoxy Laminates due to Cyclic Gradient Stress Fields

by

Kenneth J. Bonello

Submitted to the Department of Aeronautics and Astronautics on May 11th, 1990 in partial fulfillment of the requirements for the Degree of Master of Science

Abstract

The progression of damage in gradient stress fields under cyclic loading was studied in simply-supported graphite/epoxy beam-columns. Three layups, $[45_4/\text{-}45_4/(0/90)_4]_{2s}$, $[\pm 45/0/90_4]_{4s}$, and $[(45_2/\text{-}45_2/0)_2/90_5]_{2s}$, were chosen to be consistent with data collected in a previous study with static loading. Specimens were loaded statically until predetermined characteristic damage levels were obtained, after which cyclic loading began. Cyclic tests were run in load control at an R ratio of ten and a frequency of 1.5 Hz. At specific intervals, cyclic loading was stopped, a static test measuring the load and the corresponding center deflection was performed, and edge replicas of the specimen's sides were taken. Cyclic loading was then resumed until the next interval or final failure. Damage histories were pieced together for each laminate type under different maximum cyclic load levels. The damage of these specimens varied both along the length and through the thickness of the specimens with two modes of damage present. Damage due to the static loading occurred on the tension side of the specimen and was controlled by matrix cracks. Delaminations initiated and grew in areas of crack saturation. Damage due to the cyclic loading also occurred on the compression side of the specimens and was controlled by delaminations which initiated and grew independently of matrix cracks, leading to sublaminate buckling. These compression side delaminations did not initiate in static tests to failure. Increasing the maximum cyclic load changed the relative growth of the two modes of damage, thus changing the failure mode. The stiffness of the specimens increased slightly with cyclic loading but steadily declined thereafter. Stiffness degradation was less than 6% until just prior to failure. Because cyclic loading revealed critical damage modes not found with static loading, cyclic loading should be used when ascertaining all possible damage modes. Using higher cyclic load levels to reduce testing time can hide critical damage modes with the potential of overestimating cyclic lifetime.

Thesis Supervisor: Paul A. Lagace
Title: Associate Professor of Aeronautics and Astronautics

Acknowledgements

As I prepare to return to the Motor City, it occurs to me that a work such as this is hardly the effort of one person. There are many people involved, whether providing technical input and guidance to the project itself or providing friendship and support. It is these people who have been a part of my world over the last two years that have made this thesis possible.

I would not be at MIT were it not for the brilliant insightfulness of Prof. Paul Lagace. Thank you for giving me the opportunity to come to MIT and to do my research in TELAC. Your guidance, suggestions, and what seemed like endless review of this thesis have shaped it to what it is. The whole experience has been worthwhile and I learned a lot.

The experimental work would not have flowed as smoothly (if at all) without the help of Al Supple. Much thanks for your advice and patience. I would like to thank Prof. Michael Graves, Prof. John Dugundji, and Prof. James Mar for your helpful comments and questions during the final stages of this work. I would also like to thank Ping Lee for being patient with all of my questions. I would probably be still testing without the help of my UROP, Mike Clarke. I appreciate your dedication and assistance.

An important asset of TELAC is the group of graduate students that make up the lab. Whether on a technical, academic, social, or personal basis, there is always someone willing to listen and help (or go to the Muddy). Thank you Kevin, Chris, Pierre, Kiernan, Peter, Narendra (Bhatman), Wilson, Adam, Randy, Claudia, Tom, Teresa (Reese), Ed, Wai Tuck, Luca, and Kim for your friendship. I would also like to thank James

(even though you're from GT) for being a friend and maintaining some reality in my life. If I forgot someone, I'm sorry, I'm just a bozo.

There are several people who were a part of my life away from the lab these last two years. From Gordon (Gordex), Abbas (Mofo), Alex (Alecchh), and Mike, to the rest of the DT, Dan, Eric, Leif, and Smoothy, I say thanks for your friendship (and may you not spend the rest of your lives in school).

Lastly, I want to thank my parents and the rest of my family for their never ending support of my goals. My accomplishments would be meaningless without their love and understanding. I also want to acknowledge the support of my friends back in Michigan. Thank you.

Foreword

This work was performed in the Technology Laboratory for Advanced Composites (TELAC) of the Department of Aeronautics and Astronautics at the Massachusetts Institute of Technology. This work was sponsored by Boeing Military Aircraft under Boeing Purchase Order 644740.

Table of Contents

Table of Contents (continued)

List of Figures

List of Figures (continued)

List of Figures (continued)

List of Tables

List of Tables (continued)

Nomenclature

E	Young's modulus
E_i	Unidirectional ply stiffness (i=1,2,3)
G_{ij}	Shear modulus of unidirectional ply (i,j=1,2,3)
I	Area moment of inertia
L	Specimen length
P_{cr}	Euler bifurcation load
S	Maximum shear stress
X^c	Maximum longitudinal compressive stress
X^t	Maximum longitudinal tensile stress
Y^c	Maximum transverse compressive stress
Y^t	Maximum transverse tensile stress
ν_{ij}	Poisson's ratio (i,j=1,2,3)

Chapter 1

INTRODUCTION

The past two decades have seen increased attention given to advanced composite materials in the aircraft and spacecraft industries. The high specific strength and stiffness of advanced composites make them attractive alternative materials to the more traditional, heavier, isotropic materials. An important potential payoff is reduced gross weight thereby increasing range, payload, and/or maneuverability.

With the push for more fuel-efficient commercial aircraft, advanced composites were first used on a large scale for secondary structures on aircraft such as Boeing's 757 and 767 models. This usage allowed the industry to gain experience and confidence in the commercial production use of advanced composites in load-bearing capacities.

A milestone in advanced composites use was reached with the design and production of the Beechcraft Starship 1. This was the first aircraft with an all-composite airframe to be structurally certified by the FAA, leading the way for future large scale use of advanced composites for primary structures.

The use of composites has also seen extensive advancement in rotorcraft. The Boeing 360 is the world's largest all-composite helicopter. It features an all-composite fuselage and makes extensive use of composites in the landing gear components, transmission housing, drive shafts, rotor

controls, hubs, and blades, giving an overall weight reduction of approximately 25% over conventional materials.

Military applications are not exempt from the benefits of composite materials. Because of the "tailorability" of continuous fiber composites, components can be designed to perform to specific requirements. The Grumman/DAARPA X-29 forward swept wing aircraft could only have been achieved by aeroelastic tailoring the composite wing skins. The orientation of the individual plies allows the wings to be configured in a forward swept manner while still avoiding instabilities such as aeroelastic divergence.

In light of the extensive use of composite materials in aircraft, much is needed to be learned about their complex behavior. High safety factors are still being used, leaving a great deal of untapped potential. Their use tends to be in nearly quasi-isotropic layups, making the least efficient use of their properties. In order for composite structures to reach their potential efficiency, the limits and failure modes must be further understood.

While the behavior of composite structures under various loading and boundary conditions has been extensively studied, much of the work investigating damage growth and failure has been in non-gradient stress fields, except in the case of notched panels. Understanding the behavior of composite structures with gradient stress fields is the next step toward efficiently utilizing composites. The buckling of a panel is an example of a structure with a gradient stress field. Allowing the structure to buckle does not necessarily reduce its load-carrying capability and could increase its efficiency as long as the limit load requirements are still met. The current understanding of the postbuckled behavior of composite laminates is limited. Models of buckling loads and postbuckling behavior work well but

are complicated by boundary conditions and damage. Once damage occurs, the models of buckling behavior break down making predictions difficult. This lack of understanding of the effects of damage on the performance of composite structures hampers the use of composite structures in the postbuckled regime and in other applications as well. The final failure of buckled laminates is understood even less. The behavior of laminates in gradient stress fields, including damage initiation, damage growth, and ultimate failure, must be quantified before design criteria can be defined.

Many structures experience repeated, or cyclic, loading conditions which may involve gradient stress fields. Fatigue behavior in composite materials though, is much different than in isotropic materials. Composite materials exhibit many types of damage in the matrix, fiber, and matrix/fiber interface that cyclic loading can excite. Compared to metals, composites can better withstand micro-cracks and maintain cyclic load-carrying capabilities to final failure. It is known, though, that the fatigue strength is less than the static strength due to degradation of the structure during cyclic loading. It is important to fully understand the cyclic behavior of laminates in a gradient stress field. The process of damage initiation and damage growth with cyclic loading and the effects of damage on the fatigue performance of composites needs to be quantified.

Damage mechanisms in composites are complex and difficult to describe because they involve combinations of fiber and matrix interactions. These mechanisms can differ greatly between static and cyclic loading histories. Different modes of failure include fiber-matrix debonding, fiber fracture, matrix failure and delamination. Damage can be defined in terms of crack length, crack density, and amount of delaminations among other ways. The initiation of damage destroys the symmetry of the laminates

thereby increasing the complexity of the problem to the general anisotropic case and making analysis difficult.

An important mechanism of damage in composites occurs in the matrix. Matrix damage due to static or cyclic loading can affect the load-carrying capability of the component by altering the shear transfer mechanism between matrix and fibers. Material flaws, mostly in the form of voids and delaminations, can exist throughout a composite structure. Unlike static loading, cyclic loading can cause these matrix flaws to extend until they reach a critical size, leading to fracture.

It is thus necessary to understand the behavior of composite laminates cyclically loaded with a gradient stress field. This includes quantifying the progression of damage as well as defining failure modes. The occurrence of bending in a structure results in a gradient stress field along the length as well as through the thickness. The objective of this investigation was to understand the damage accumulation in graphite/epoxy laminates due to cyclic gradient stress fields. This will help to give insight into the cyclic behavior of composite structures operating in the postbuckled regime and for other configurations as well. Column specimens of three laminate types under simply-supported boundary conditions providing a simple gradient stress field were chosen as the medium. With the maximum stress at the center of the specimen, damage will initiate at the center away from the boundary conditions. A test program was developed to obtain damage accumulation histories for the three layups subjected to cyclic loading. Initial damage was first created statically on the specimens. Damage accumulation and stiffness degradation was monitored during compression-compression cyclic

loading until ultimate failure. The maximum cyclic load level as well as the amount of initial damage was varied.

In chapter two, a summary of previous efforts to study the general effects of fatigue on composite laminates as well as damage growth and stiffness reduction due to cyclic loading is presented. The specimen, test jig, test program, specimen manufacture, and test procedures are described in chapter three. The results of the experiments, with a section for each laminate type, are explained in chapter four. A discussion of the results follows in chapter five. Conclusions and recommendations are presented in chapter six. In Appendix A, the specimen thicknesses and widths are listed. The specimen stiffness data in the form of Southwell buckling loads at each cyclic interruption is given in Appendix B.

Chapter 2

FATIGUE EFFECTS ON COMPOSITES

Fatigue behavior of composites has been studied extensively. The effects of cyclic loading on stiffness and damage growth, along with frequency and load level effects are popular research topics. The work however, has been almost exclusive of fatigue behavior in a gradient stress field such as in a buckled structure. Since composites can carry significant loads after buckling, it is important to understand how damage modes initiate and interact in cyclic gradient stress fields and how the fatigue performance is affected by the damage. An understanding of previous work studying the general effects of cyclic loading as well as damage growth and stiffness reduction is needed before investigating the behavior of laminates subjected to cyclic gradient stress fields.

2.1 General Effects

The effects of frequency and load level on the life of composites have been studied for many types of laminates. Fatigue life of composites has frequently been characterized by S-N curves. It is apparent, as more research is done, that simple characterizations such as S-N curves cannot adequately describe the fatigue behavior of composites due to the many damage types which occur and their interactions.

Much experimental work has been done to develop an understanding of composite fatigue behavior so that adequate characterizations can be developed. Using unidirectional coupon specimens, Awerbuch and Hahn [1] measured the life to failure and residual static strength over a range of peak stress levels. The effects of a proof load on the fatigue life distribution were also included. A proof load is an initial static load applied before cyclic loading begins. It was hoped that a relationship would be found between the static strength distribution of virgin coupons and their fatigue life by eliminating specimens of low static strength, but nothing conclusive was found. The data did serve as a source for statistical fatigue life predictions.

The idea that there was a relationship between static strength and fatigue life was studied by Hahn and Kim [2], with the strength-life equal rank assumption. This hypothesis contends that the specimens with the greatest static strength will also have the longest fatigue life with the lowest strength specimen being the first to fail. Evidence of a unique relationship between static strength and life through proof testing was found to exist for unidirectional glass/epoxy composites. Chou and Wang [3] compiled data from different tensile fatigue experiments and compared several strength degradation and failure models based on the equal rank assumption. None were found to satisfactorily describe every set of experimental data.

Residual strength measurements are a common method of assessing the effects of fatigue on the laminates. A surprising discovery concerning fatigue tests with notched or flawed laminates was that the static strength often increased substantially after fatigue cycling. Romani and Williams [4] show residual static strength increasing by as much as 40% after five million tension-tension cycles. A explanation of this was given by Reifsnider, Stinchcomb, and O'Brien [5] using a two process interaction.

First, a wear-in process occurs locally as the multiple damage modes which occur in a composite laminate erase the stress concentration at the discontinuity. The second process, a wear-out process, consists of a general degradation of the entire laminate by repeated loading with this second process becoming dominant later in the fatigue life. This result shows how multiple damage modes can interact and influence the behavior of a laminate.

Much of the early work on fatigue focused on the material response to cyclic tensile stresses. Inclusion of compressive loads in fatigue loading histories has been shown to significantly reduce life to specimen failure. Ryder and Walker [6] show results of tension-tension, tension-compression, and compression-compression tests of two different laminates. The slope of the S-N curves for the tension-tension tests was less steep than for the other two tests with compression loads. Tension-compression fatigue tests were found to be the most severe conditions. Rosenfeld and Huang [7] suggest that matrix strength degradation allows the fibers to buckle under the compressive loads. There tends to be more damage per cycle with compression loads, accounting for a reduced fatigue life. It is evident from the literature that fatigue testing of composites should include compression to achieve the most severe conditions.

Compressive cyclic loading in composites differs greatly from that of metals. Whereas the compressive loads in metals tend to close the gap created by a microcrack causing little tendency to extend the damage, compressive loads in composites can excite various damage modes such as fiber breaks, delamination, fiber/matrix debonding, and matrix cracking. In addition, as the literature shows, compressive cyclic loading in composites is much more critical to damage development than tension-

tension loading. Sublaminate buckling, which effectively reduces the laminate to two, or more, laminates with less stiffness, can occur with compressive cyclic loading. More attention is needed to understand the effects of compressive cyclic loading in composites on damage and failure.

2.2 Damage Growth

Much of the work on the cyclic behavior of composites has centered on damage accumulation and failure. There are various nondestructive techniques used to experimentally study damage accumulation. In 1986, Stinchcomb [8] evaluated these techniques. Using the progressive damage due to cyclic loading as a medium for evaluation, five damage states to failure were summarized. Different damage modes were found to interact, forming a complex network of damage making up each damage state. Edge replication and microscopy are techniques to provide damage information on the exposed edge of the laminate giving through-the-thickness but not across-the-width data. The interior damage can be detected by X-ray radiography and ultrasonic methods, but determining the ply in which damage occurs is difficult. The ultrasonic method works better for detecting large delamination areas. Thermography is another technique for detecting internal damage. High frequency - low amplitude or low frequency - high amplitude mechanical vibrations excite the thermal frequencies of particular damage modes which create internal sources of heat due to friction. Stiffness was also used to quantify the effects of damage leading to failure.

Damage in composites can be distinguished between the two constituents: matrix and fiber. With these types of damage, different modes

can exist. Talreja [9] describes the different modes caused by tensile fatigue in unidirectional composites. Cracks can be confined to the matrix only, as well as causing fiber breaks or leading to interface failure. Progressive damage is matrix dependent. Fibers can bridge matrix cracks or can break increasing matrix cracking. During fatigue loading, these various damage mechanisms can grow at different rates, interchanging their dominance. In the same work, Talreja introduces damage mechanism maps for composites as a way of characterizing fatigue behavior that is more useful than the usual S-N curves. The critical damage mechanisms are plotted as regions using strain as a variable versus the logarithm of the number of cycles. This characterization shows the ranges of dominance of multiple damage mechanisms.

Reaching a better understanding of the initiation, growth, and interaction of different damage modes, requires detailed damage accumulation studies using nondestructive techniques. Graves [10] conducted an investigation of damage progression in four graphite/epoxy laminates. The experiments included compression-compression fatigue of four-point bending specimens with holes. Visual and tactile inspections made at various intervals of cyclic testing allowed a progressive damage sequence to be developed for each laminate type. It was found that stacking sequence and ply orientation both play a significant role in fatigue life. A more precise nondestructive evaluation technique needs to be used to gain a better understanding of the actual damage mechanisms.

The effects of cyclic loads on composites can be further established by comparing the fatigue damage and failure modes with static modes. Mar, Graves, and Maass [11] found that the failure modes in fatigue generally differ from that in static tests for balanced graphite/epoxy notched

composites subjected to compression-compression fatigue. Interlaminar stresses at the free edge degrades the compressive strength leading to delaminations. Daken and Mar [12] investigated the development of splitting in notched unidirectional specimens under tension-tension cyclic loading. Splitting was found to relieve stress concentrations at the notch and developed at cyclic loads well below the static splitting stress, suggesting a degradation of properties with cyclic loading.

In another effort, Mar [13] reinforces the difference in failure modes between cyclic and static loading histories. He proposes that the research emphasis should be on the propagation of damage under cyclic loads and the amount of damage which will cause catastrophic failure. Experiments and analyses should be aimed at understanding the damage initiation and accumulation in the epoxy material and at the fiber/matrix interface.

Further work on multiple damage modes was conducted by Fanucci and Mar [14] in their investigation of the damage initiation and propagation in graphite/epoxy laminates with circular holes during compressive fatigue. Sandwich specimens were used to avoid buckling. Damage initiation and progression were monitored using Moire interferometry, a method of optically producing surface contour lines. They found that different damage modes can occur in the same laminate under various conditions reinforcing the idea that cyclic behavior of composites cannot be characterized by general tests. Final failure was preceded by a rapid growth of damage area, suggesting that a warning of specimen failure may be obtained by monitoring cyclic damage.

While it is necessary to understand what different damage modes develop and interact to influence failure, it is also important to understand the method by which each mode progresses. The growth of damage in

terms of transverse cracks was investigated by Reifsnider *et al* [15]. It was discovered that at a sufficiently large number of cycles, patterns of cracking would develop to saturation and remain stable under the same loading. These patterns, labelled as characteristic damage states, are dependent on the laminate configuration.

Much of the work in damage growth due to cyclic loading has dealt with delamination crack growth since there are severe implications on the integrity of the laminate with this damage mode. For non-gradient stress fields, Ye [16] found that increasing matrix strength and ductility increases the critical loads for delamination onset, while reducing the delamination growth under cyclic loading.

There are several standardized tests for quantifying delamination crack growth based on strain energy release rate [17]. This approach equates the energy created by the formation of new fracture surfaces with the strain energy release in the fracture process. Each of these tests evaluate a different mode of crack growth depending on the loading condition. Empirical models of damage growth due to loading can be developed from these tests. Hwang and Han [18] investigated the effects of fiber bridging on Mode I cyclic loading. A modified Paris power law was derived to interpret fatigue crack growth under the influence of fiber bridging which increases the critical load and fracture energy. Under constant cyclic strain energy release rate loading, the crack growth rate decreases due to the fiber bridging.

Varying the cyclic load level can affect crack growth. A delamination crack growth threshold was found for Mode I and mixed mode (I and II) cyclic loading [19,20]. Above the threshold growth rate, crack propagation rate was expressed as a power function of the stress intensity range. Below

this threshold growth rate, there was very little or negligible crack growth with low stress intensity ranges. Mode II crack growth rates under reversed cyclic loading were found to obey a power law depending on the cyclic strain energy release rate [21].

Much effort into understanding damage growth with cyclic loading is directed to the development of theoretical models to predict fatigue life. These models rely on accurate damage accumulation models. Approaches to modelling damage accumulation can range from the global degradation of specimen stiffness to a micromechanics approach separating the fiber and matrix responses. Ye [22] introduces a damage variable to define phenomenologically the degree of damage based on stiffness change. A power law relationship was proposed between the rate of damage development and the ratio of the square of fatigue load level to the current damage level. A micromechanics approach to predicting fatigue failure of unidirectional composites under any loading system was developed by Aboudi [23]. The micro-failure criteria is applied separately to fiber and matrix regions requiring only the S-N curves of fibers and unreinforced matrix. Good agreement with experimental results were found for several fiber-matrix systems. Harris *et al* [24] developed a mechanics approach to predict progressive damage, laminate strength, and fatigue life using damage dependent constitutive relationships. As damage developed, stiffness was degraded, allowing further damage to progress, eventually leading to failure. Rotem and Nelson [25] propose a fatigue failure envelope to reveal the behavior of composites subjected to all types of loading based on a couple of experiments and laminate strengths. This envelope will distinguish between tensile and compressive failure modes for reversed loading. It agreed with limited experimental results. A failure envelope

such as this though, does not include the effect of multiple damage mode interaction which can vary for different conditions.

Because there are different modes of damage in composites, models should also include multiple modes of damage and their interactions. Talreja [26] developed a continuum mechanics approach to characterize damage resulting from fatigue or any other loading condition. Damage is represented by a set of vector fields, each representing a damage mode and orientation. These damage modes are allowed to develop simultaneously and at different growth rates. Constitutive equations relate the elastic constants of a damage state to those of the undamaged state, thereby characterizing the current elastic response of a damaged composite. This methodology does not describe damage development, however. Talreja calls for a better understanding of damage in composites before a proper mechanics treatment of damage accumulation is developed.

Real structures are seldom subjected to the same load levels over long periods of time. An analytical study of cumulative damage during multilevel fatigue loading was performed by Hwang and Han [27]. The models developed could be useful in predicting multi-stress fatigue life. Fatigue modulus and resultant strain were used as parameters representing damage as a function of the number of cycles and applied stress level. It is concluded that much work is needed to establish a universal fatigue damage model which would explain multi-stress level fatigue phenomena without an S-N curve.

A damage tolerance approach for predicting fatigue life was presented by O'Brien [28]. First, matrix cracks are assumed to exist throughout the off-axis plies. Edge delamination initiation is predicted using the strain energy release rate. Delamination growth is then

accounted for by either experimentally measuring stiffness, analytically using growth laws based on strain energy release rate, or assuming catastrophic delamination growth. Failure prediction is made after accounting for the accumulation of local delaminations through the thickness, each of which reduce the failure strain. This methodology was used to predict the tension-tension fatigue life of glass-epoxy laminates and the data fell within the ranges predicted. This approach could also be extended to compressive fatigue loading by first assuming that edge delaminations grow throughout the interface immediately. Models for local and global buckling of damaged laminates would then have to be used to assess the failure strain. This methodology is limited, though, for cases where various damage modes interact because unique characterizations of damage modes in terms of energy release rate become complex.

It has been shown that damage which occurs under cyclic loading can be quite different than that which occurs due to static loads. Most of the work in the literature studying damage growth involves tension-tension loading or restricts buckling of the laminates, ignoring the potential effects of cyclic gradient stress fields. In the cases where bending was allowed, the damage detection techniques used did not allow precise quantification of the damage. Conducting standardized delamination crack growth experiments can aid in the prediction of such damage, but the interaction of various damage modes further complicates the problem for general laminates. Damage growth in cyclic gradient stress fields, such as in a buckled structure, needs to be understood before models can accurately predict real conditions.

2.3 Stiffness Reduction

A proposed method of predicting failure is by monitoring stiffness reduction with cyclic loading as a result of damage. Rotem [29] and Maier *et al* [30] found that the stiffness degradation of specimens subjected to tension-compression and tension-tension cyclic loading can be described by three stages. After initial cycling, the stiffness is reduced by a few percent. For most of the rest of the fatigue life the stiffness is reduced slightly at a constant rate. At approximately 80-90% of the fatigue life, regardless of load level, the stiffness degrades at an accelerated level until failure. Saunders and Van Blaricum [31] found that failure in their laminates occurred after stiffness degraded approximately 15%. These results indicate the potential use of stiffness measurements as a nondestructive evaluation technique to predict laminate failure.

Razvan *et al* [32] found that for notched laminates subjected to reverse loading at different maximum load levels, stiffness degradation was more severe for low load levels than for high load levels. The fundamental types of damage were not altered by load level but the manner in which different damage modes interacted up to failure was strongly dependent on load level. The low load level tests saw an increase in the contribution of delaminations leading up to failure. This suggests that the fatigue response of composite structures is dependent on load history and that the most severe case is not necessarily represented by the highest load levels.

The behavior of composites in fatigue in terms of stiffness can vary depending on the layups used. Various fiber orientations react differently, making it necessary to study each desired layup until reliable prediction

methods are developed. Poursartip *et al* [33] saw that the stiffness of their laminates increased after cyclic loading with some initial damage. They attributed this to a shearing of the 45° plies and a realignment of the 0° fibers. Failure occurred after the stiffness was degraded approximately 35% allowing a prediction of failure based on quantitative measurements of stiffness reduction. Lifshitz [34] looked at compression-compression loading without restricting buckling of the specimen. The 0° uniaxial specimens showed no apparent change in stiffness before catastrophic failure where the 90° specimens saw a slight increase in stiffness during the early stages of fatigue life with a reduction before failure. A slight increase in stiffness was also found for the ±45° shear test specimens with a drop in stiffness prior to failure.

Many researchers have developed models to predict stiffness changes and fatigue life which are based on experimental data. Talreja [35] classifies the effects of transverse cracking into four types to qualitatively assess laminate performance with cracking. A method for quantitatively predicting the stiffness changes due to transverse cracking was found to have good accuracy. Whitworth [36] developed an empirical model relating the stiffness degradation to the fractional life expended at a given stress level and also to the residual strength degradation. This model, based on three parameters that are experimentally evaluated, is restricted to constant amplitude fatigue loadings. Hwang and Han [37] introduced the concept of "fatigue modulus" which is defined as the slope of applied stress versus the resultant strain at a specific cycle. Their empirical model uses the assumption that the fatigue modulus degradation rate follows a power function of fatigue cycle. The equation for predicting fatigue life, using the fatigue modulus and its degradation rate, works better than S-N curves.

These models were compared to non-gradient stress field tests. Experiments with gradient stress fields are needed to assess these models to accurately predict the behavior of composites under these conditions.

The significant decrease in stiffness prior to failure reported in the literature indicates an experimental technique for predicting failure. An understanding of how damage modes interact and accumulate under cyclic loading coupled with an understanding of how damage affects laminate stiffness can aid in the development of accurate models to predict laminate failure. A logical extension of the above work is to investigate the effects on stiffness of laminates subjected to cyclic gradient stress fields. It is suggested that load level is also a variable and that loading history should be considered when designing tests or developing models.

2.4 Summary

Though much work has been done on the fatigue behavior of composites, most of it has been done in non-gradient stress fields. While it is generally agreed that compressive cyclic loading represents a severe case, most experiments were designed to prevent the buckling of the specimen. The studies summarized are insightful as to the effects of fatigue on strength, delamination growth, and specimen stiffness, but the subject of repeated bending behavior of laminates is not fully addressed. It is clear that compressive cyclic loading reduces the fatigue life of a specimen but the effects of adding bending to the problem is still uncertain.

Wolfe [38] investigated the progression of damage in statically loaded beam-column specimens in a bending state. Damage accumulation histories for three layups were developed and structured into four

characteristic damage states. A two-dimensional finite element model was developed to predict the damage accumulation and failure using the maximum stress failure criterion for in-plane damage as well as the Quadratic Delamination Criterion for out-of-plane damage. In-plane damage and delamination initiation was predicted with good accuracy, but the progression of the delaminations was overpredicted.

This work represents a first step in assessing the damage accumulation in laminates with a gradient stress field. The next step is to assess the damage accumulation due to cyclic gradient stress fields. Just as different damage mechanisms are present in cyclic loading as compared to static loading, the damage mechanisms due to repeated bending may differ as well compared to that due to non-gradient stress fields.

Prediction methods for cyclic damage accumulation, stiffness reduction, and fatigue life are based largely on empirical data. A better understanding of the various damage mechanisms and the interaction of these mechanisms with respect to different loading conditions in various stress fields is needed before composite structures can be efficiently designed to operate in gradient stress field environments.

Chapter 3

THE EXPERIMENT

3.1 Specimen Geometry and Test Jig

The specimen type chosen was designed and utilized by Wolfe and Lagace [38]. There were three requirements for the test specimen to meet. First, the stress field had to be straightforward to calculate. A complex stress state would have been difficult to calculate and would hinder a study of failure mechanisms. Second, the location of damage needed to be predictable. It was necessary that damage initiation occurred away from load introduction points, since the stress state at the boundaries would be very complex. Third, an observable accumulation of damage was desired. It was necessary to identify several stages of damage accumulation prior to final failure so it was important that initial damage and final failure did not coincide. It was also necessary to be able to physically inspect the specimens during the course of the test to document the accumulation of damage.

In light of these requirements, a simply-supported column specimen was chosen as the specimen type. The stress state varies along the length with the maximum stresses and hence initial damage occurring in the middle of the specimen, away from the boundary conditions. Thus, the gradient stress field is simple to calculate and the location of damage initiation is known.

The specimen geometry is shown in Figure 3.1. The specimen has a length of 200 mm and a width of 37.5 mm. The side of the specimen exhibiting the greatest tensile stresses due to bending will be referred to as the tension side, with the other side referred to as the compression side. Three configurations of laminates of fifty-six, sixty, and sixty-four plies, with a ply thickness of 0.134 mm, were chosen. The length was chosen such that the buckling loads of the three laminates, as given by the Euler buckling equation:

$$P_{cr} = \pi^2 EI / L^2 , \tag{3.1}$$

were within the ten percent load range of the test machine (4.45 kN to 44.5 kN). Testing a new laminate of a different thickness may require a new length as governed by the above equation. The specimens were thick enough to provide an observable accumulation of damage, wide enough to avoid an interaction of edge effects from the sides, and long enough to ensure bending preventing failure by squashing.

The test jig used in the previous damage accumulation study [38] was used for this investigation. The requirement of the jig was to provide simply-supported boundary conditions for all loads applied. Any friction in the mechanism would cause the column to first behave in a clamped column manner. It was therefore desired to avoid any friction problems while trying to achieve ideal simply-supported boundary conditions. The jig used is shown in Figure 3.2. In this jig, the specimen ends fit into end pieces which rest on rounded knife edges through which the load is introduced. The end pieces are slotted steel blocks. A tight fit between the specimen and end pieces is ensured with thin steel and brass shims. The

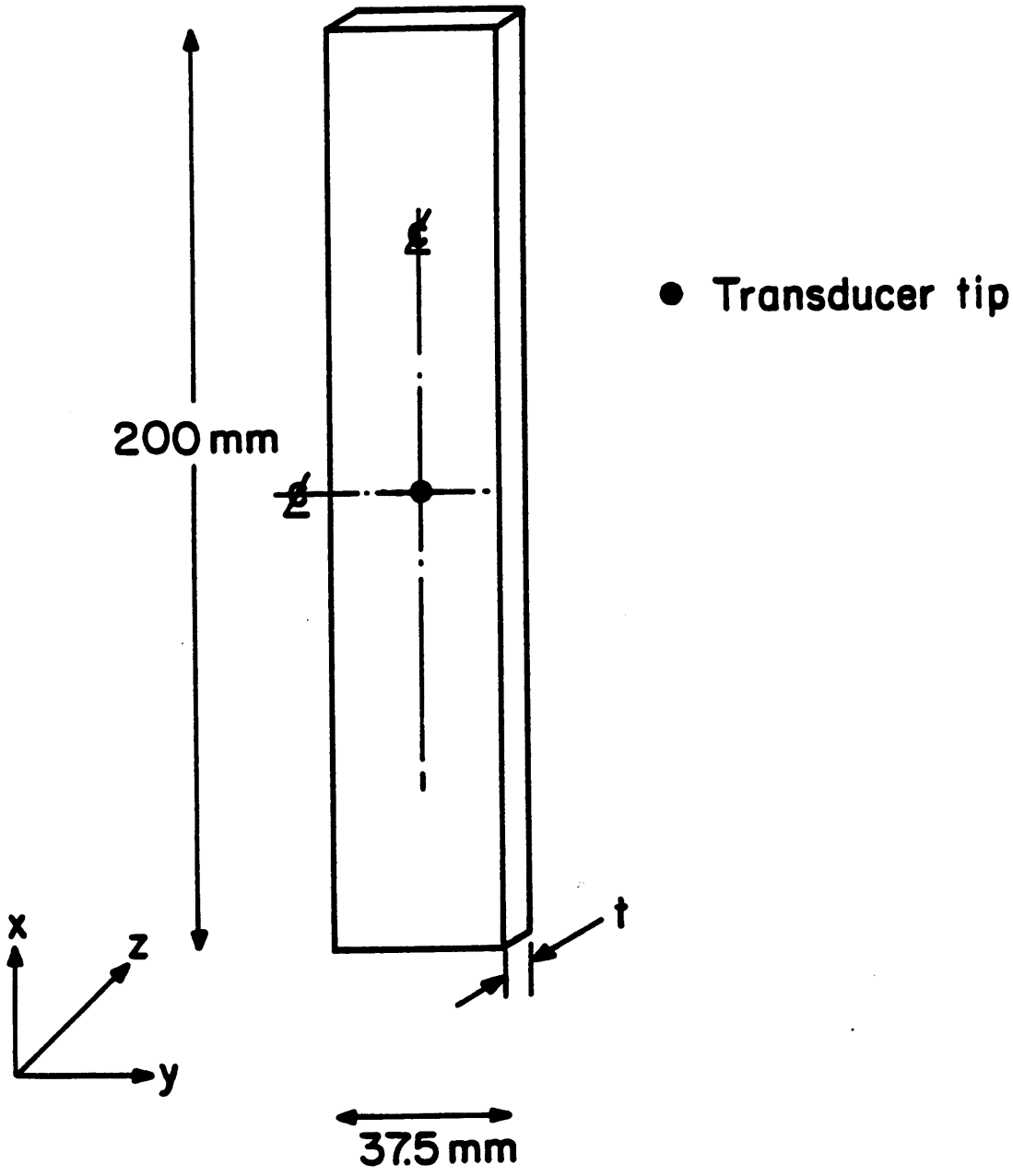

Figure 3.1 Specimen geometry.

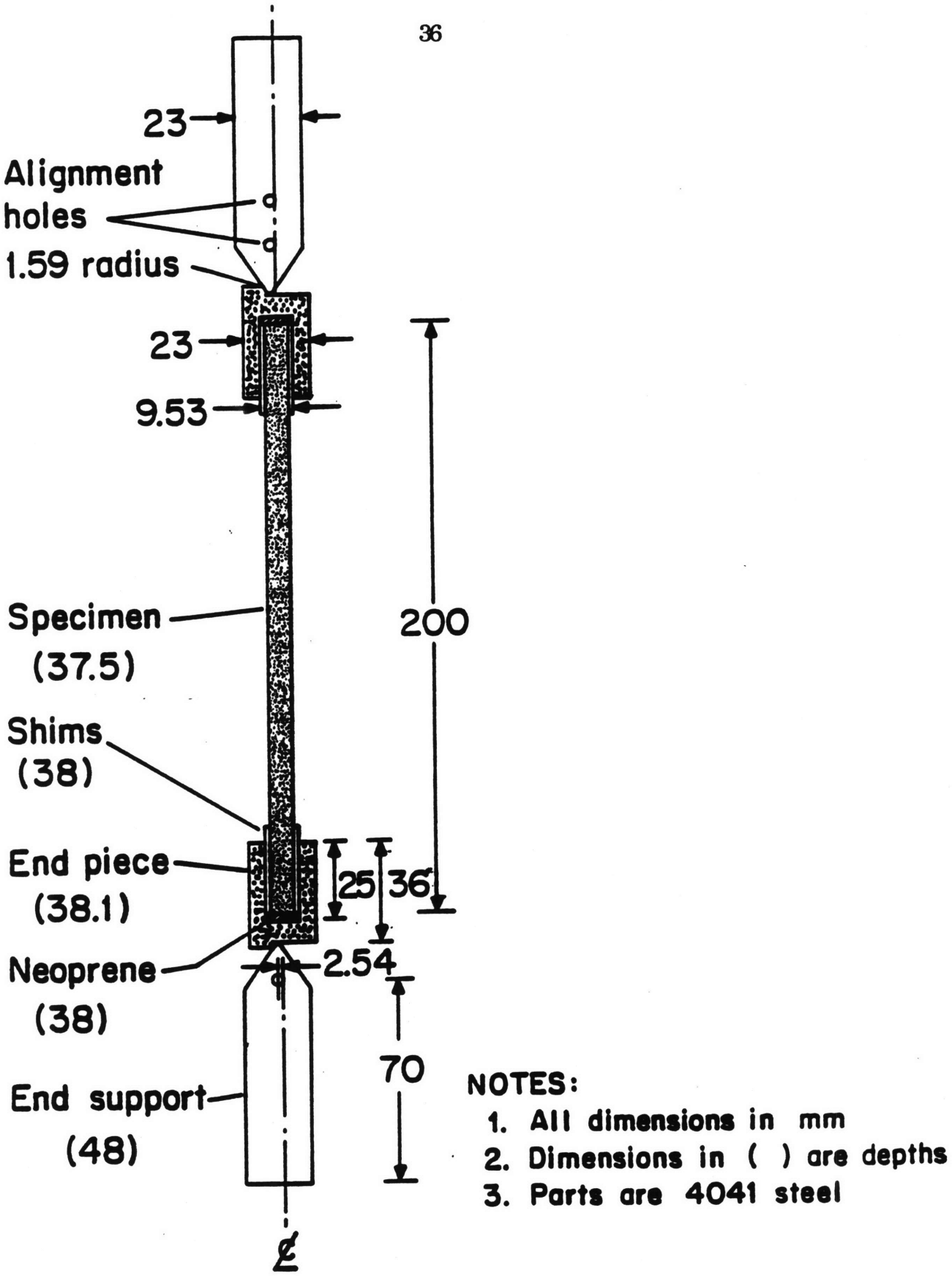

Figure 3.2 Illustration of test jig.

shims are placed on both sides of the specimen to keep it symmetric with respect to the centerline of the end pieces. The slots in the end pieces are 25 mm deep, reducing the test section length of the specimen to 150 mm. The total length of the column including the end pieces is 222 mm. On the opposite surface of the end pieces, a groove is cut into which the knife edges of the end supports fit. The end supports are blocks of 4041 steel, hardened to 36 Rockwell, with one end machined to a wedge with a rounded edge. This rounded knife edge has a radius of 1.59 mm. These end supports are placed into the grips of the test machine. Alignment of the top and bottom end supports is important to provide the correct loading conditions. Proper alignment is assured by bolting an alignment plate to both end supports. Once the top end support is gripped by the test machine, the plate is attached to the end support by two bolts preventing the plate from rotating. The bottom end support is then bolted to the alignment plate, after which the bottom end support is gripped. After both grips are closed, the alignment plate is removed. A side view of the jig with the alignment plate in place is shown in Figure 3.3.

The groove on the end pieces is not at the centerline of the specimen, thus making the load introduction eccentric. The groove is 2.54 mm (0.1 inch) from the centerline creating a moment at the specimens ends. This moment is large enough to overcome any friction present at the knife edge. Thus the specimen behaves as a simply-supported beam-column from the start of load introduction. The eccentricity is large enough to overshadow any eccentricity resulting from slight manufacturing defects in the specimens. This eccentricity will cause the specimens to always deflect in the same direction.

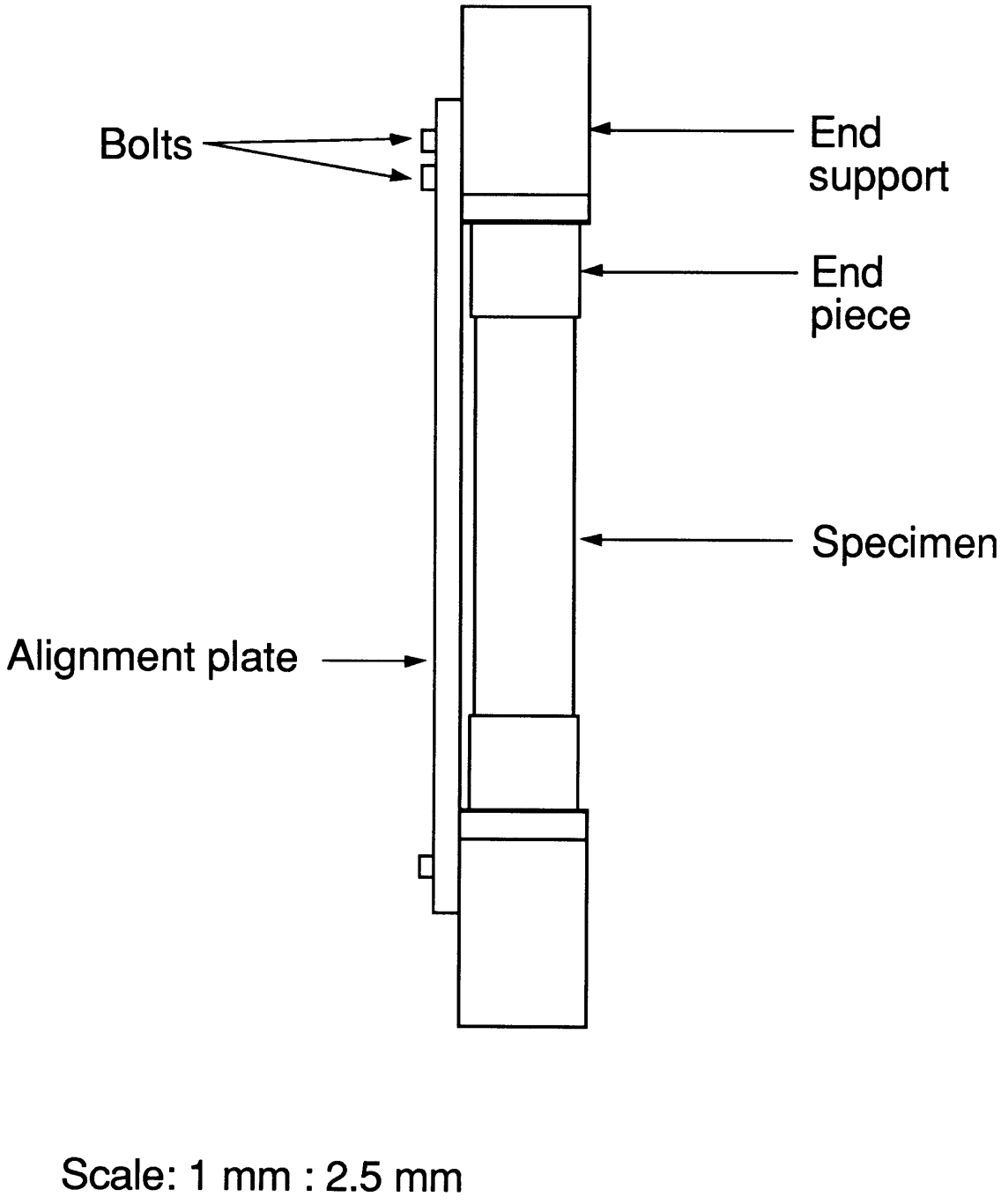

Figure 3.3 Side view of jig with alignment plate.

Neoprene rubber blocks are placed between the specimen and the end pieces. Without the rubber blocks, contact between the specimen and the end pieces might be reduced to the edge of the surface of the specimen because the end pieces tend to rotate slightly more than the end of the specimen. Premature failure could occur due to a resulting shear stress concentration. The addition of the rubber blocks in the bottom of the slots provided a more even load distribution. The addition of a plastic material through the load path meant that the end displacement data as recorded by the test machine load cell is not useable.

A lip on the compression side of the end pieces exists to attempt to prevent the specimen from flying out of the jig upon ultimate failure. Aside from safety concerns, additional damage can occur due to the specimen becoming ballistic and striking a hard surface, which was considered undesirable. A plastic shield was also attached to the test machine to restrain a specimen leaving the jig in this manner.

3.2 The Test Program

Hercules AS4/3501-6 material was used throughout this investigation. This consists of unidirectional AS4 graphite fibers in a thermoset 3501-6 matrix system. It is in a semi-cured (B-stage) state as preimpregnated tape and must be stored at -18°C or colder. This prepeg roll is nominally 305 mm wide. Nominal elastic and strength properties of a cured unidirectional ply are shown in Table 3.1.

In order to provide consistent results with the previous work [38], the same three laminates were chosen: $[45_4/\text{-}45_4/(0/90)_4]_{2s}$, $[\pm 45/0/90_4]_{4s}$, and $[(45_2/\text{-}45_2/0)_2/90_5]_{2s}$. These laminates were originally chosen in order that

Table 3.1 AS4/3501-6 material properties.

Stiffness Properties			Strength Properties		
E_1	142	GPa	X^T	2356	MPa
E_2	9.8	GPa	X^C	1468	MPa
E_3	9.8	GPa	Y^T	49.4	MPa
G_{12}	6.0	GPa	Y^C	186	MPa
G_{13}	6.0	GPa	S	105	MPa
G_{23}	4.8	GPa			
ν_{12}	0.3				
ν_{13}	0.3				
ν_{23}	0.34				

initial damage would occur in the form of matrix cracks, making the accumulation of damage observable. Damage would be expected in groups of at least 4 plies of the same fiber orientation. These groups, called "effective plies", behave as a single ply. Thus, when a crack appears, it propagates through the entire thickness of the ply. With an effective ply of less than four plies, the experimentally observed tensile strength is higher. It has been found that the *in situ* ply strength for transverse cracks in $[0_2/90_n]_s$ laminates is related to ply thickness [39]. In fact, for a value of n equal to one, failure stresses could exceed the nominal transverse strength of the 90° plies by a factor of 2.5. Classical Laminated Plate Theory and the Maximum Stress failure criterion were used in laminate selection. Two of the laminates, $[\pm 45/0/90_4]_{4s}$ and $[(45_2/-45_2/0)_2/90_5]_{2s}$, were chosen such that initial damage would occur in 90° plies on the tension side, and one, $[45_4/-45_4/(0/90)_4]_{2s}$, such that initial damage would occur in the 45° plies on the tension side.

A test program was designed to determine the damage accumulation history of the three layups when subjected to cyclic loading. First, specimens of each layup were tested statically to failure. These tests were interrupted and edge replicas taken such that a damage accumulation history could be pieced together in the same manner as the previous work [38]. With the specimens loaded in displacement control, the Load Drop Technique was used to detect a drop in load, interpreted as the occurrence of damage. Edge replicas were taken at each interruption to record the damage state on both sides of the specimens. X-ray photos were not taken since the damage across the width of the specimen was not seen to significantly vary in the previous work [38]. Center deflection versus load measurements were also recorded. These static tests verified that the

specimens and the test set-up used were comparable to what had been previously done. The remainder of the specimens were tested cyclically to failure to fulfill the objectives of this work.

These specimens were first loaded quasi-statically in displacement control using the Load Drop Technique. A predetermined level of initial damage would be achieved statically before starting the cyclic portion of the test. Once this initial damage was created, the specimens would be loaded cyclically to failure. At predetermined cyclic intervals, a static test sequence would be performed in which a static load versus center deflection measurement was taken as well as edge replicas. This allowed the monitoring of the accumulation of damage and stiffness degradation with respect to the number of cycles.

The four characteristic damage states noted for these layups for static loading [38] were used to define the initial damage levels desired before cyclic loading. These damage states are reviewed in chapter 4. The level of initial damage statically induced and the maximum fatigue load was varied to determine their effect on the damage accumulation histories and failure modes. Competing damage modes may be initiated and interact differently depending on the damage state at the start of cyclic loading as well as the cyclic load level. The entire test program is shown in Table 3.2.

3.3 Specimen Manufacture

Three 305 mm by 350 mm laminates of each layup were manufactured for this investigation. The procedures used were developed in TELAC [40], and are summarized herein.

Table 3.2 Test matrix.

Layup	Number of Specimens	Type of Test [a]
$[45_4/-45_4/(0/90)_4]_{2s}$	4	Static test to failure Edge replicas at load drops
	7	Static to damage level one Cyclic to failure at maximum static load [b]
$[\pm 45/0/90_4]_{4s}$	2	Static test to failure Edge replicas at load drops
	4	Static to damage level one Cyclic to failure at maximum static load
	6	Static to damage level three Cyclic to failure at maximum static load
$[(45_2/-45_2/0)_2/90_5]_{2s}$	2	Static test to failure Edge replicas at load drops
	4	Static to damage level one Cyclic to failure at maximum static load
	3	Static to damage level three Cyclic to failure at maximum static load
	3	Static to damage level three Cyclic to failure at damage level one load level

[a] All cyclic tests include edge replicas and stiffness measurement at intervals.

[b] R ratio of ten used in all cyclic tests.

The prepeg tape is stored at or below -18°C. Upon being taken out of the freezer, the roll is left sealed at room temperature for thirty minutes. This is to help prevent condensation from forming on the material.

The tape is cut into appropriate shapes required for each of the ply orientations using aluminum templates covered in teflon-coated glass fabric and razor blades. The 45° plies are cut into trapezoidal shapes which are placed together to form a 305 mm by 350 mm rectangle. These trapezoids are designed such that there are no fiber breaks in any ply. The joint where the two trapezoids meet is parallel to the fiber direction making it a "matrix joint" which becomes indistinguishable during the cure cycle. The 0° and 90° plies are made using squares and rectangles.

Because the laminates were thick laminates, they were each divided into three sublaminates of approximately twenty plies. These sublaminates were layered separately and compacted in a vacuum of 740 mm Hg for two hours. The backing paper was not removed on each surface of a sublaminate during this process. This compaction helps remove any air pockets and results in a lower void content after curing. After compaction, the sublaminates were then stacked to form the laminate.

Many materials are used in the curing process of a laminate as can be seen in Figure 3.4. Peel-ply, a nylon-like fabric which is porous to the epoxy, is placed on the surface of the laminate. The laminate is placed on an aluminum caul plate. This caul plate is first covered by Mold Wiz® mold release, manufactured by Axel Plastics Research Laboratories, and nonporous teflon-coated glass fabric (TCGF). A sheet of porous teflon-coated glass fabric is placed on top of the laminate. In order to absorb excess epoxy as it flows out of the laminate during the cure, sheets of bleeder material are placed on top of the porous teflon. The number of

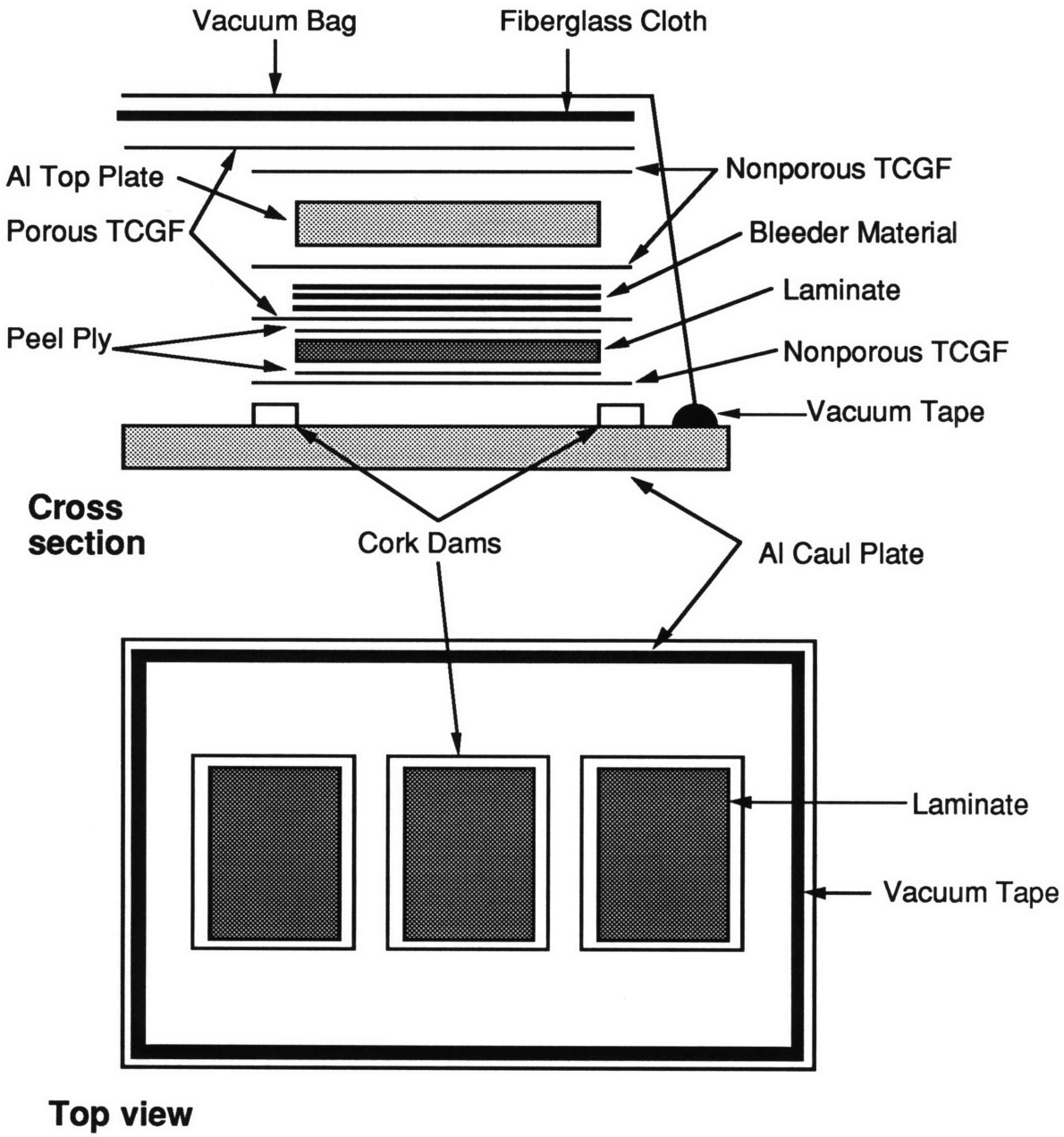

Figure 3.4 Schematic of cure setup.

sheets is half the number of plies of the laminate, although for thick laminates, it was found that less mess was created by using 3 to 5 more sheets. Aluminum top plates, the same size as the laminates, wrapped in a high grade nonporous teflon-coated glass fabric (GNPT) are placed on top of the bleeder material. Corprene rubber material (cork) is used to build up dams around the laminate and top plate assembly to ensure that neither shifts during the cure.

Usually, two or three laminates were cured at a time on one caul plate. The manner in which three laminates were placed on the caul plate is shown in Figure 3.4. Sheets of porous teflon-coated glass fiber were placed over all the top plates, and a heavy fiberglass cloth serving as an air breather was placed over this. This air breather allowed air and other gases to escape into the vacuum system. The entire system is sealed with a high-temperature nylon bagging material and vacuum tape.

Curing the laminates is a two stage process. First, excess epoxy is allowed to flow away during a one hour flow stage at 117°C. At this time, the epoxy is at its lowest viscosity. Second, the chemical cross-linking of the polymer chains occurs during a two-hour set stage at 177°C. During both stages, a vacuum of 740 mm Hg is applied as well as pressure of 0.59 MPa. To avoid thermally shocking the laminates, heating and cooling rates are kept between 1°C and 3°C per minute. A postcure of eight hours at 177°C in an unpressurized oven follows these stages. This cure cycle is illustrated in Figure 3.5.

Six specimens were machined from each laminate to the proper dimensions (200 mm by 37.5 mm) upon the completion of the cure cycle. A water-cooled diamond grit cutting wheel mounted onto a milling machine was used. A table speed of 28 mm per minute was used because of the

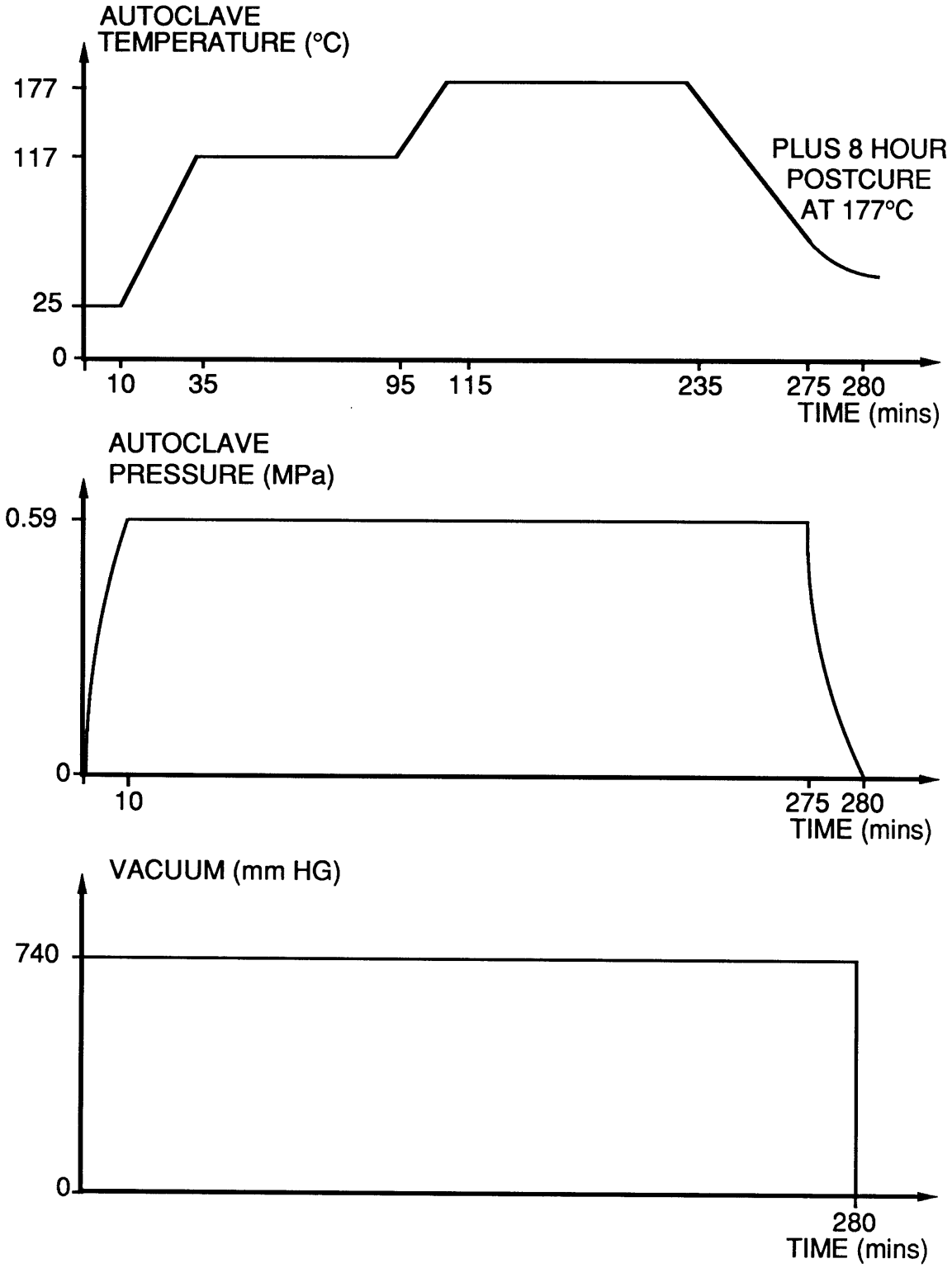

Figure 3.5 Schematic of cure cycle.

thickness of the laminates. A faster rate may cause the laminate and the wheel to heat excessively.

The specimens were measured in three locations for width and nine locations for thickness. The locations of these measurement points is shown in Figure 3.6. The average measured thicknesses are 8.965 mm, 8.317 mm, and 7.600 mm for the $[45_4/-45_4/(0/90)_4]_{2s}$, $[(45_2/-45_2/0)_2/90_5]_{2s}$, and $[\pm 45/0/90_4]_{4s}$ layups respectively. The nominal thicknesses are 8.576 mm, 8.040 mm, and 7.504 mm respectively. The average ply thickness for all of the specimens is 0.138 mm, with a coefficient of variation of 2.6%, compared to the nominal thickness of 0.134 mm. Generally, the specimens from the middle of the laminate were slightly thicker than those from the outer portions by approximately 4%. The average thickness and average width for each specimen are listed in appendix A.

In order to obtain good edge replicas, the edges of the specimens must first be polished to a glossy finish. This involved mounting felt bobs, which had been dipped into a solution of a fine abrasive, onto a drill press. Kaopolite-SF, with an average particle size of 0.7μm, was hand mixed with tap water. The mixing ratio used was two parts water to one part of abrasive. The spinning felt bobs polished the edges of the specimens after which the specimens were rinsed with water to eliminate any residue left by the abrasive solution. Once the specimens were dry, a line was scribed across the thickness of the sides at the center of the specimen with a machinist's scribe. This line was used as a reference when documenting the damage from the replicas. Care had to be taken so as not to scribe the line too hard thereby damaging the surface plies.

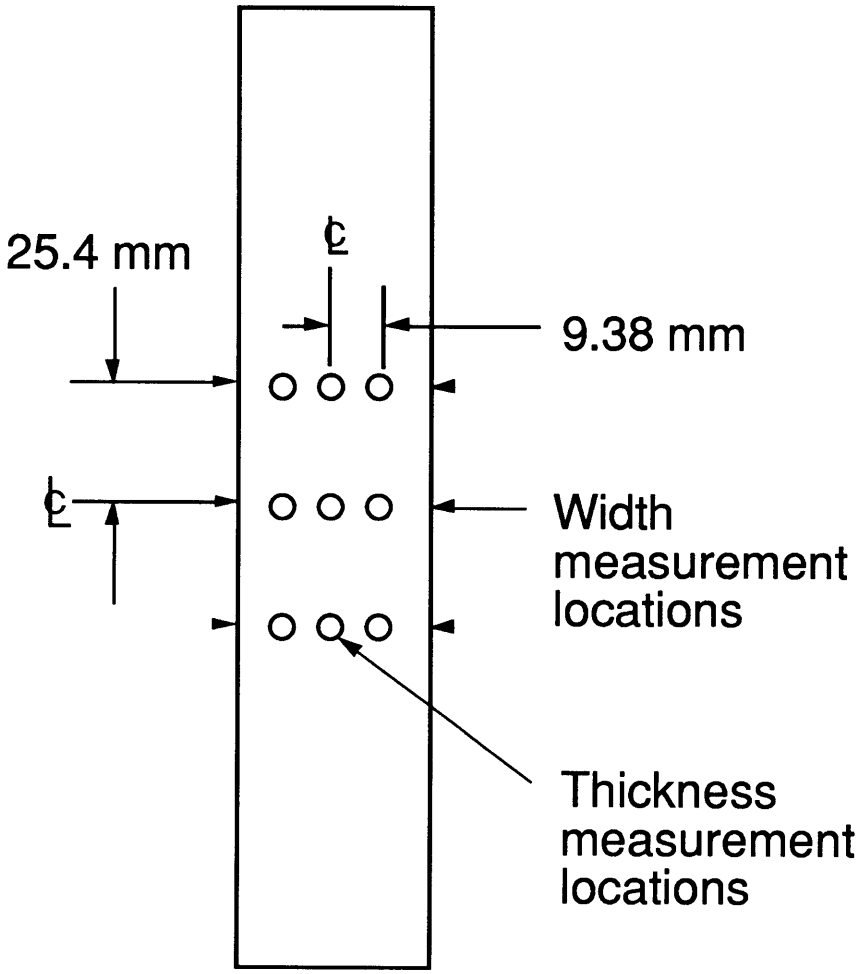

Figure 3.6 Locations of measurements.

3.4 Instrumentation

The only measurements taken requiring instrumentation was the center deflection of the specimens. This measurement was taken during the static portions of the test sequencing. A Linear Variable Differential Transducer (LVDT) was used to record the center deflection. This was a Trans-Tek DC-DC model 355 with a range of ±51 mm and an accuracy of ±0.5% linearity. The transducer was mounted onto a jig which was affixed to the vertical side supports of the testing machine. Vertical and horizontal adjustments could be made to the jig allowing for proper transducer placement with respect to the center of the specimen.

3.5 Damage Detection

The Load Drop Technique was used as a method of detecting the possible occurrence of damage in the static tests. Once this technique indicated that damage may have occurred, the edge replication technique was used to examine the type and severity of the damage. Edge replication is a nondestructive evaluation technique in which a permanent record of the damage state is made and can then be easily examined.

3.5.1 The Load Drop Technique

The Load Drop Technique is a method for detecting the occurrence of damage [41]. As damage occurs, the overall compliance of the specimen increases. A slight change in compliance is difficult to detect for a small amount of damage in the beam-column specimens. By loading the specimen in stroke control, though, each occurrence of damage causing an increase in compliance will result in a drop in the magnitude of the applied

load. Thus, it is possible to detect the occurrence of damage by monitoring the applied load of a specimen loaded quasistatically in stroke control. Caution must be taken so that the increase in load magnitude due to normal loading does not obscure a load drop due to the occurrence of damage.

A computer program has been written which monitors the applied load during a test and interrupts the test with the occurrence of a drop in the load magnitude. Several factors control the ability of the program to detect load drops. The magnitude of the load drop, the loading rate, and the time interval chosen between data points determine the sensitivity of the program. The load data, in the form of analog voltage data from the testing machine, is digitized using analog-to-digital converters. Thus, the load is represented by discrete computer units which are input into the computer and monitored by the program. The resolution, or load corresponding to a computer unit, is dependent on the load range selected on the testing machine. At each time interval, the program compares the new load value with the previous one and interrupts the test if the new one is lower.

If the normal increase in the load magnitude is larger than the drop in load due to damage, the load drop can be hidden, as illustrated in Figure 3.7. If the time interval between data points is too large with respect to the loading rate, a drop in load may be overlooked. If the time interval is too small, the noise in the system can be larger than the normal rise in load and taken as a load drop, thus false stops can interrupt the test. An optimum time interval was needed to achieve the desired sensitivity so that all load drops were detected while avoiding problems with noise in the system. An interval for each layup was chosen so that false stops might occur but all legitimate load drops would be detected. The optimum time

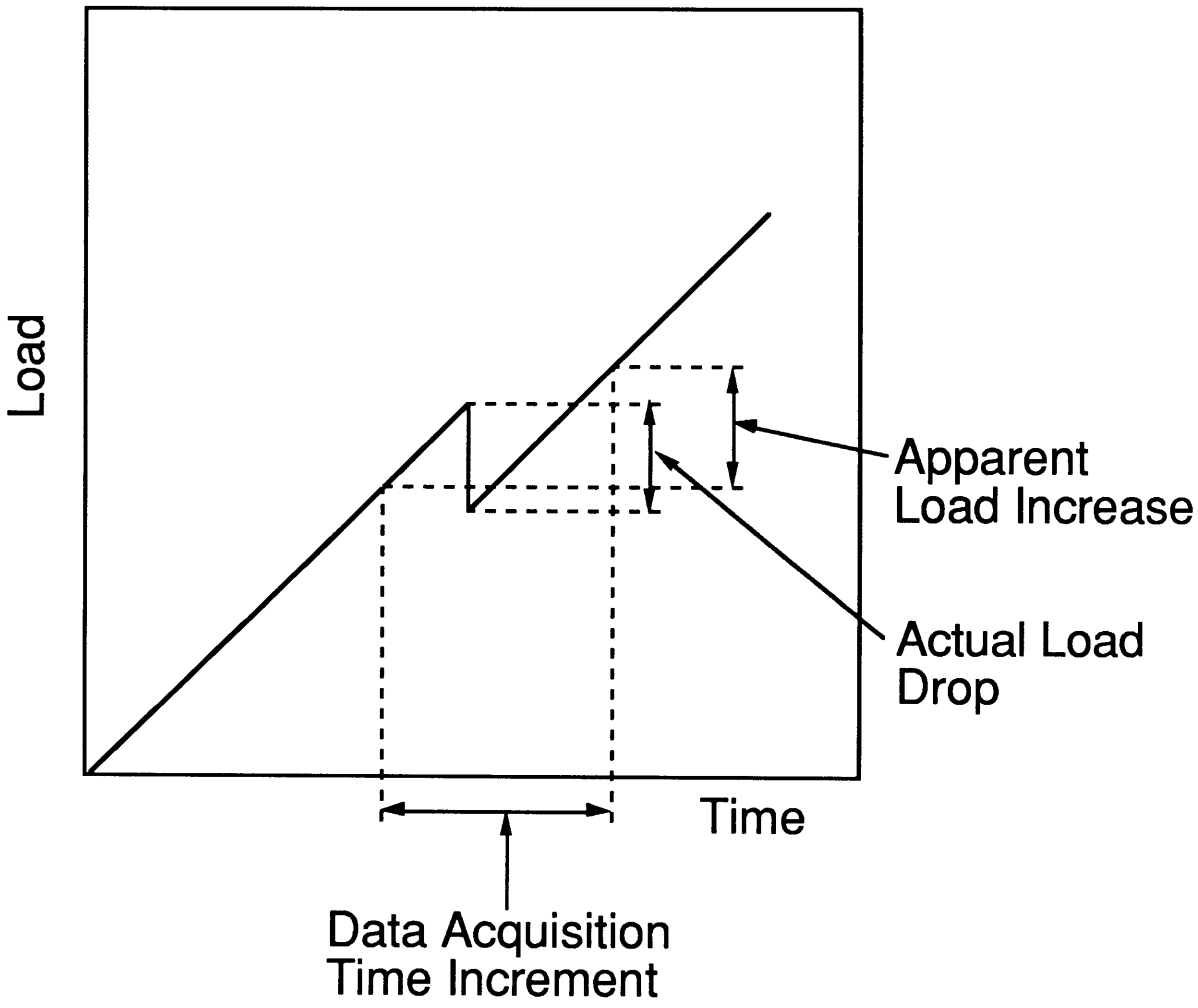

Figure 3.7 Illustration of load increase obscuring a load drop.

interval for both the $[\pm 45/0/90_4]_{4s}$ and $[(45_2/-45_2/0)_2/90_5]_{2s}$ layups was 1.0 seconds. A time interval of 0.7 seconds for the $[45_4/-45_4/(0/90)_4]_{2s}$ layup was used. It was noticed during initial testing that using 1.0 second for the $[45_4/-45_4/(0/90)_4]_{2s}$ layup caused some damage events to be overlooked. Reducing this time interval eliminated the problem.

3.5.2 Edge Replication

Edge replication is the nondestructive technique used to monitor the type and severity of damage occurring on all of the specimens throughout the duration of the tests. During the static tests, replicas were taken at every interruption, while replicas were taken at every static test sequence during the fatigue portion of the tests. A permanent record of the side of a specimen is obtained by making its impression on a strip of clear acetate tape. Replicas were taken of both edges of a specimen.

Replicas were made while the specimens were under load, eliminating the need for removing the specimen from the jig for each replication. The matrix cracks and delaminations on the tension side of the specimen open up when the specimen is loaded, giving them better visibility on the replica. Detection of compression side damage was usually not difficult even though the compressive loads might tend to close the cracks. It is possible that the cyclic motion created gaps at crack locations due to friction, aiding the detection of damage in the compressive stress field.

Since the length of the section of the specimen easily accessible between the end pieces was approximately 125 mm, a strip of replicating tape of this length was cut for each replica. By holding one end of the tape to the lower end of the specimen's edge, acetone was applied to the rest of the edge using a squeeze bottle. The acetone softens the tape, allowing it to fill

the gaps left by cracks and delaminations when smoothed onto the edge with a finger. While the tape was drying, it was labelled with a felt tip pen. After approximately one minute, the tape was removed.

Upon removal, the replicas were inspected with the naked eye for smudges and other markings that would inhibit the detection of damage. These smudges and markings could result from uneven pressure or a lifting of the tape before complete drying. Unacceptable replicas were discarded and new ones taken. Acceptable replicas were placed between two sheets of glass to keep them from curling.

Good replicas can allow individual fibers to be seen. Laminate features, such as individual plies and interlaminar resin layers, can easily be seen due to a change in surface texture. Damage is detected as the softened tape can seep into the gaps created by the cracks and delaminations. Compression side damage can also be detected by surface texture changes. These damage features are easy to detect when examining the replicas under a microscope with backlighting due to the surface texture of the tape after drying. The same damage is difficult to detect when examining the specimen directly because there is no backlighting and the features appear as dark details on a dark background.

A microscope, at a magnification of thirty, was used to examine the replicas. The replicas, placed between two sheets of glass, were elevated allowing the placement of a small lamp to provide backlighting. The damage as seen on the replicas was transcribed to schematics of the specimen's edge. These schematics, or transcriptions, are drawn to scale along the length of the specimen and expanded by a factor of about seven through the thickness with each effective ply drawn in. The cracks and delaminations are drawn on the appropriate plies on one transcription for

each replica. The damage can then be quantified by determining the number of cracks over a unit length, referred to as crack density. Due to the end pieces and shims, only approximately 100 mm of the central portion of a specimen's edge was consistently replicated. A photograph of a typical replica along with the corresponding transcription is shown in Figure 3.8.

3.6 Test Procedures

Two types of tests were conducted in this investigation. Static tests were carried out for three purposes; quasistatic tests to failure on two specimens of each laminate to obtain basic damage information, quasistatic tests to create initial damage prior to cyclic loading, and quasistatic tests to obtain stiffness measurements during interruptions in the cyclic portion of the tests. Cyclic tests were conducted to failure with static test sequences at predetermined intervals.

3.6.1 Static Tests

Static tests were conducted under quasistatic monotonic compressive loading in stroke (displacement) control on an MTS 810 Material Testing System. The stroke rate of 0.0254 mm per second for all laminates combined with the time interval chosen between data points made the Load Drop Technique an effective tool. The test machine was run on the 10% load range (±44.5 kN, ±10,000 lbs) and on the 20% stroke range (±25.4 mm, ±1 inch).

It was considered important to have correct edge alignment in order to achieve the proper simply-supported boundary conditions. To achieve this, the top knife edge end fixture was first aligned with a machinist's

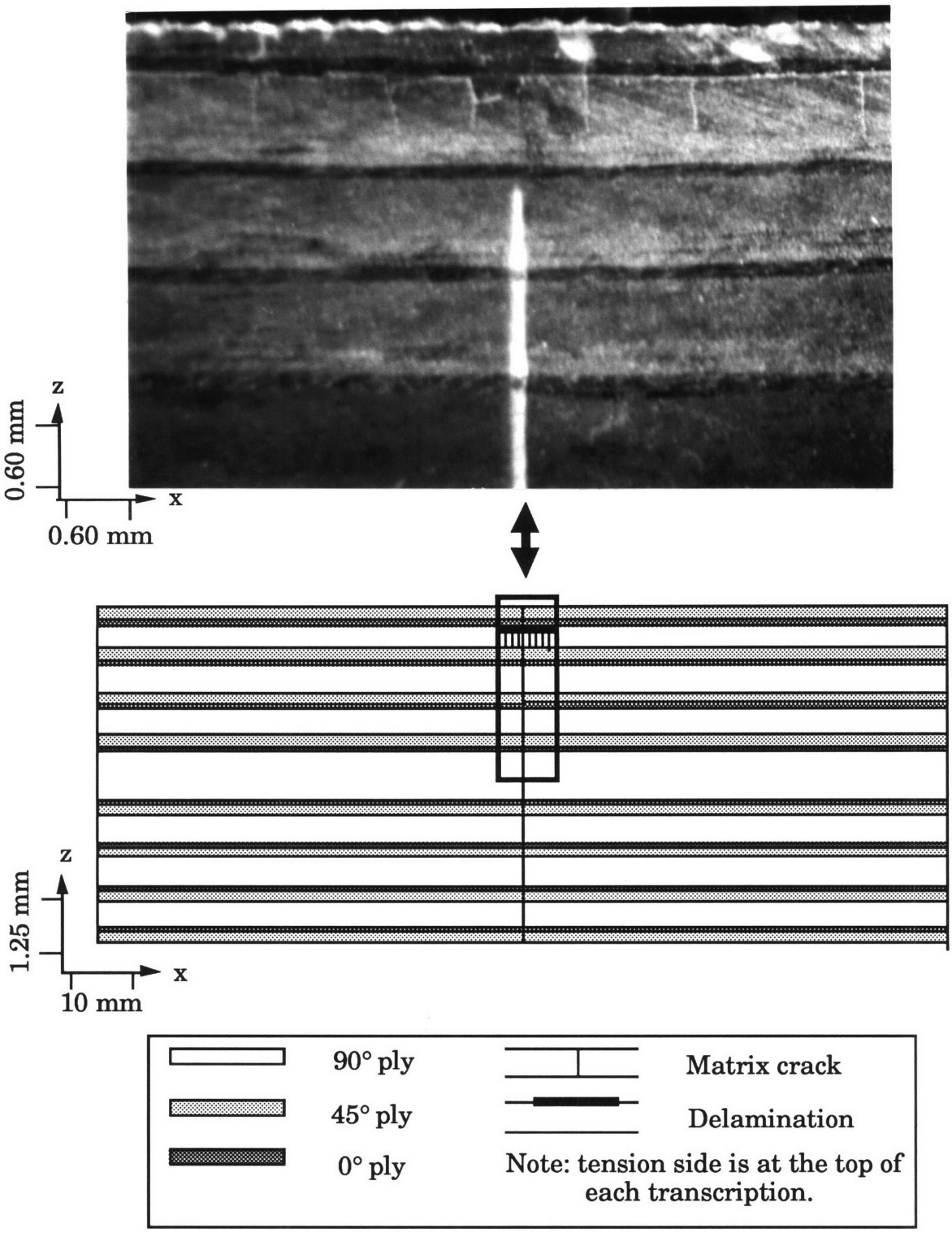

Figure 3.8 Photograph of an edge replica of a $[\pm 45/0/90_4]_{4s}$ specimen with the corresponding transcription.

square into the machine's upper grip. A grip pressure of approximately 400 psi was used. After bolting the alignment plate (see Figure 3.3) to the top knife edge, the lower knife edge end fixture was bolted to the alignment plate. The whole assembly was then lowered so that the lower knife edge could be gripped by the lower grips. The alignment plate was then removed. The lower grip could be adjusted to move vertically so the correct distance between the knife edges could be easily set. Once this distance was set, the specimen could be slipped in between the knife edges with no load applied.

Once the specimen was placed into the jig at zero load, the transducer was aligned with the center of the specimen. The lateral and vertical position of the transducer could be adjusted via the fixture mounted to the side uprights of the test machine. The transducer was checked to be horizontal using a water level. Calibration of the transducer was accomplished by placing a 1.000 inch block between the transducer tip and the specimen. The difference in the number of computer units with and without the block gave the calibration factor in inches per computer unit. A voltmeter was also hooked up to the transducer to be able to monitor the center deflection real time.

For all of the static tests, the testing machine was run under computer control. During the static tests to failure, the load drop program stopped the test when the load at time interval n was lower than that recorded at time interval n-1, thus signalling the possible occurrence of damage. At each interruption, the maximum load level reached by the test machine was recorded. The program then reduced the stroke by a factor of two to eliminate the chance of creating more damage while the replicas were taken.

After the replicas were taken, the specimen was unloaded and another test iteration was started. For each iteration, the computer was instructed to ignore any load drops prior to the previous load level. These iterations were repeated until the specimen failed, with a new data file created for each iteration.

For the specimens to be cyclically loaded, static tests were first run to create initial damage. The Load Drop Technique was again used to detect the possible occurrence of damage. Each iteration, consisting of loading to the next load drop, was contingent upon immediate examination of the replicas. Based on the characteristic damage states for these laminates as documented by Wolfe [38] and on the damage history obtained from the current static to failure tests, each replica was carefully examined to determine if the current damage state was suitable for the start of the cyclic portion of the test. If it was deemed that more damage needed to be created statically, then another iteration would be performed. These iterations continued until the desired damage state was reached. The voltmeter hooked up to the transducer to monitor the center deflection assisted this process by allowing a real time look at the response of the specimen in case some load drops were not detected. The iteration could be halted manually if it was felt that the center deflection was becoming large enough to indicate there was more damage than desired. Audible signs of damage, crackling sounds heard within one or two meters from the specimen, also triggered some manual stops. A replica was taken to verify the damage state. This process helped to avoid overshooting the desired damage state.

The static test performed for each static test sequence during the cyclic portion of the test did not utilize the same program to control the test machine. A similar program was used that loaded the specimen the same

way, but did not look for load drops. Since the purpose of this static test was to obtain center deflection versus load data to calculate a Southwell buckling load, the computer instructed the test machine to stop loading at a predetermined load level which was manually input into the computer for each specimen. The level at which loading was stopped was usually 10-20% below the maximum cyclic load to prevent the creation of additional damage under static loading. The stroke was then reduced by a factor of two to allow for replicas to be taken. After the replicas were taken, the specimen was unloaded and cyclic loading was resumed.

3.6.2 Cyclic Tests

The cyclic tests were carried out on the same MTS 810 Material Testing System. These tests were run in load control with the load range at 10% (±44.5 kN, ±10,000 lbs). A function generator provided the waveform for the haversine loading at a frequency of 1.5 Hz. This was the maximum frequency physically possible due to the magnitude of the stroke required to reach the maximum cyclic load. It was desired to use as high a frequency as possible to make the most use of available testing time.

It has been reported that heat can be generated due to friction effects in a damaged laminate cyclically loaded [1]. Excessive heat can degrade the matrix material and alter the outcome of the test. Temperature effects were also considered in determining a test frequency. Several damaged specimens were cyclically loaded at 1.5 Hz with a thermocouple monitoring the temperature of the specimen surface adjacent to the damage. No significant increases in temperature were found throughout the duration of the tests. This frequency was thus considered safe for the remainder of the specimens.

A load ratio, R, of ten was used for this investigation. Load ratio is the ratio of the minimum load to the maximum load used for the cyclic tests. A positive value greater than one indicates compression-compression loading. The lowest numerical load (absolute value) was first dialed into the test machine using the "set point" knob. The largest numerical load (absolute value) was dialed in using the "span 1" dial. The span 1 value is actually the difference between the maximum and minimum load values. This setting was reduced slightly to ensure that the maximum compressive load was not exceeded upon start-up. These settings were adjusted after several single cycle attempts at the proper frequency. The maximum and minimum load levels were then finetuned once continuous cyclic loading began.

As damage accumulated during the cyclic portion of the tests, the stiffness of the specimen changed slightly. Near specimen failure, with the damage becoming extensive, the stiffness changes caused the load levels to drift as much as 5%. This drift in load was due to the feedback loop of the testing machine which constantly adjusts the loading to match the control position. As the stiffness of the specimen changes, the control position of the testing machine will not be at exactly the right setting for the desired loading. The load level needed to be monitored to ensure that the correct conditions were met.

In order to monitor the accumulation of damage during cyclic loading, static test sequences were conducted on an interval basis. A schematic of the sequence of tests is shown in Figure 3.9. As explained above, these test static sequences involved a center deflection versus load measurement as well as edge replications. These intervals occurred every 2,500 cycles up to 10,000 cycles, then every 5,000 cycles. For one specimen

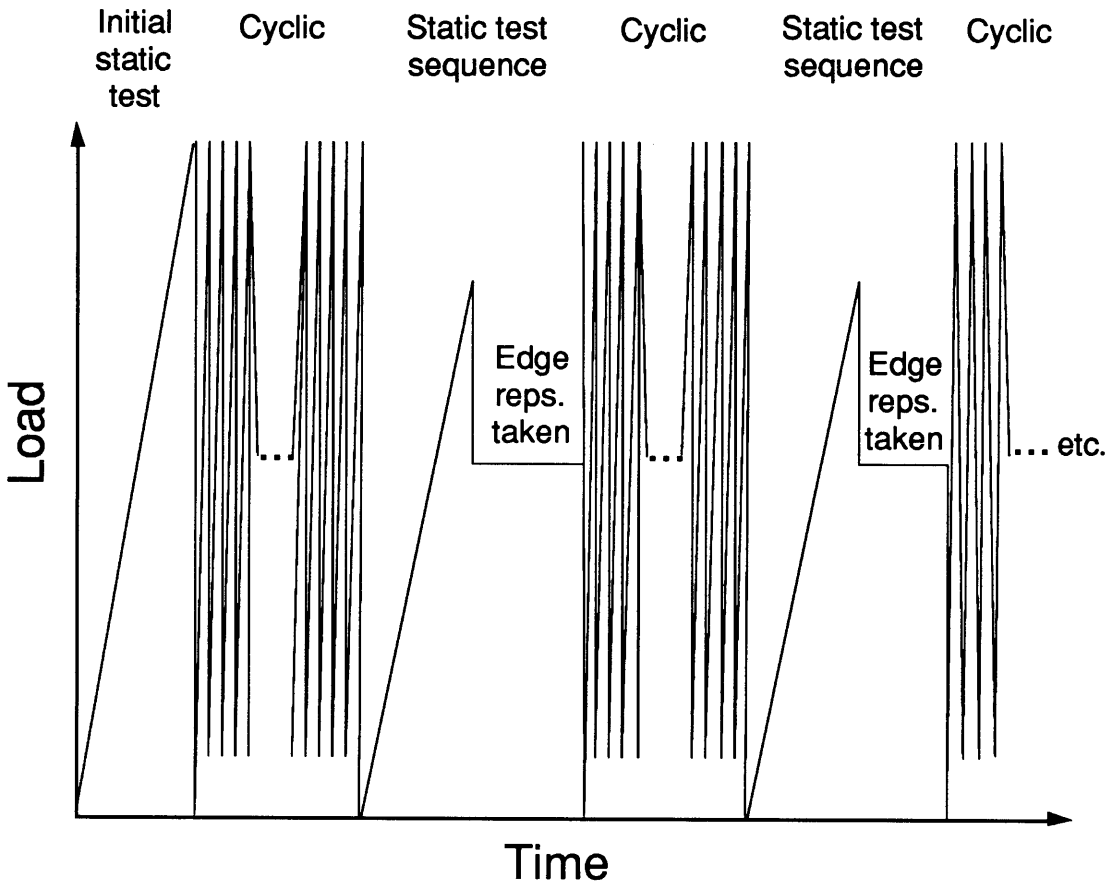

Figure 3.9 Schematic of sequence of tests for cyclic specimens.

that went over 600,000 cycles, intervals of 10,000 and 20,000 cycles were used beyond 60,000 and 200,000 cycles respectively. Cyclic loading was halted at each interval with the aid of a resetable counter on the testing machine console. This counter could be preset to halt the test at any value and was not the same counter used to count the total number of cycles for a specimen.

The cyclic tests were continued until specimen failure. Failure was defined as the inability of the specimen to carry 50% of the maximum load and was usually catastrophic. Often, the testing machine would shut down due to the stroke limits being reached in trying to obtain the load levels and maintaining the same frequency. At failure, the specimen sometimes left the jig, striking the plexiglass shield attached to the machine.

Chapter 4

RESULTS

The results of the experiments described in Chapter 3 are presented herein. Each laminate type is treated in its own section, with subsections for the static and cyclic tests. The damage states are presented in the form of transcriptions of a typical specimen for each test condition. Transcriptions cover only half of the length of the test section up to the centerline parallel to the z axis. They are drawn to scale along their length, but are magnified by a factor of approximately eight through the thickness.

Southwell buckling loads were used as a means of characterizing the load versus center deflection data. Center deflection divided by load was plotted against center deflection, and a line was fit to the straight section of the graph, the slope of which gives the buckling load. A typical load versus center deflection plot is shown in Figure 4.1 followed by the corresponding Southwell plot in Figure 4.2.

4.1 $[45_4/-45_4/(0/90)_4]_{2s}$ Laminates

Before discussing the static and cyclic behavior of these specimens, it is necessary to first point out the existence of matrix cracks in some of the untested specimens. The presence of this damage was not consistent throughout all of the specimens of a particular laminate panel. This damage also varied across the width of a specimen since the replicas of both

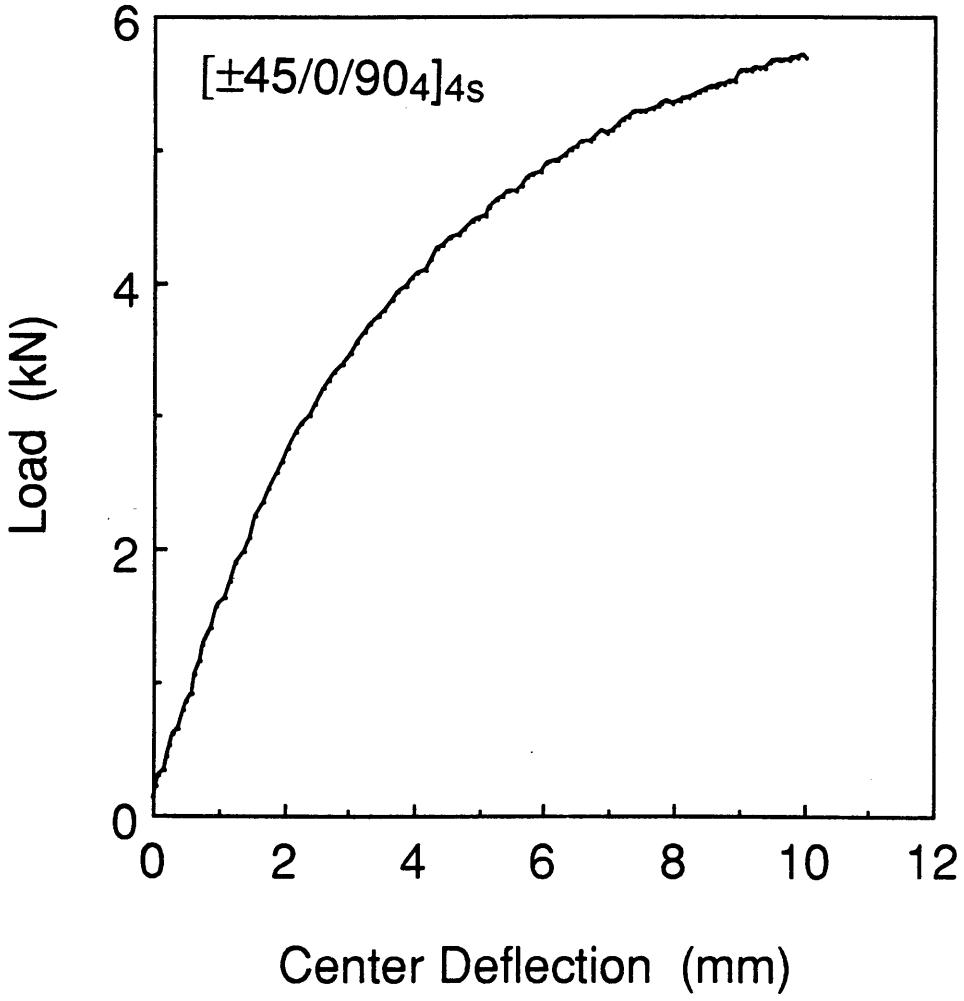

Figure 4.1 Typical load versus center deflection plot for a $[\pm 45/0/(90)_4]_{4s}$ specimen.

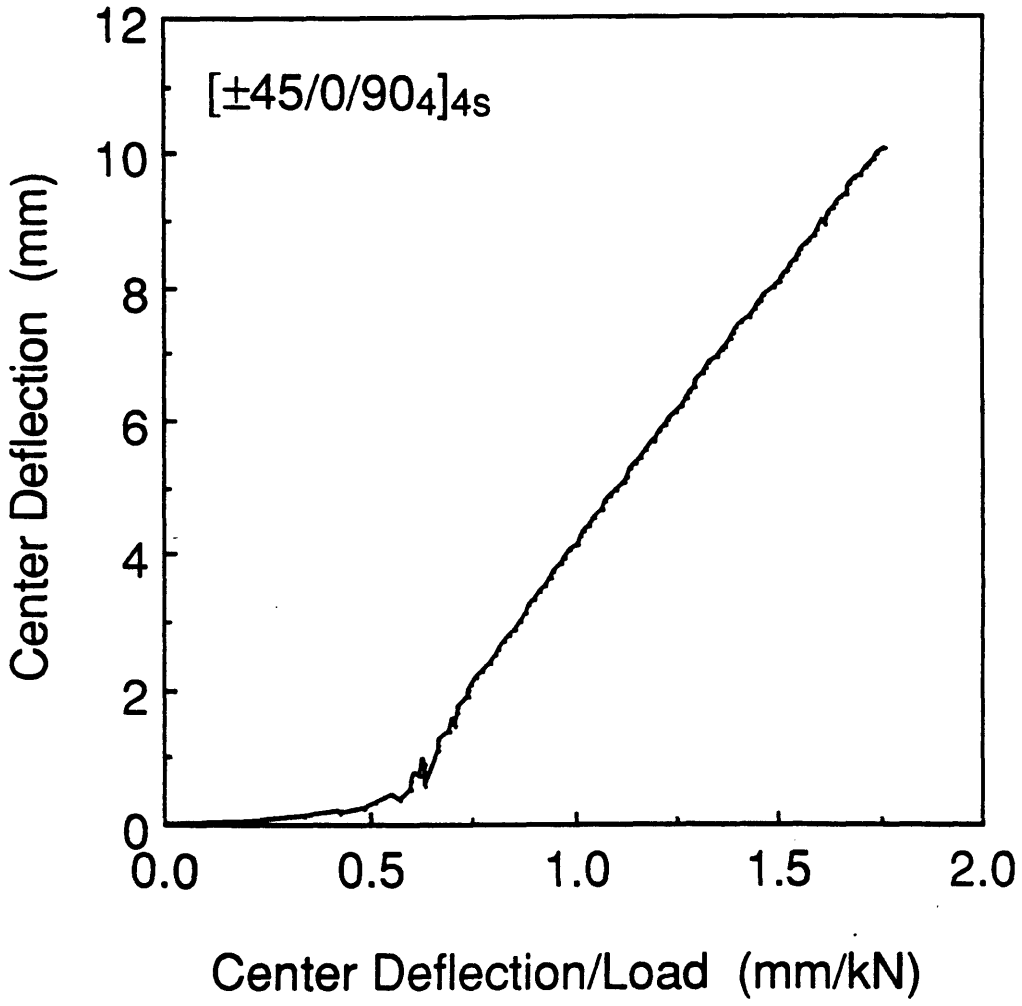

Figure 4.2 A typical Southwell plot for a $[\pm 45/0/(90)_4]_{4s}$ specimen.

edges of some specimens showed different damage states. A typical transcription of the matrix cracks of an untested specimen is shown in Figure 4.3. When these matrix cracks were present, they were always in the 45° and -45° effective ply groups. A surface 45° ply usually had most of the damage with the opposite surface 45° and adjacent -45° plies showing no damage. Some of the interior 45° and -45° plies also contained cracks. The severity of the cracking varied from specimen to specimen. The possible reasons for the existence of such damage are discussed in the following chapter.

The damage histories for both the static and fatigue tests were dependent on the orientation of the specimens in the test jig in regards to this initial cracking. Placing the specimen on the jig such that these cracks were biased toward what would be the compression side once center deflection occurred produced a different damage history than if the cracks were biased toward the tension side of the specimen. The behavior for both conditions is presented.

4.1.1 Static Behavior

Four specimens were tested to failure under static loading conditions. Two were tested such that the initial matrix cracks were on the compression side of the specimen and two with the cracks on the tension side. For specimens of both orientations, damage due to applied loads was initiated as expected: matrix cracks in the central region of the specimen in the outermost 45° and -45° plies on the tension side. The damage accumulated in the form of matrix cracks and delaminations until failure. Failure was defined for all of the specimens tested statically to be when the applied load dropped to less than half of the maximum load reached.

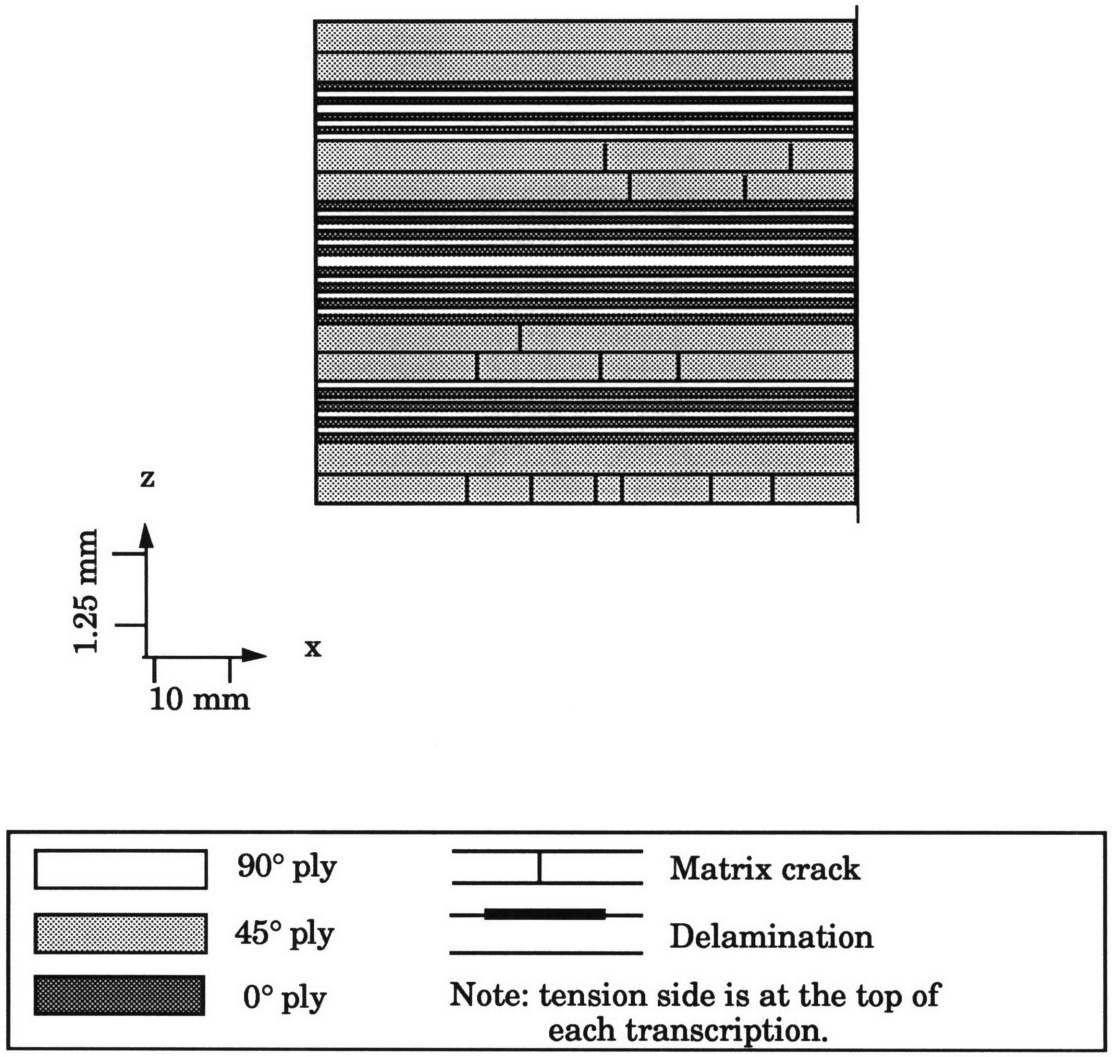

Figure 4.3 Transcription of a typical untested $[45_4/-45_4/(0/90)_4]_{2s}$ specimen.

The effect of the initial damage on the virgin specimens is clearly seen when looking at the damage histories of the two orientations. The four characteristic damage states for the specimens where the initial damage was biased toward the tension side are summarized in Table 4.1 and illustrated in Figure 4.4. The damage accumulation histories for these specimens are comparable to previous results [38]. The first characteristic damage state consists of sporadic cracks in the outermost tension side 45° and -45° plies. A couple of small discontinuous delaminations connected some of the cracks. There are more cracks and the discontinuous delaminations spread in the second damage state. By the third damage state, the delaminations grow together, becoming one continuous delamination across the central 60 mm of the specimen. The damage is clearly visible to the naked eye by the fourth damage state with a gross delamination separating the central 80 mm of the outermost 45° and -45° plies. Crack saturation is reached in the central 60 mm portion of the -45° ply, with the crack density dropping to between 50 and 75% saturation 15 mm to either side of this region. The average crack spacing at saturation is 1.69 mm. Final failure occurs when the 0° plies on the tension side fail. All of the damage at failure was on the tension half while the compression half was still intact as shown in the photograph in Figure 4.5.

For the orientation where the initial cracks were on the compression side of the specimen, the damage history is significantly different as shown in Figure 4.6. The damage progression on the outermost tension side 45° and -45° plies follows the same stages as outlined in Table 4.1 for the other orientation above, but there was also damage growth on the outermost compression side 45° ply where initial cracks existed on the untested specimens. The growth of damage on the compression side was mostly in

Table 4.1 Description of the four characteristic damage states of the $[45_4/-45_4/(0/90)_4]_{2s}$ laminate.[a]

Characteristic Damage State	Description
1	Sporadic cracks on outermost tension side 45° and -45° effective plies. Small discontinuous delaminations at 45°/-45° interface.
2	More cracking. Delaminations begin to spread.
3	Delaminations grow together creating one continuous delamination across the central 60 mm of specimen. Crack density increases.
4	Crack saturation reached in central 60 mm of -45° ply with an average crack spacing of 1.69 mm. Delamination visible to naked eye. *(On compression side, delaminations initiate at 45°/-45° interface, linking existing cracks, and grow rapidly to become one continuous delamination.)*

[a] Comments in parentheses and italics pertain only to specimens with initial damage on compression side.

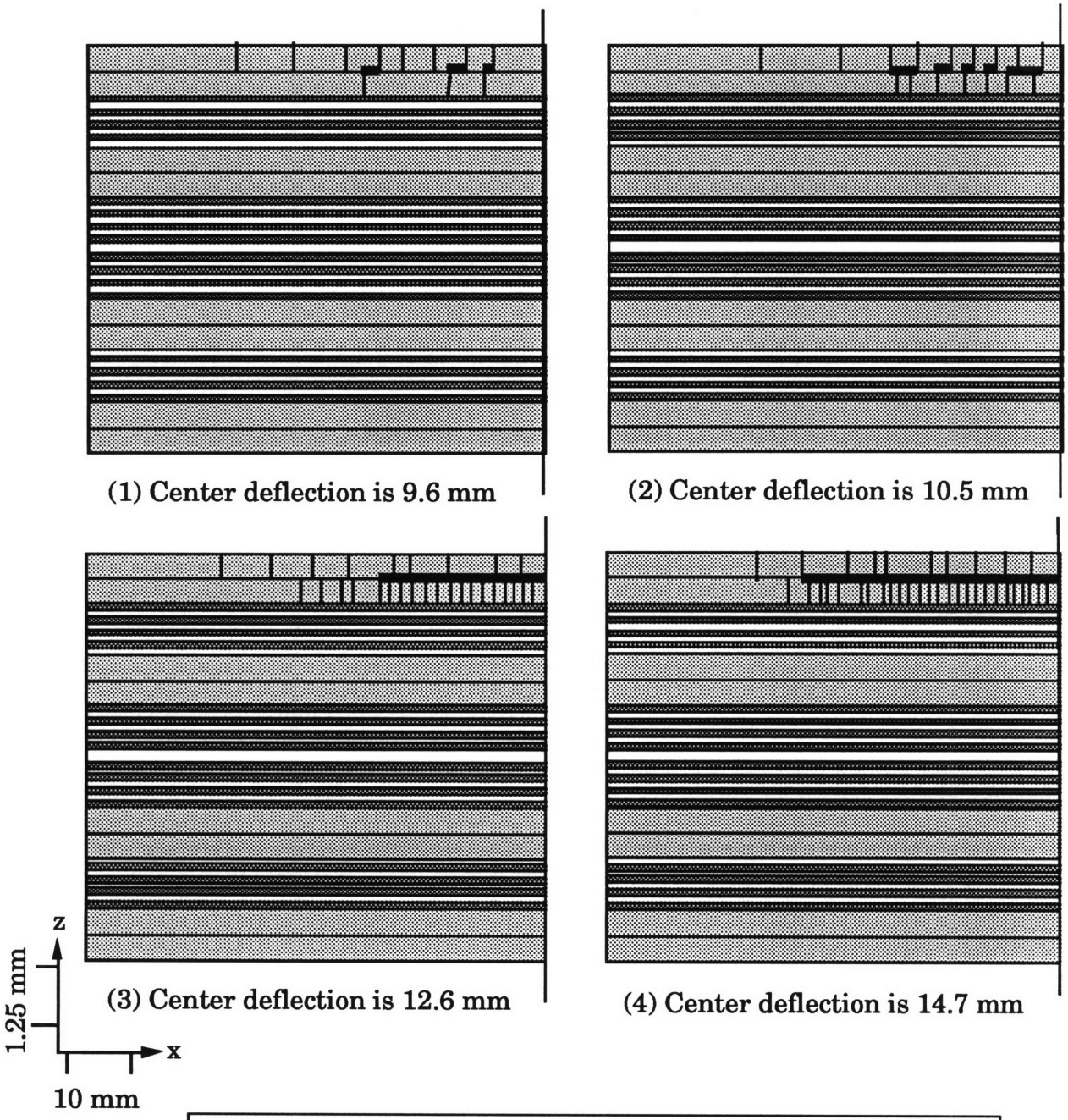

Figure 4.4 Damage history of a typical $[45_4/-45_4/(0/90)_4]_{2s}$ specimen statically tested with the initial damage biased toward the tension side.

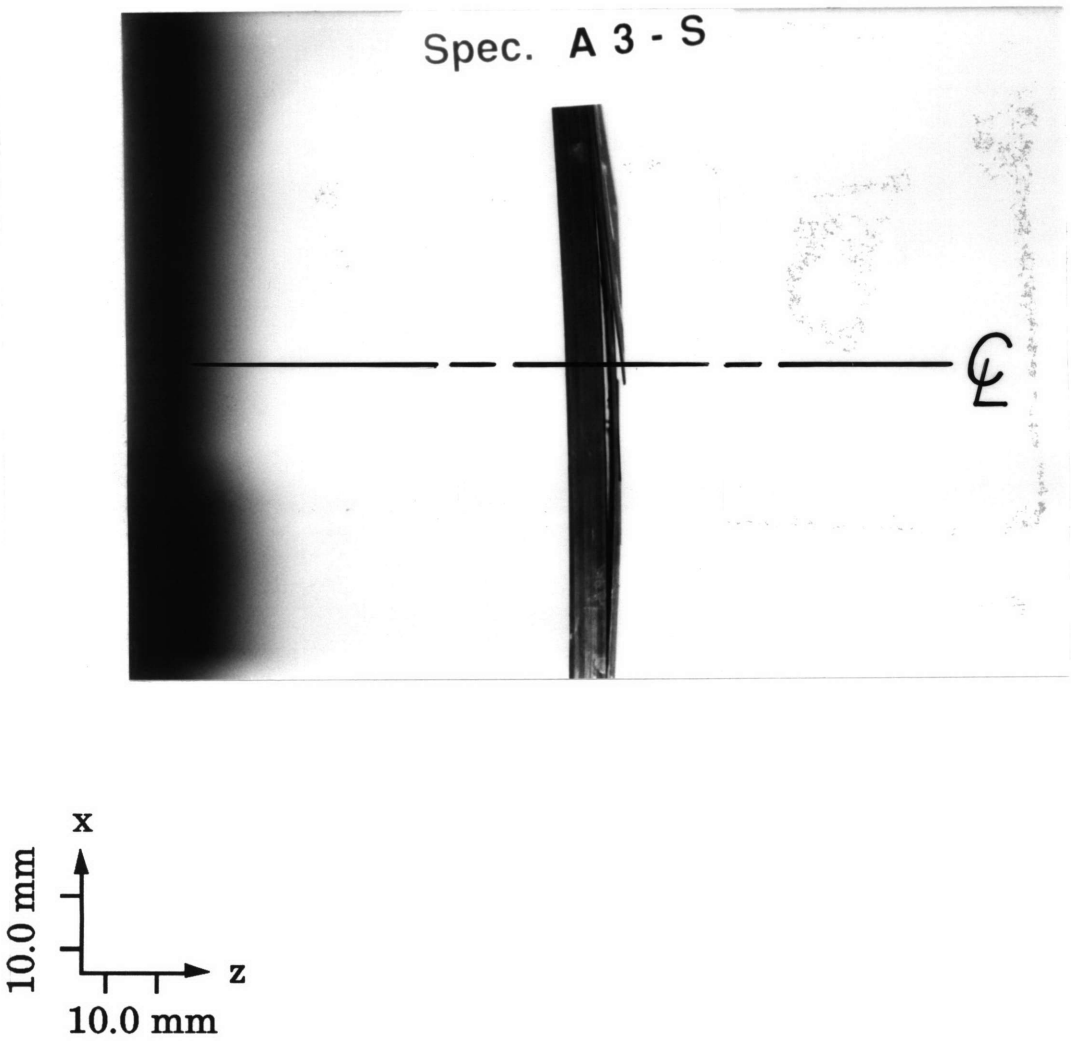

Figure 4.5 Photograph of a typical failed $[45_4/-45_4/(0/90)_4]_{2s}$ specimen statically tested with initial damage biased toward the tension side.

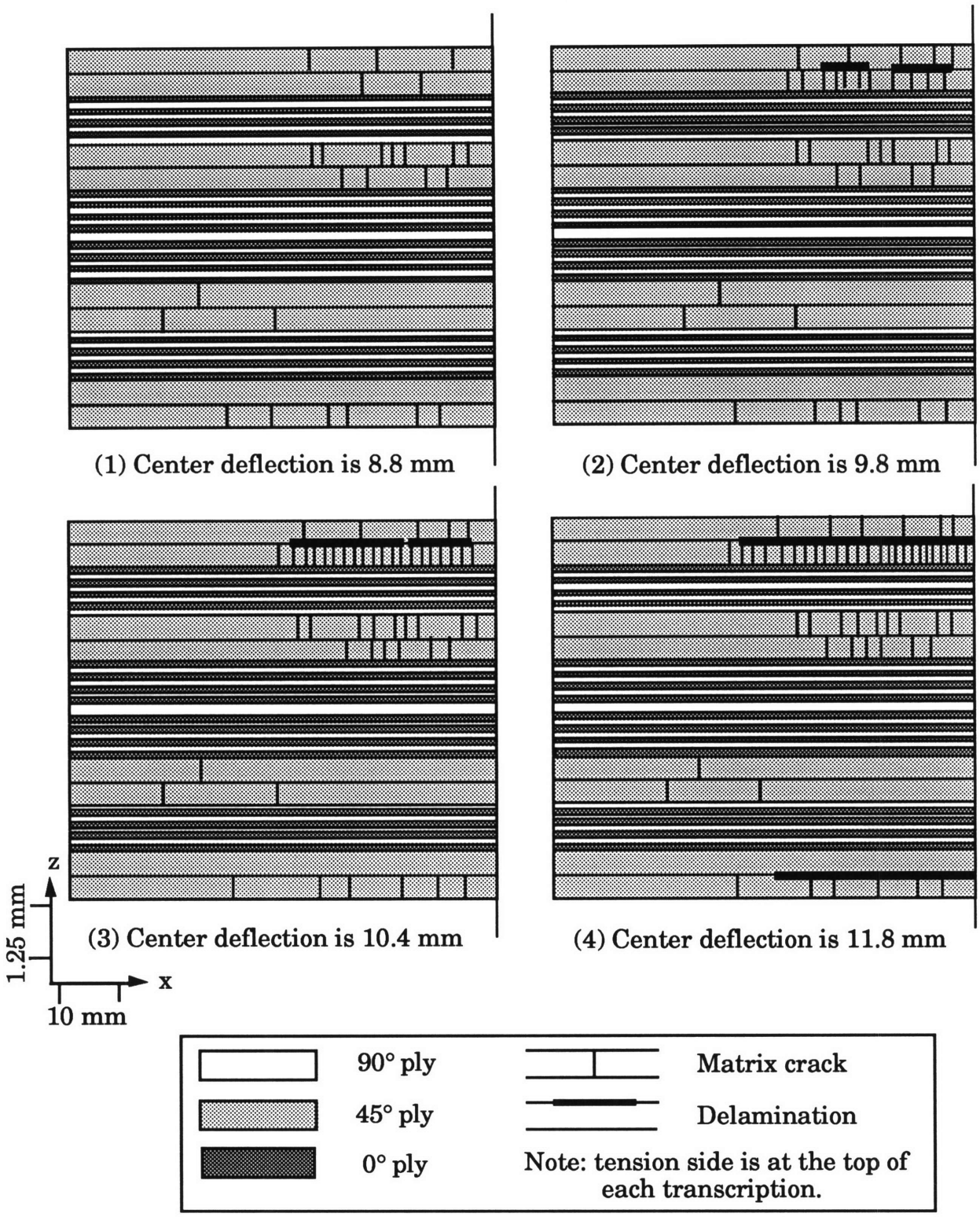

Figure 4.6 Damage history of a typical $[45_4/\text{-}45_4/(0/90)_4]_{2s}$ specimen statically tested with initial damage biased toward the compression side.

the form of delaminations linking the existing cracks, growing rapidly after the third damage state. The damage on the inner 45° and -45° plies did not significantly grow. Failure occurred with both tension and compression side delaminations with the center intact as shown in the photograph in Figure 4.7.

The maximum load as well as the buckling load and center deflection at each characteristic damage state for the specimens tested are shown in Table 4.2. The maximum loads reached at failure are 70 to 80% of the Southwell buckling loads of the specimens prior to damage due to loading. The load versus center deflection results of these tests show that prior to final failure, the damage did not have a significant effect on the flexural stiffness of the specimens. The Southwell buckling load is not reduced by more than 10% at the fourth characteristic damage state although there is a steady, discernable decrease. The specimens with the damage biased toward the compression side had a lower maximum center deflection due to the growth of the compression side delaminations causing failure. The results for the specimens with the initial damage biased toward the tension side are consistent with previous results [38].

4.1.2 Cyclic Behavior

Seven specimens were cyclically tested to failure. All of the specimens were statically loaded up to the first characteristic damage state and then cyclically loaded using the maximum load reached statically as the maximum cyclic load. Three specimens were tested with the initial damage on the untested specimens on the tension side. The other four specimens were orientated with the initial damage on the compression side. The initial damage state, buckling load before load induced damage,

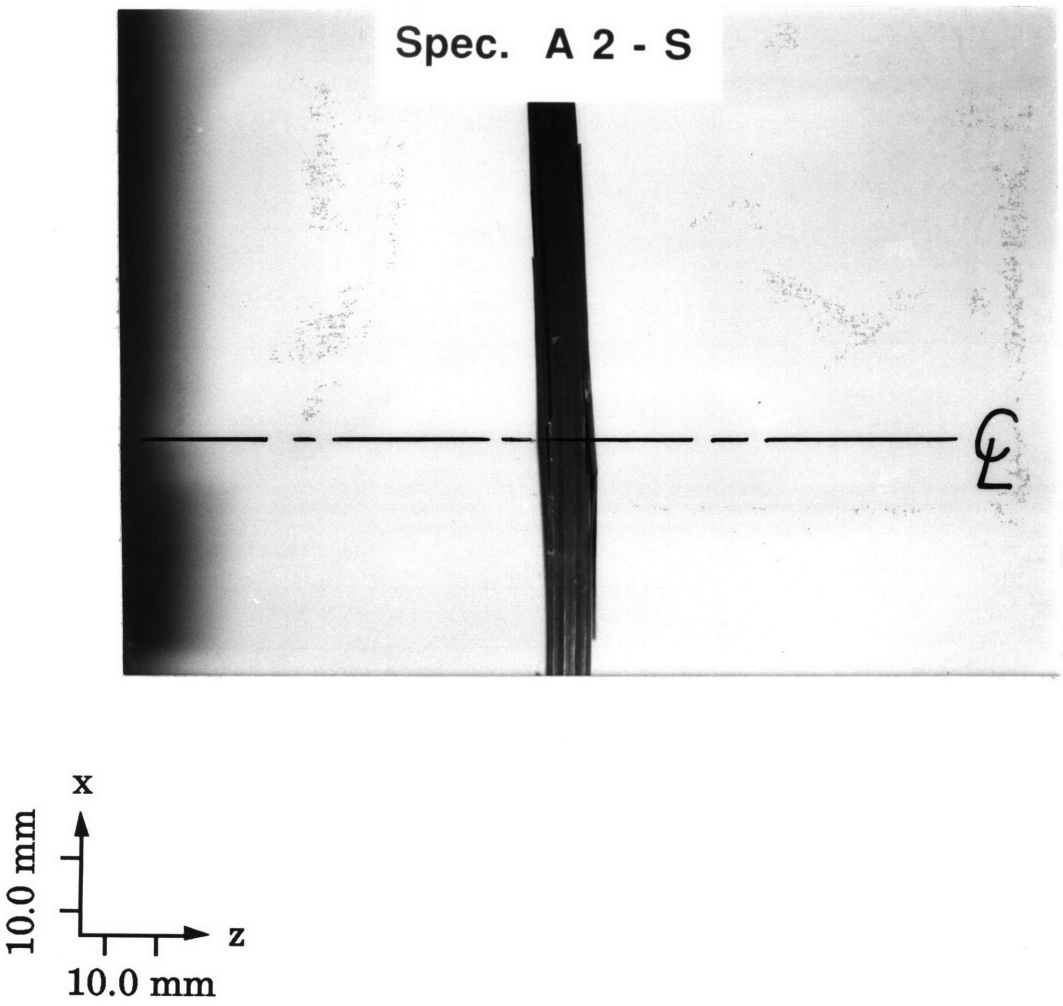

Figure 4.7 Photograph of a typical failed $[45_4/-45_4/(0/90)_4]_{2s}$ specimen statically tested with initial damage biased toward the compression side.

Table 4.2 Buckling load and center deflection at each characteristic damage state and maximum load for the $[45_4/-45_4/(0/90)_4]_{2s}$ specimens statically tested.

Specimen	Characteristic Damage State	Southwell Buckling Load (N)	Center Deflection (mm)	Maximum Load (N)
1[a]	0[c]	18,143	8.4	—
	1	18,094	9.6	—
	2	18,010	10.5	—
	3	17,965	12.6	—
	4	17,694	14.7	—
	failure	—	—	13,833
2[a]	0[c]	17,636	6.1	—
	1	16,798	9.0	—
	2	16,778	10.5	—
	3	16,655	11.1	—
	4	15,783	12.0	—
	failure	—	—	11,974
3[b]	0[c]	19,126	6.7	—
	1	17,436	8.8	—
	2	17,249	9.8	—
	3	17,129	10.4	—
	4	17,085	11.8	—
	failure	—	—	13,211
4[b]	0[c]	19,054	6.3	—
	1	17,781	8.9	—
	2	17,987	9.5	—
	3	17,765	10.6	—
	4	17,621	11.0	—
	failure	—	—	13,495

[a] Original damage biased toward tension side.
[b] Original damage biased toward compression side.
[c] Indicates only original damage present.

maximum loads, and the number of cycles to failure for each specimen are shown in Table 4.3. As with the specimens tested statically, the damage histories for the fatigue specimens were dependent on the orientation of the initial damage.

The damage history for the specimens orientated with the initial damage on the tension side before any loading was applied is illustrated in Figure 4.8. Four damage states are shown with the first being the damage state of the specimen after statically inducing damage but before any cyclic loading was done. Regardless of the number of cycles to failure for specimens with a particular loading history, a pattern of damage accumulation was noticed with respect to the fraction of the number of cycles completed to failure. The second cyclic damage state occurred approximately halfway to failure. At this second state, the damage on the tension side progressed similarly to that of the static tests. The short discontinuous delaminations grew into each other with the cracks becoming more dense. This second cyclic damage state was also characterized by the initiation of damage on the compression side. This compression side damage, which did not occur under static loading, consisted of a delamination on the outermost 45°/-45° interface with one or more matrix cracks. The delamination on the compression side did not terminate at matrix cracks as they did on the tension side. The third cyclic damage state was characterized by the further growth of the tension side damage. The matrix crack density neared saturation in the central 70 mm portion of the specimen and dropped to between 25 and 50% saturation 20 mm to either side of this region. The tension side delaminations became continuous. The compression side damage grew mostly in the form of a large continuous delamination. This damage state generally occurred

Table 4.3 Initial damage state, buckling load, maximum loads, and the number of cycles to failure for each $[45_4/-45_4/(0/90)_4]_{2s}$ specimen tested cyclically.

Specimen	Initial Damage State	Southwell Buckling Load (N)	Maximum Static Load (N)	Maximum Cyclic Load (N)	Number of Cycles to Failure
1[a]	1	18,120	12,899	12,899	8330
2[a]	1	15,745	12,188	12,188	1920
3[a]	1	16,971	12,099	12,099	13,200
4[b]	1	16,400	11,520	11,520	7150
5[b]	1	18,646	13,211	13,211	35,370
6[b]	1	18,975	14,990	14,990	20
7[b]	1	18,327	12,810	12,810	31,080

[a] Specimens orientated with the original cracks biased toward tension side.
[b] Specimens orientated with the original cracks biased toward compression side.

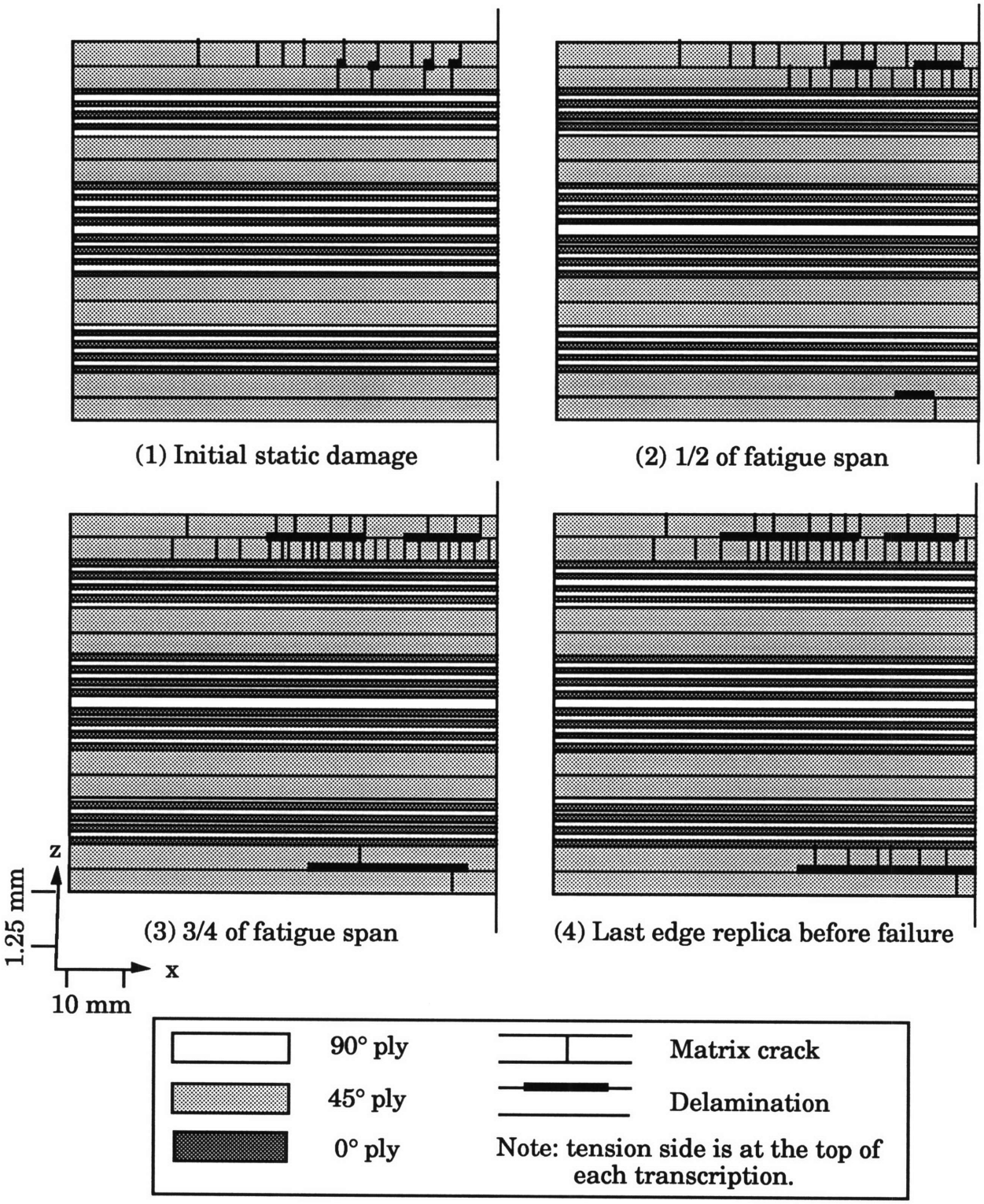

Figure 4.8 Damage history for a typical cyclic $[45_4/-45_4/(0/90)_4]_{2s}$ specimen with the initial damage biased toward the tension side.

three-quarters of the way to failure. The fourth cyclic damage state corresponded to the edge replica just prior to failure. The tension side damage did not progress much further from the last state except for slight growth of the delaminations but the compression side damage progressed significantly. The crack density increased and the central 60 mm of the outermost compression side 45° ply became separated from the laminate.

Thus, the first half of the test was dominated by the growth of tension side damage with the growth of compression side damage dominating the latter half. The failure of these specimens was predictable with the compression side damage becoming easily visible to the naked eye late in the test. Failure occurred on both the tension and compression sides with both damage modes contributing to the failure. A photograph of a failed specimen is shown in Figure 4.9. There were 0° ply failures on the tension side with delaminations and angle ply splits on the tension and compression sides.

The damage history for a typical specimen orientated with the initial damage on the compression side is shown in Figure 4.10. The first damage state, after the static tests but before any cyclic loading, consisted of the compression side cracks that were present before any load was applied. On the tension side there was some matrix cracking in the outermost 45° and -45° plies. Most of the tension side matrix cracking resulting from the applied load was in the second group of 45° plies. Damage in these plies was not seen with the specimens having the initial damage biased toward the tensions side. Halfway to failure for the second cyclic damage state, the tension side damage did not progress significantly but discontinuous delaminations appeared on the compression side linking the matrix cracks. The crack density on the tension side increased on the second

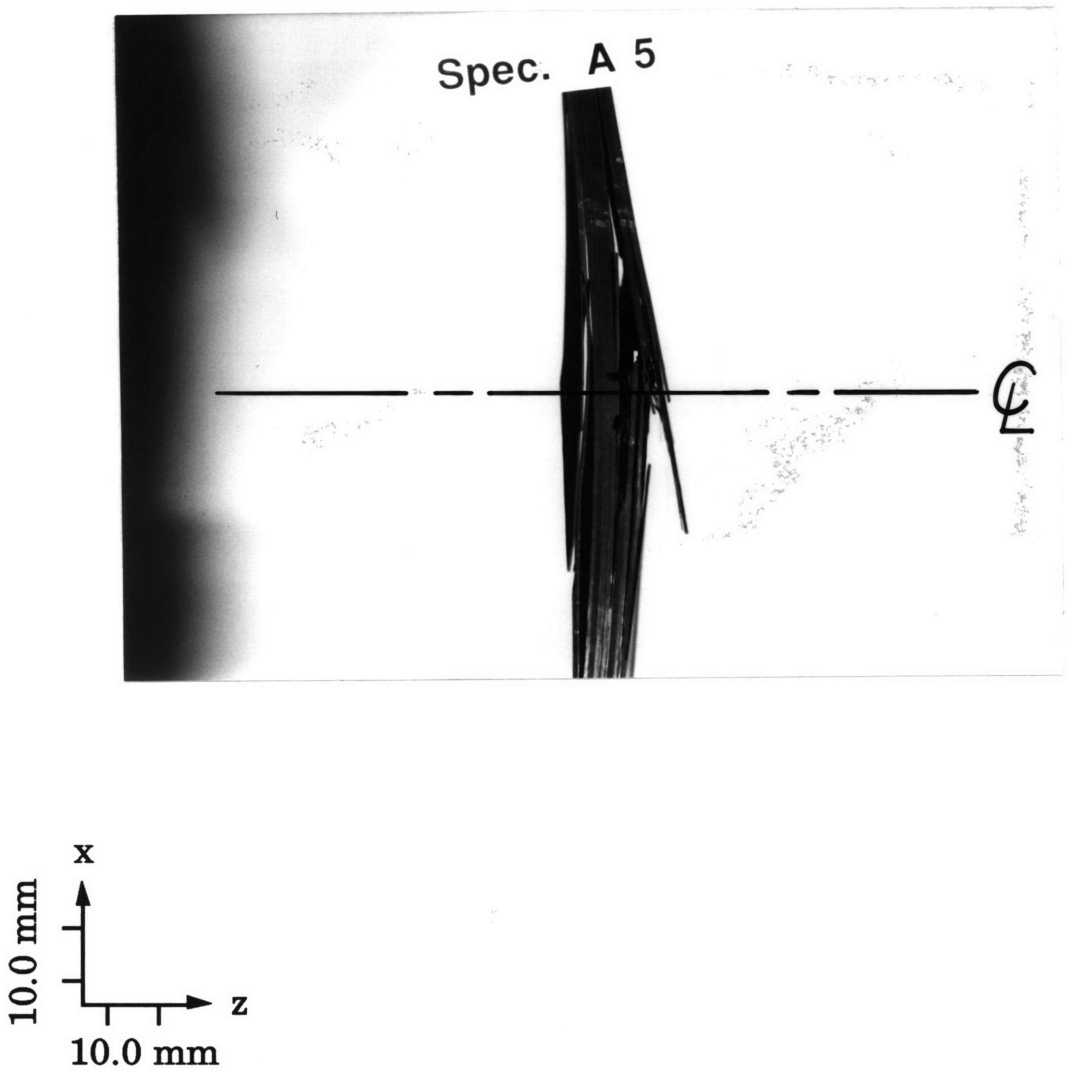

Figure 4.9 Photograph of a typical failed $[45_4/-45_4/(0/90)_4]_{2s}$ specimen tested cyclically with the initial damage biased toward the tension side.

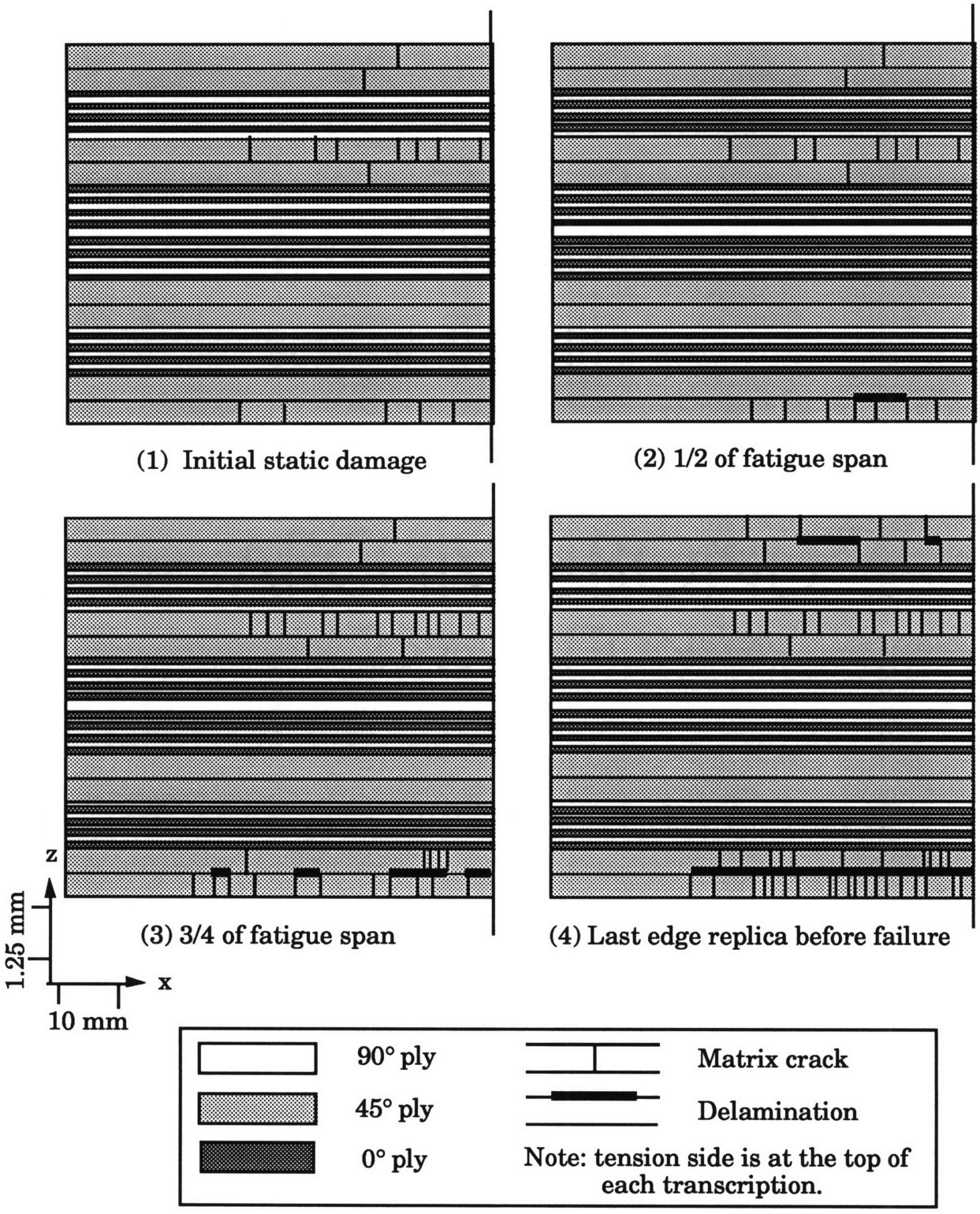

Figure 4.10 Damage history for a typical cyclic $[45_4/-45_4/(0/90)_4]_{2s}$ specimen with the initial damage biased toward the compression side.

outermost 45° ply by the third cyclic damage state. On the compression side, more cracks appeared along with more discontinuous delaminations. The last cyclic damage state before failure was characterized by a growth in cracks and the initiation of delaminations in the outermost tension 45° and -45° plies. On the compression side, the crack density reached saturation in the central 50 mm of the specimen, dropping to between 50 and 75% saturation 20 mm to either side of this region. The average crack spacing at saturation is 1.75 mm. The delaminations became continuous, spreading across approximately 80 mm of the central portion of the outermost compression side 45° ply. Failure of these specimens occurred abruptly with both tension and compression sides failing. A photograph of a failed specimen is shown in Figure 4.11. Again, there was 0° ply failure on the tension side with delaminations and angle ply splits on both sides. The failure of these specimens was similar to that of the specimens with the initial damage biased toward the tension side although there was no easily visible warning that failure was going to occur as in the other specimens. With the initial damage present on the compression side, damage in these plies grew closer to the specimen ends throughout the cyclic testing, but the failure mode was unchanged from that of the previous orientation.

During each static test sequence when edge replicas were taken, load versus center deflection data was taken to obtain a measure of the flexural stiffness of the specimen as a result of the cyclic loading. In Figure 4.12, a plot of the Southwell buckling loads versus the number of cycles for five of the specimens tested is shown. Two of the specimens failed before adequate data could be taken. The data is presented in tabular form in Appendix A. The buckling loads are normalized with respect to the buckling load of the specimen after static testing but before any cyclic loading. The abscissa is

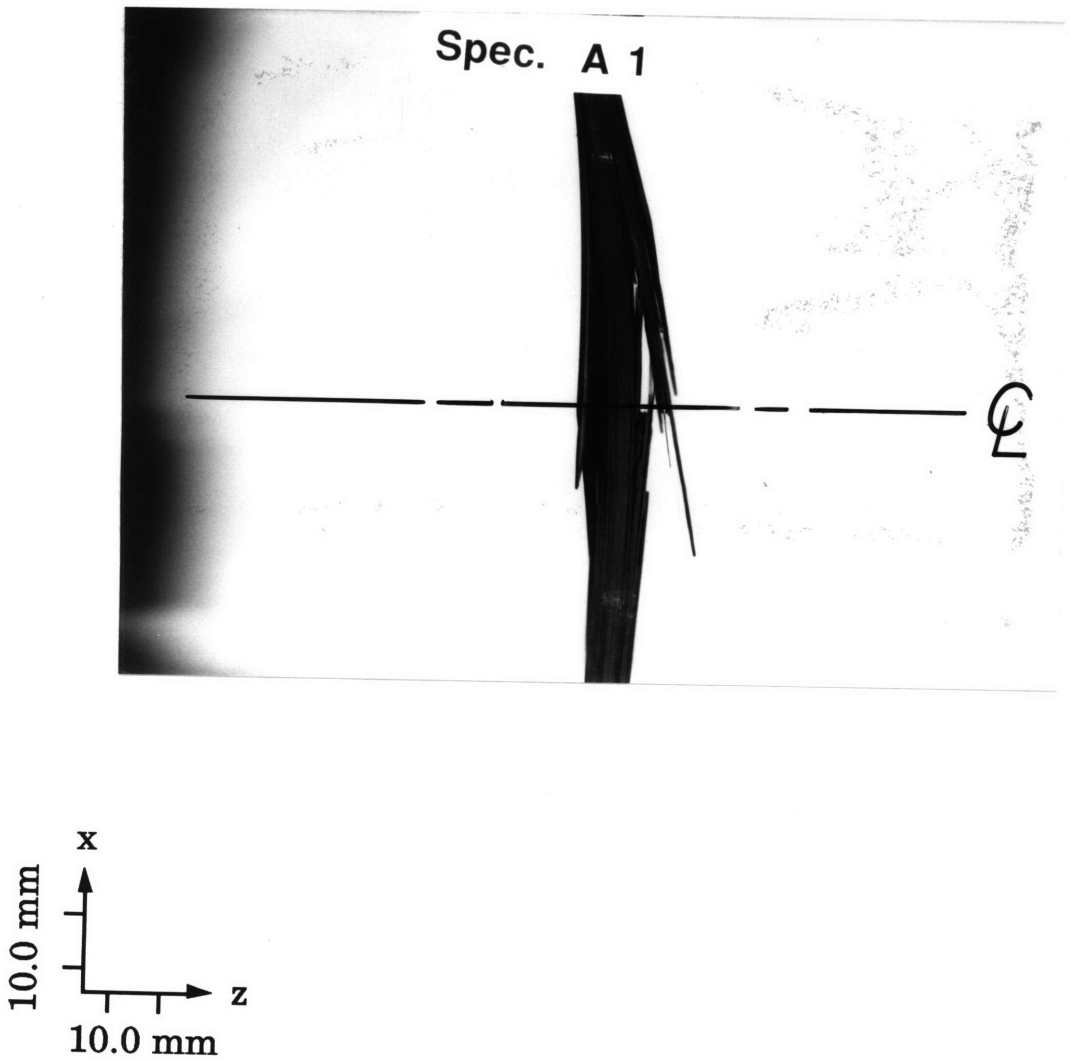

Figure 4.11 Photograph of a typical failed cyclic $[45_4/-45_4/(0/90)_4]_{2s}$ specimen with the initial damage biased toward the compression side.

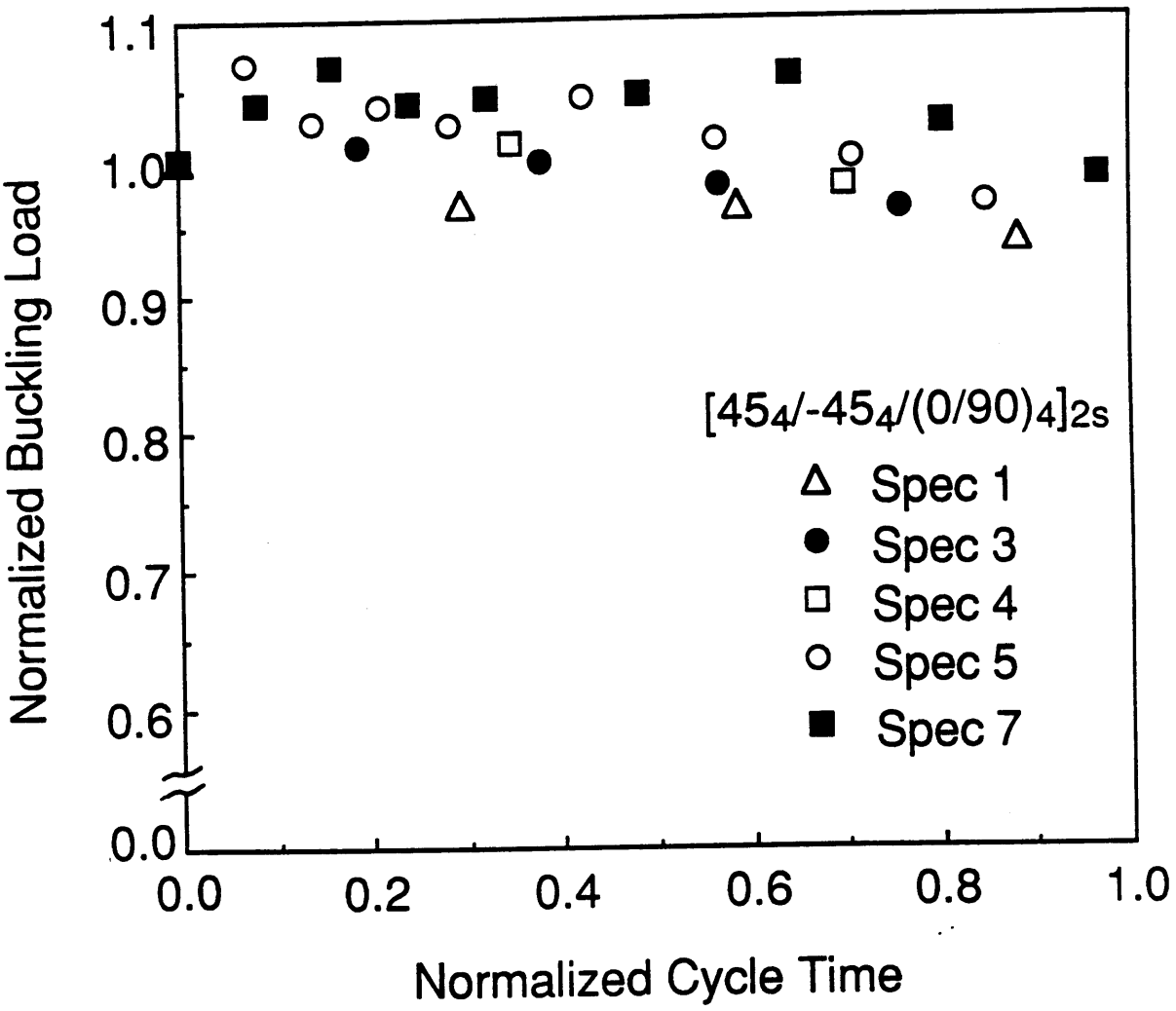

Figure 4.12 Normalized Southwell buckling loads versus normalized cycle time for $[45_4/-45_4/(0/90)_4]_{2s}$ specimens.

normalized with respect to the maximum number of cycles each specimen reached. Stiffness did not degrade significantly until just prior to failure. Any stiffness degradation just prior to failure could not be captured since stiffness was only measured during the static test sequences, the last of which was usually several thousand cycles before failure. This was approximately 5 to 30% of the total cycle time depending on the number of cycles to failure of a particular specimen. The data reveals a slight increase in stiffness at first with a slight decline throughout most of the cyclic loading. This behavior is similar to what is reported in the literature for laminates containing ±45° and 90° plies under non-gradient and gradient stress fields [33,34].

4.2 $[\pm 45/0/(90)_4]_{4s}$ Laminates

4.2.1 Static Behavior

Two specimens were tested to failure under static conditions. The four characteristic damage states for these specimens are outlined in Table 4.4 and illustrated in Figure 4.13. Damage in the form of matrix cracks initiated in the locations expected: at the center of the specimen in the outermost 90° ply on the tension side. Scattered cracking makes up the first damage state. The second damage state is characterized by a crack density of approximately 50% saturation over the central 50 mm of the specimen on the outermost 90° ply with short discontinuous delaminations forming at the 0°/90° interface. A crack density of approximately 25% saturation is present 15 mm to either side of this region. Some scattered cracking was found on the second outermost 90° ply. A crack density at about 75% saturation over the central 60 mm of the specimen was reached on the first

Table 4.4 Description of the four characteristic damage states of the $[\pm 45/0/(90)_4]_{4s}$ laminate.

Characteristic Damage State	Description
1	Scattered cracking in the outermost 90° effective ply.
2	Crack density at 50% saturation over the central 50 mm of the outermost 90° effective ply with cracks linking short discontinuous delaminations at the 0°/90° interface.
3	Crack density at 75% saturation over the central 60 mm of the outermost 90° effective ply. Delaminations grow together.
4	Crack saturation in central 80 mm of the outermost 90° effective ply with an average crack spacing of 0.83 mm. Continuous delamination separating central 80 mm portion of specimen.

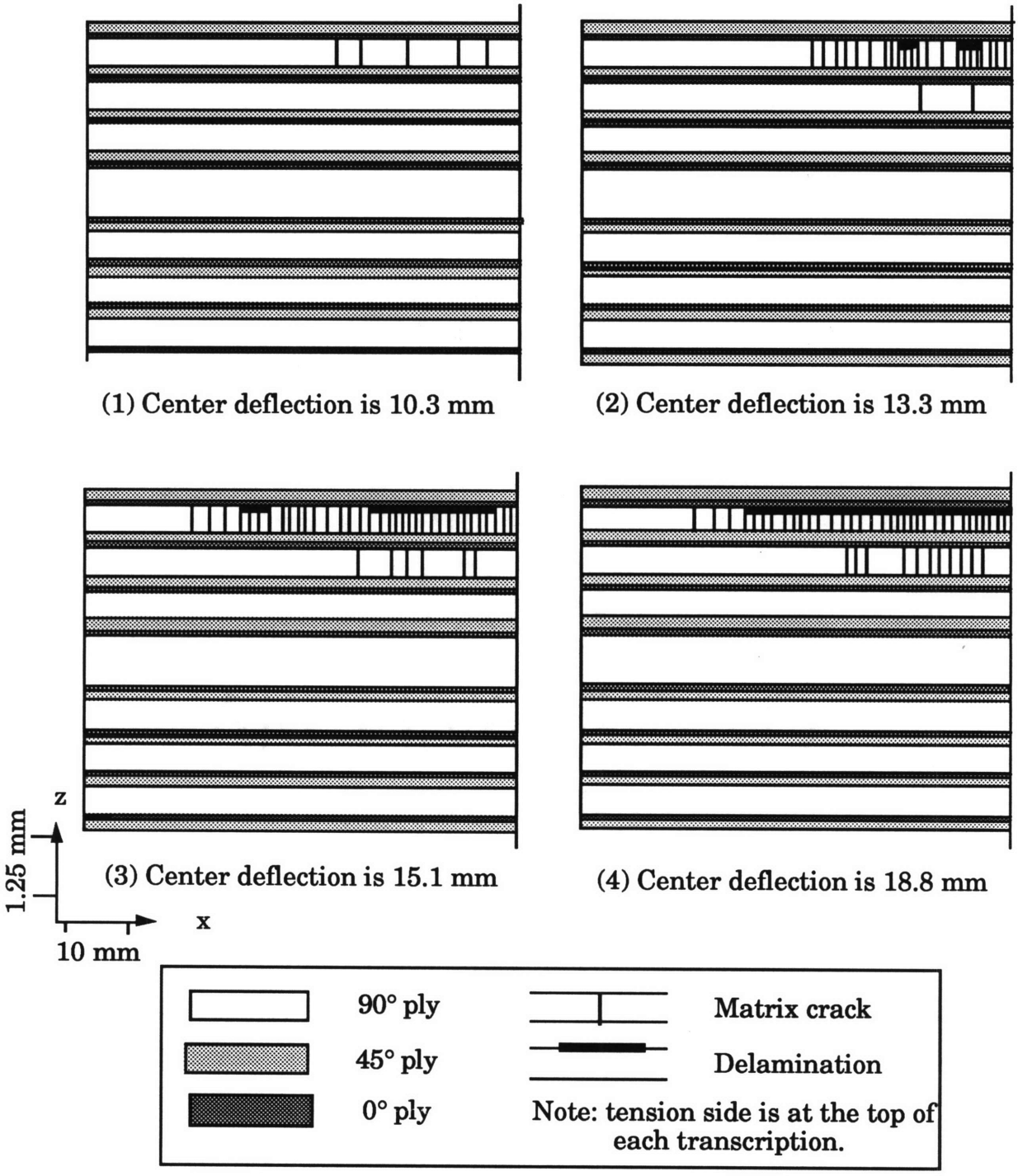

Figure 4.13 Damage history of a typical $[\pm 45/0/(90)_4]_{4s}$ specimen statically tested.

outermost 90° ply by the third damage state. A crack density between 50 and 75% was present on approximately 15 mm either side of this region. The delaminations began to grow into each other with more of them forming. The fourth damage state was characterized by crack saturation in the central 80 mm portion of the outermost tension side 90° ply with crack density dropping to approximately 50% saturation 10 mm to either side of this region. The average crack spacing at saturation is 0.83 mm. A continuous delamination separated the central 80 mm portion of the specimen at the outermost tension side 0°/90° interface. Increased cracking in the second 90° ply occurred, but no delaminations formed there.

At failure, sublaminate buckling occurred on the compression side along the outermost 0°/90° interface with the tension side of the specimen remaining intact. A photograph of a failed specimen is shown in Figure 4.14. Although the damage history is similar to that reported previously [38], the failure mode is different with no 0° ply failure on the tension side occurring. The center deflection at failure is approximately 15% higher than in the previous work. It is believed that these specimens represent a borderline situation where a slight change in specimen thickness or material properties can influence the failure. This discrepancy in failure mode would not interfere with the objective of statically inducing damage and obtaining a damage history to failure due to cyclic loading since the stress level required to statically fail the specimen would never be reached.

The load versus center deflection data, Southwell buckling loads, and maximum load of both specimens were similar to the previous experiments [38]. The maximum loads reached were approximately 75 to 80% of the Southwell buckling loads. The flexural stiffness of the specimens did not degrade more than 8% at the fourth characteristic damage state compared

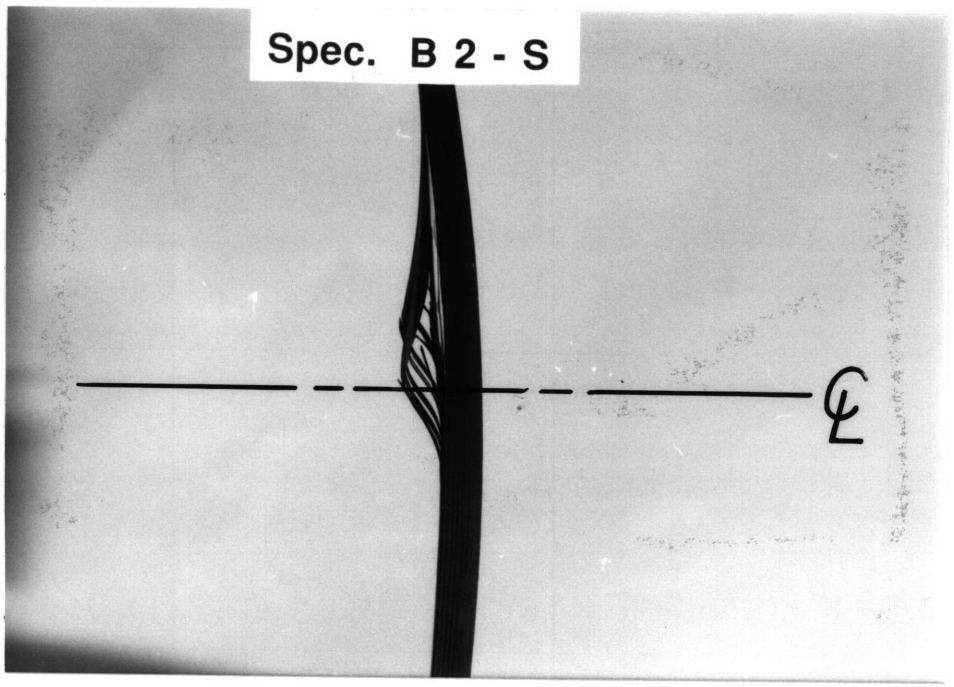

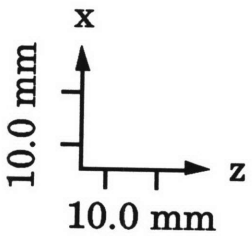

Figure 4.14 Photograph of a typical failed $[\pm 45/0/(90)_4]_{4s}$ specimen statically tested.

to the undamaged specimen although there was a steady decrease. The maximum load as well as the buckling load and center deflection at each characteristic damage state for both specimens tested are shown in Table 4.5.

4.2.2 Cyclic Behavior

A total of ten specimens were cyclically tested to failure. Four of the specimens were statically damaged to the first characteristic damage state and then loaded cyclically using the maximum load reached statically as the maximum cyclic load. The other six specimens were statically damaged to the third damage state and loaded cyclically using the maximum load reached statically as the maximum cyclic load. The latter six specimens can be further distinguished from each other by the relative severity of the damage state at the end of the static portion of the test. For three of the specimens statically damaged to the third damage state, the damage was slightly more severe than the other three. During the static portion of the test for these specimens, the third characteristic damage state was overshot with the delaminations on the tension side 0°/90° interface becoming nearly continuous. The damage histories of the six specimens were similar but the failure mode and number of cycles to failure were different depending on the severity of the initial damage. The initial damage state, Southwell buckling load before damage, maximum loads, and the number of cycles to failure for each specimen are presented in Table 4.6.

For the specimens statically damaged to the first damage state, the corresponding damage history is shown in Figure 4.15. The first damage state is the state of the specimen at the end of static loading before cyclic

Table 4.5 Buckling load and center deflection at each characteristic damage state and maximum load for the $[\pm 45/0/(90)_4]_{4s}$ specimens statically tested

Specimen	Characteristic Damage State	Southwell Buckling Load (N)	Center Deflection (mm)	Maximum Load (N)
1	undamaged	8856	9.8	—
	1	8816	10.3	—
	2	8700	13.3	—
	3	8669	15.1	—
	4	8380	18.8	—
	failure	—	—	7117
2	undamaged	8312	8.0	—
	1	7848	11.0	—
	2	7834	13.2	—
	3	7831	15.4	—
	4	7656	19.2	—
	failure	—	—	6169

Table 4.6 Initial damage state, buckling load, maximum loads, and the number of cycles to failure for each $[\pm 45/0/(90)_4]_{4s}$ specimen tested cyclically.

Specimen	Initial Damage State	Southwell Buckling Load (N)	Maximum Static Load (N)	Maximum Cyclic Load (N)	Number of Cycles to Failure
1	1	9287	7250	7250	62,540
2	1	8771	6494	6494	58,380
3	1	8073	6094	6094	47,730
4	1	9910	7784	7784	46,190
5	3	9780	8184	8184	44,430
6	3	9206	7473	7473	52,220
7	3	9234	7384	7384	29,810
8	3+ [a]	10,333	8006	8006	13,940
9	3+ [a]	9986	8006	8006	7760
10	3+ [a]	9158	7784	7784	4200

[a] Initial damage was just beyond the third characteristic damage state.

loading began. Halfway to failure, the second cyclic damage state is defined on the tension side by approximately 50 to 75% crack saturation in the central 60 mm portion of the outermost tension side 90° ply. On the compression side, there was the introduction of damage in the form of delaminations along the outermost 0°/90° and 0°/-45° interfaces. The 0°/90° delaminations did not have matrix cracks as boundaries. Cracking of the outermost 45° and -45° plies on the compression side also occurred. Crack saturation in the central 65 mm portion of the tension side 90° ply was reached at the third cyclic damage state with the crack density dropping to between 50 and 75% saturation 15 mm to either side of this region. The average crack spacing at saturation is 0.83 mm. A continuous delamination separated the central 70 mm of the specimen at the tension side 0°/90° interface. On the compression side, the delaminations were significantly larger, becoming visible to the naked eye. The fourth cyclic damage state is characterized by gross damage on the compression side with the delaminations spreading across most of the length of the specimen but still not terminating at matrix cracks. The tension side damage, having reached saturation in the previous state, did not progress other than moving slightly closer to the specimen ends.

The tension side damage thus dominated the early portions of the test with the initiation and growth of the compression side damage dominating the latter half. The failure of these specimens was predictable with the compression side damage becoming easily visible to the naked eye. The failure of these specimen occurred on both the tension and compression sides. A photograph of a failed specimen is shown in Figure 4.16. The entire tension half of the specimens was destroyed with sublaminate

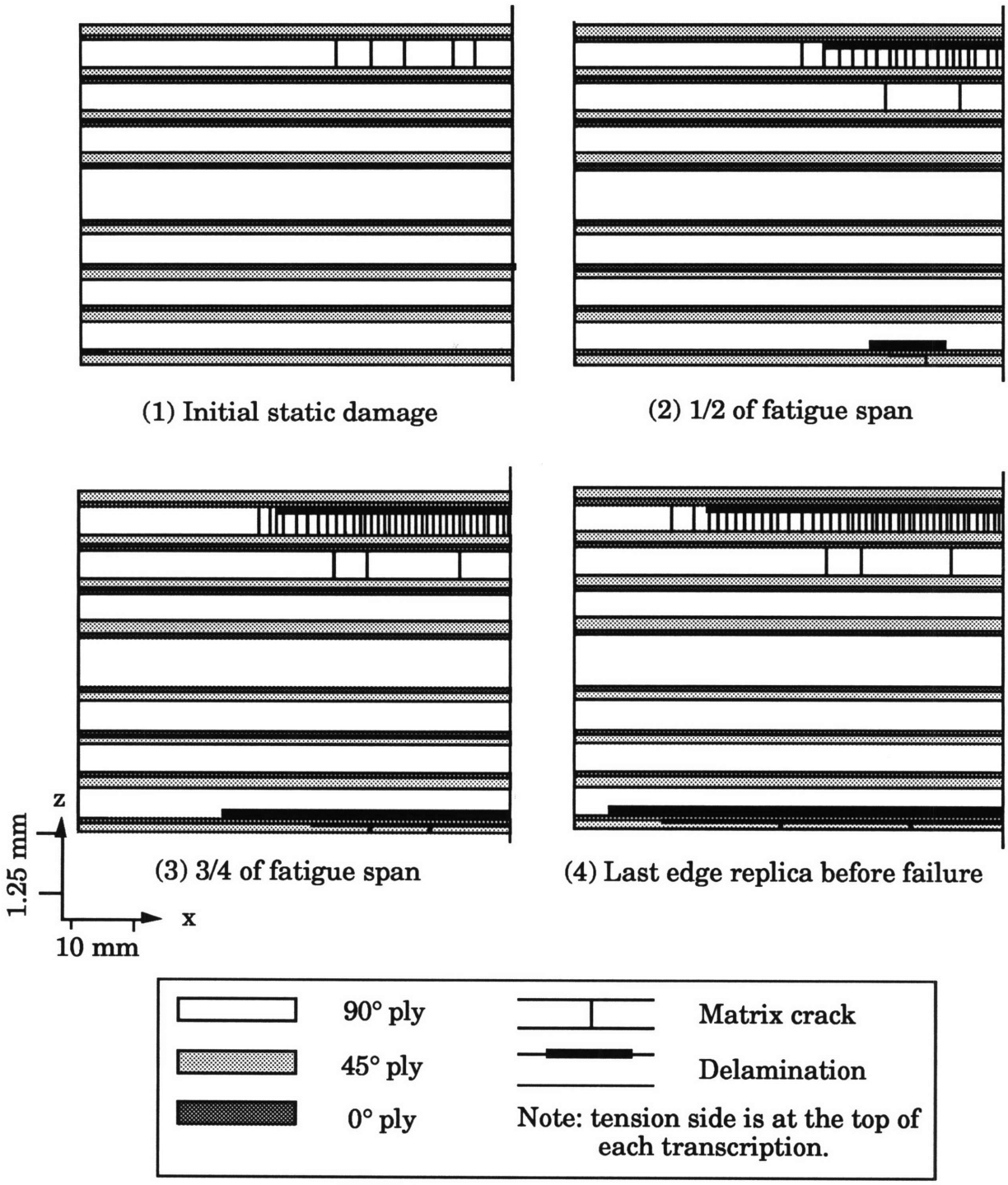

Figure 4.15 Damage history for a typical cyclic $[\pm 45/0/(90)_4]_{4s}$ specimen statically damaged to the first damage state.

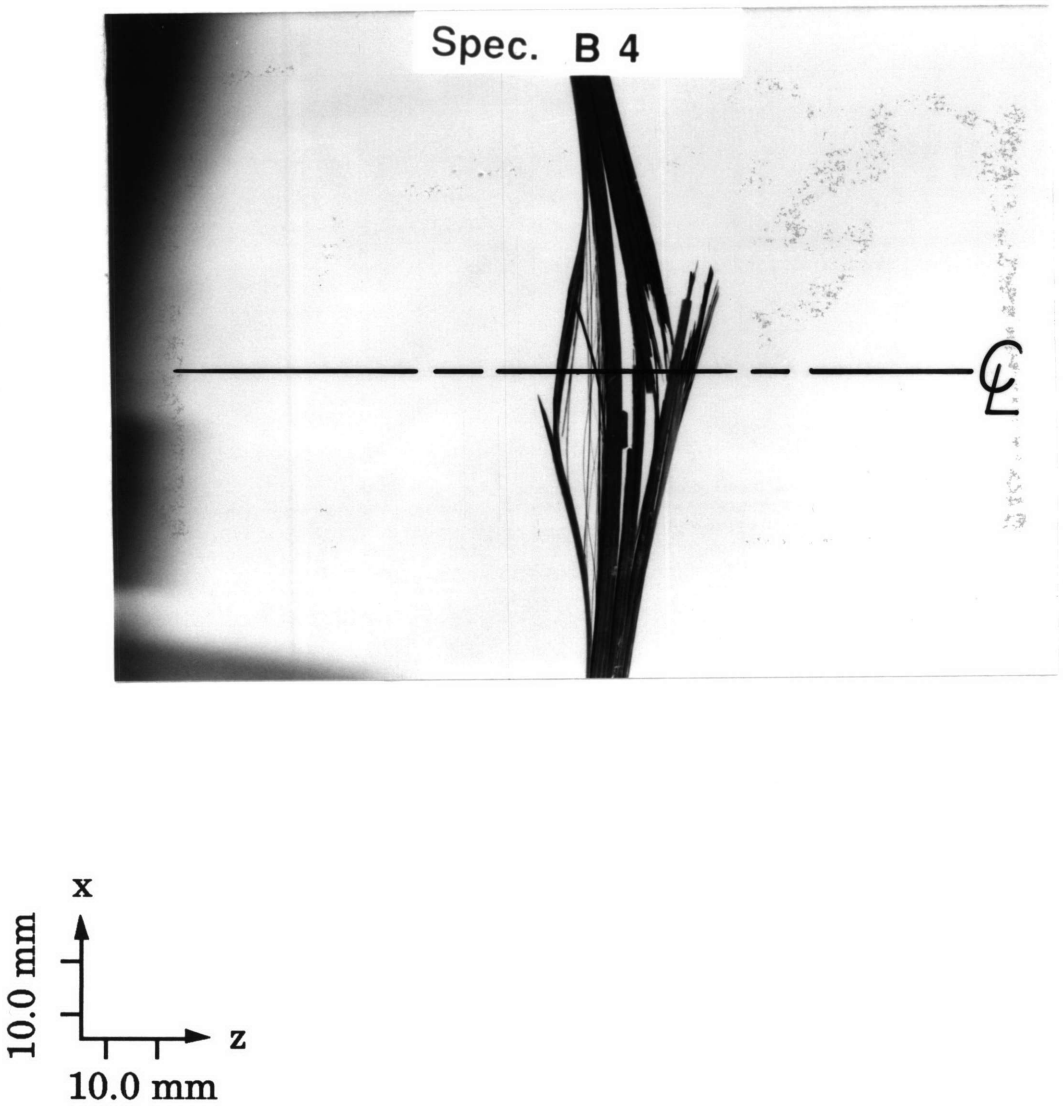

Figure 4.16 Photograph of a typical failed cyclic $[\pm 45/0/(90)_4]_{4s}$ specimen statically damaged to the first damage state.

buckling occurring on the compression side along the outermost 0°/90° interface.

As previously mentioned, the damage histories of the six specimens (specimens 5 to 10) statically damaged up to and just beyond the third damage state are similar after cyclic loading begins. The difference in severity of the initial damage of three of the six (specimens 8 to 10), reflected by a higher cyclic load level, affected the failure modes and number of cycles to failure. The damage histories of these two groups are illustrated in Figures 4.17 and 4.18 and are similar except for the initial damage state and the extent to which the damage grows toward the specimen ends. The first damage state is the damage state at the end of static loading before cyclic loading began. Matrix cracks at approximately 75% saturation along with some discontinuous delaminations were present in the central 60 mm of the outermost tension side 90° ply. For the three specimens with slightly more severe damage (specimens 8 to 10), the delaminations were on the verge of becoming continuous. The growth of these delaminations was consistently closer to the specimens ends throughout the cyclic testing. The second cyclic damage state, halfway to failure, is characterized by matrix cracks nearing saturation level in the central 60 to 70 mm portion of the outermost tension side 90° ply. Crack density dropped to between 50 and 75% saturation 15 mm to either side of this region. A continuous delamination separated the central 60 to 70 mm of the specimen at the 0°/90° interface. At the second cyclic damage state for these specimens though, there is no compression side damage. In fact, compression side damage is not initiated until the third cyclic damage state, three-quarters to failure. At this third cyclic damage state, the tension side damage reached crack saturation in the central 70 to 80 mm of the specimen with crack

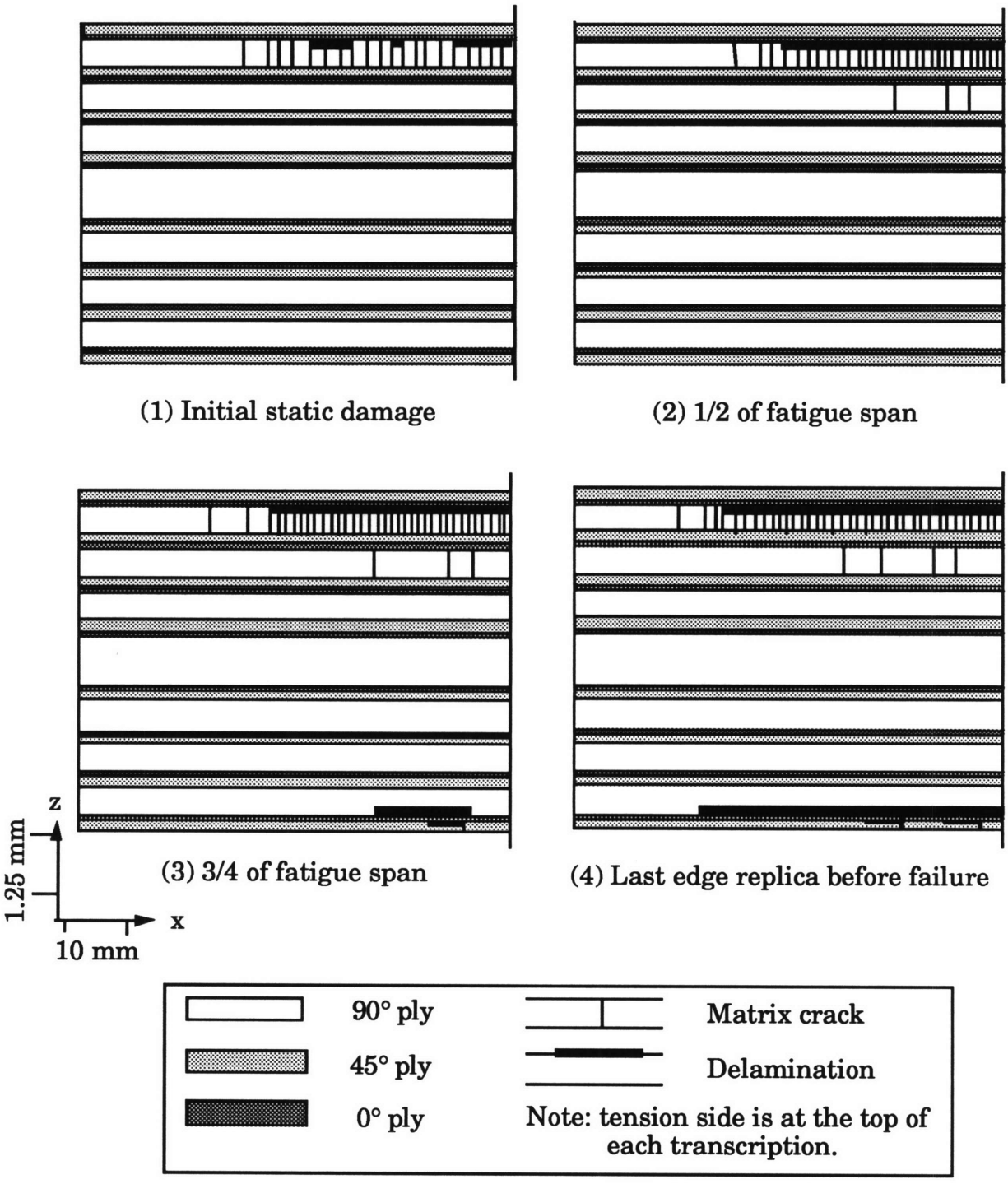

Figure 4.17 Damage history for a typical cyclic $[\pm 45/0/(90)_4]_{4s}$ specimen statically damaged up to the third damage state.

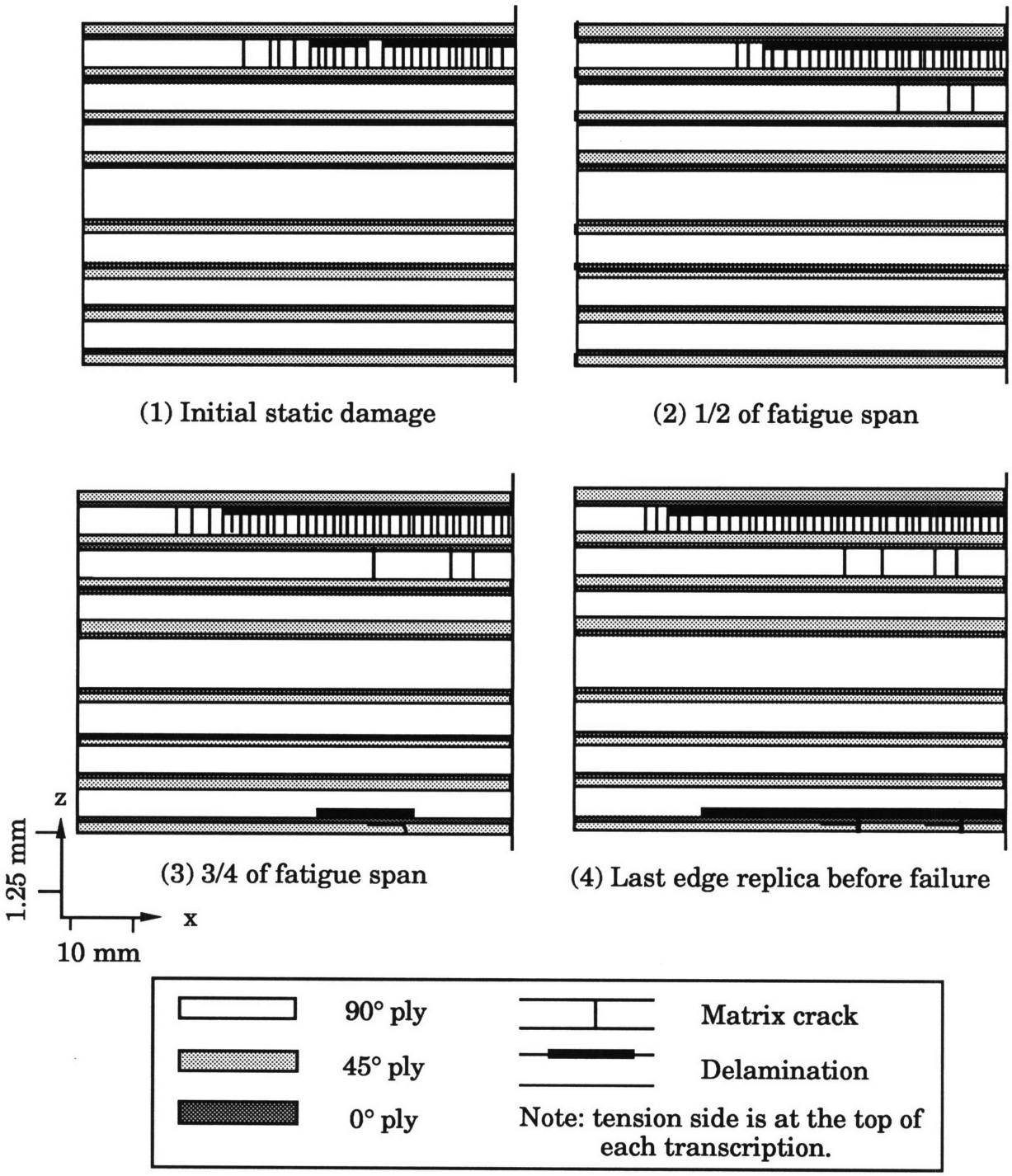

Figure 4.18 Damage history for a typical cyclic $[\pm 45/0/(90)_4]_{4s}$ specimen statically damaged just beyond the third damage state.

density dropping to approximately 50% saturation 10 mm to either side of this region. The average crack spacing at saturation was 0.83 mm. The continuous delamination propagated towards the specimen ends, separating the central 70 to 80 mm of the specimen at the 0°/90° interface. The damage in specimens 8 to 10 was approximately 10 mm closer to the edges than in specimens 5 to 7. The compression side damage initiated much in the same way it did with specimens 1 to 4, in the form of delaminations along the outermost 0°/90° and 0°/-45° interfaces with some matrix cracking in the 45° and -45° plies. The delaminations at the 0°/90° interface were not bounded by matrix cracks. The fourth cyclic damage state was characterized by the accumulation of the compression side damage with the delaminations growing towards the edges. The progression of the compression side damage in all six specimens was not as close to the specimen ends at the fourth cyclic damage state as in specimens 1 to 4 when this damage initiated earlier in the cyclic portion of the test.

For specimens 5 to 7, where the initial damage was less severe, failure occurred on both the tension and compression sides, much in the same way as in specimens 1 to 4, as shown in the photograph in Figure 4.19. The failures were predictable since the gross compression side damage was easily visible to the naked eye just prior to failure. For specimens 8 to 10, with the more severe initial damage, failure occurred on the tension side in the form of delaminations along 0°/90° and 90°/45° interfaces with some 0° ply failure. The midthickness region also exhibited failure with delaminations along 0°/90° interfaces. It appears that the growth of the tension side delaminations closer to the specimen ends became prominent in failure before the compression side damage. The

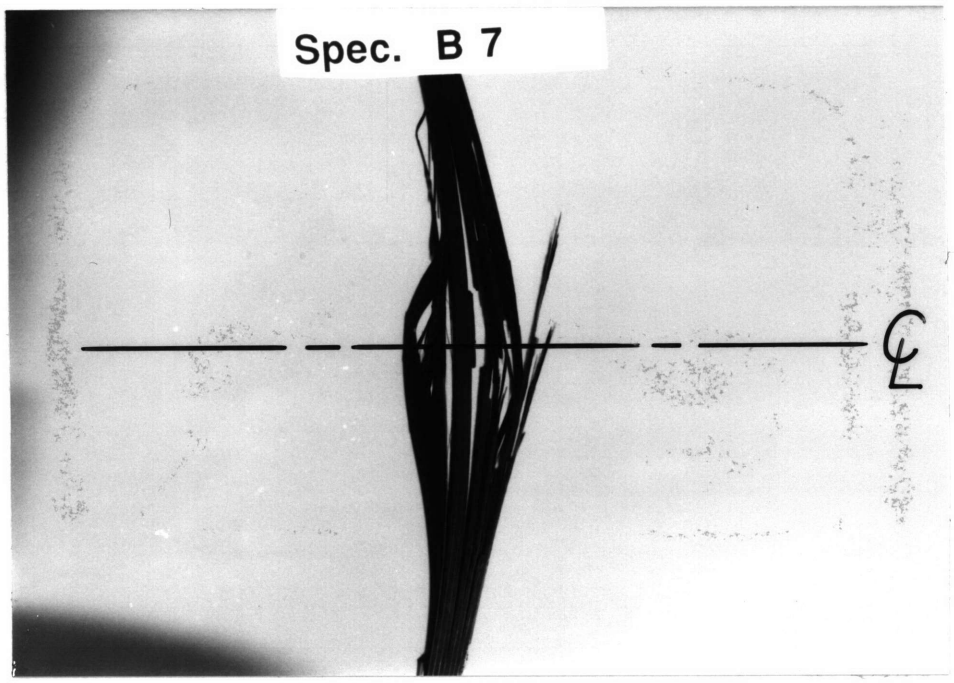

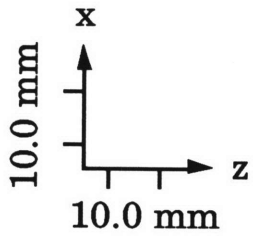

Figure 4.19 Photograph of a typical failed cyclic $[\pm 45/0/(90)_4]_{4s}$ specimen statically damaged up to the third damage state.

failure mode of a typical specimen initially damaged just beyond the third damage state is shown in the photograph in Figure 4.20. It is interesting to note how a small increase in initial damage state before cyclic loading, thus increasing the cyclic load level, can significantly affect the failure mode of a specimen and significantly decrease the number of cycles to failure.

Prior to the compression side damage becoming easily visible to the naked eye on some of the specimens, the stiffness as measured by Southwell buckling loads for all of the specimens of this laminate type did not degrade significantly, although there was a slight decline as shown in Figure 4.21. Several of the specimens exhibited a slight increase in stiffness early in the test before steadily declining. Specimen 10 is not plotted because it failed before sufficient stiffness data could be obtained. The data is presented in tabular form in Appendix A. Stiffness reduction of the specimens was observed just prior to failure by an increase in the stroke necessary to reach the required load levels. This was not captured by the data since there were usually several thousand cycles between the last measurement and ultimate failure making up approximately 5 to 20% of the total cycle time depending on the number of cycles to failure of a particular specimen.

4.3 $[(45_2/-45_2/0)_2/90_5]_{2s}$ Laminates

4.3.1 Static Behavior

For this laminate, two specimens were tested to failure under static loading. First ply failure occurred in the 90° effective ply on the tension side at the middle of the specimen as expected. The four characteristic damage states of this laminate are outlined in Table 4.7 and illustrated in Figure

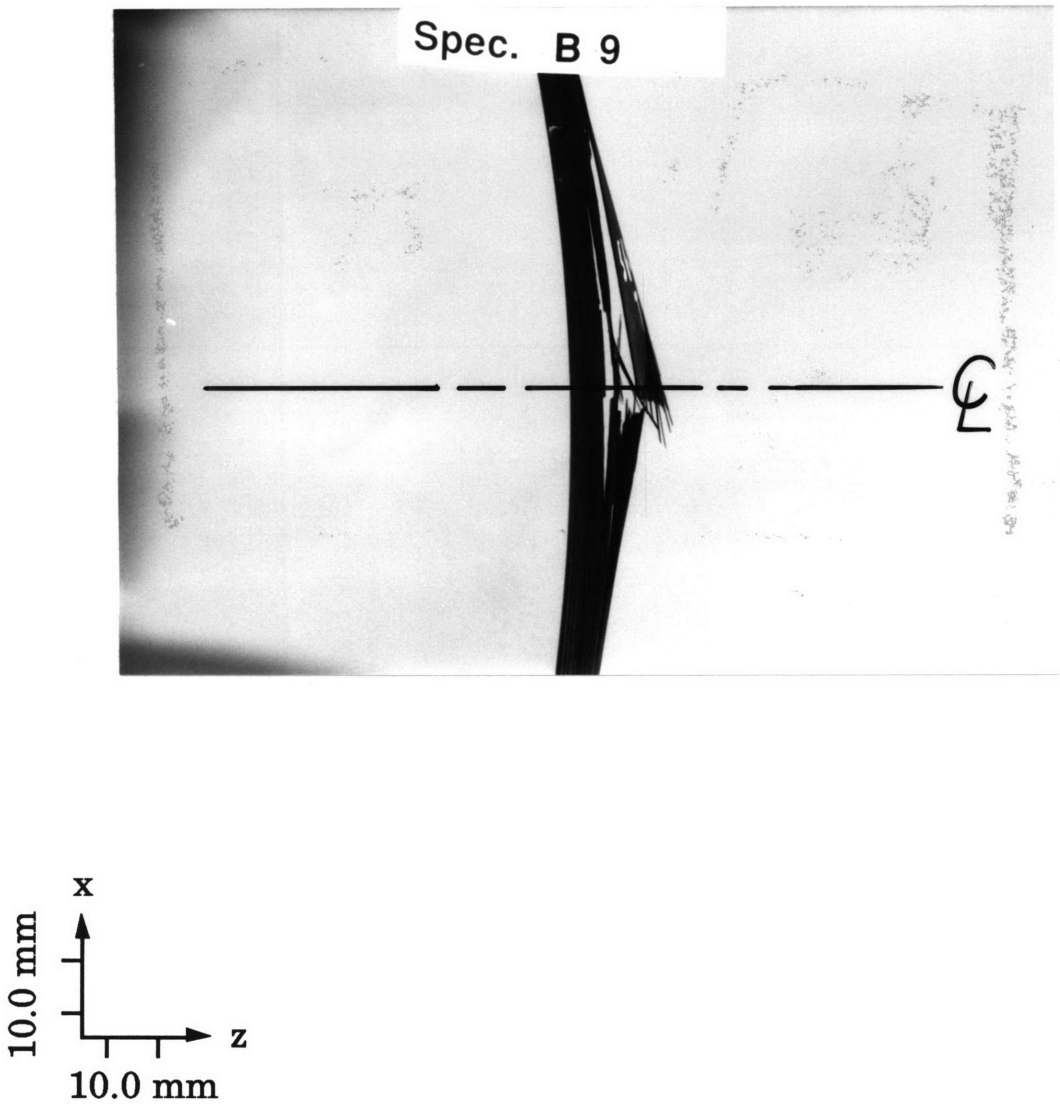

Figure 4.20 Photograph of a typical failed cyclic $[\pm 45/0/(90)_4]_{4s}$ specimen statically damaged just beyond the third damage state.

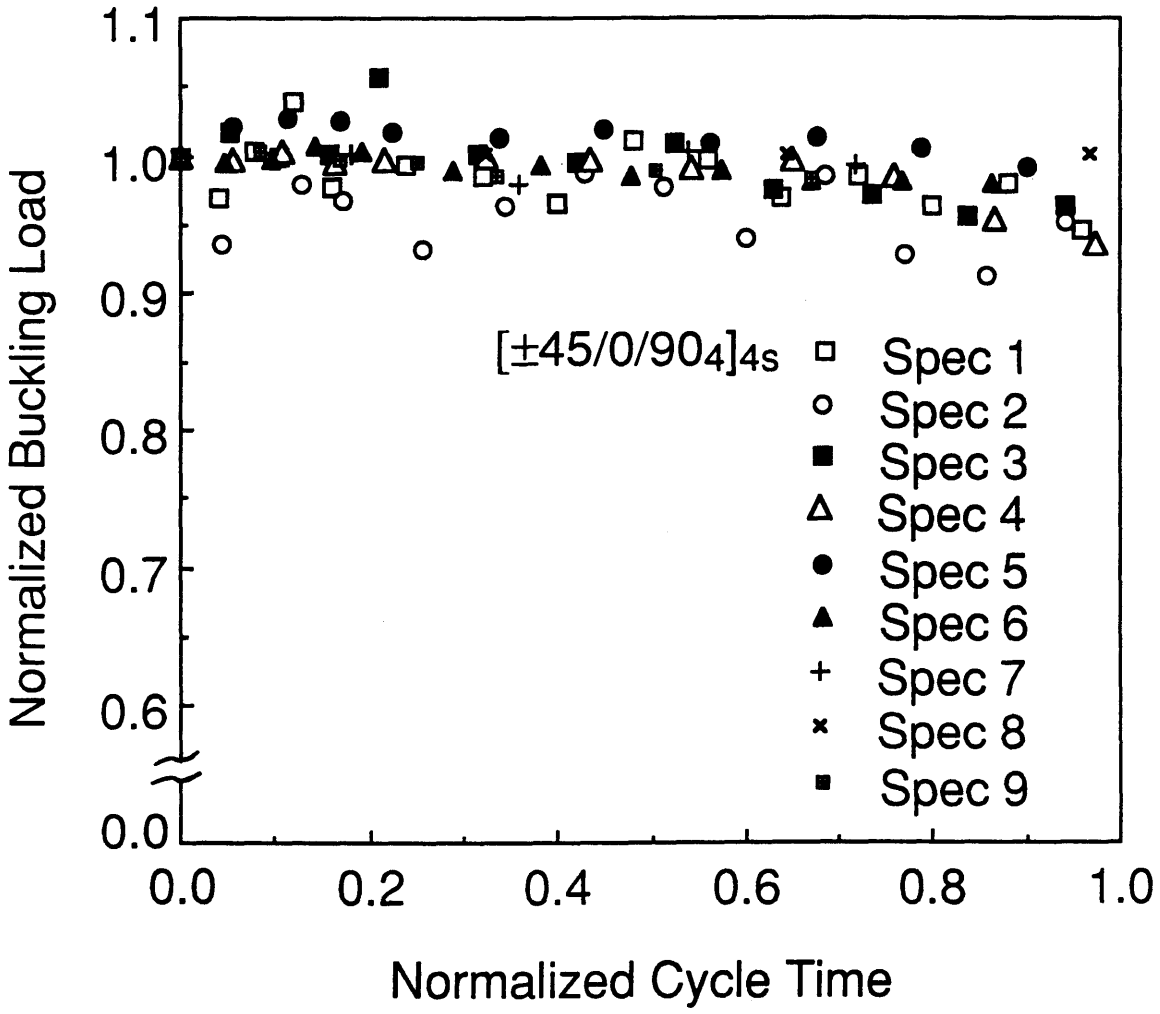

Figure 4.21 Normalized Southwell buckling loads versus normalized cycle time for $[\pm 45/0/(90)_4]_{4s}$ specimens.

4.22. The first characteristic damage state consists of scattered cracks at a density of approximately 25% saturation in the central 50 mm of the specimen. The second damage state is characterized by a crack density between 50 and 75% saturation in the central 60 mm portion, with the higher densities closer to the center of the specimen. Discontinuous delaminations appeared at the outermost tension side 0°/90° interface. The delaminations became continuous in the third damage state with the crack density reaching saturation throughout the central 70 mm portion of the specimen. The crack density was between 50 and 75% saturation 15 mm to either side of this region. The average crack spacing was 1.25 mm at saturation. In the fourth state, discontinuous delaminations appeared between the outermost tension side 90° ply and the neighboring 45° ply. The other damage present progressed closer to the specimen ends. Final failure occurred with a series of delaminations between individual 90° plies along the length of the midthickness 90° effective ply as well as delaminations along the central and tension side 0°/90° interfaces. This midthickness 90° effective ply damage was not present in the edge replica just prior to failure indicating that this damage initiated and quickly grew as the occurrence of matrix cracks in that ply caused catastrophic failure. The damage at failure was restricted to the midthickness 90° ply and the tension side of the specimen as the compression side remained intact. A photograph of a failed specimen is shown in Figure 4.23.

Again, the load versus center deflection data, Southwell buckling loads, and damage history of both specimens was similar to previous results [38]. The maximum loads reached were approximately 75% of the Southwell buckling loads. The flexural stiffness did not degrade more than

Table 4.7 Description of the four characteristic damage states of the $[(45_2/-45_2/0)_2/90_5]_{2s}$ laminate.

Characteristic Damage State	Description
1	Scattered cracking in outermost 90° effective ply.
2	Crack density between 50-75% saturation in central 60 mm portion of specimen. Cracks linking short discontinuous delaminations at 0°/90° interface.
3	Delaminations become continuous with crack density reaching saturation throughout the central 70 mm of the specimen. Crack density between 50-75% saturation 15mm to either side of this region. Average crack spacing of 1.25 mm at saturation.
4	Damage progresses closer to specimen ends. Discontinuous delaminations appear at outermost 90°/45° interface

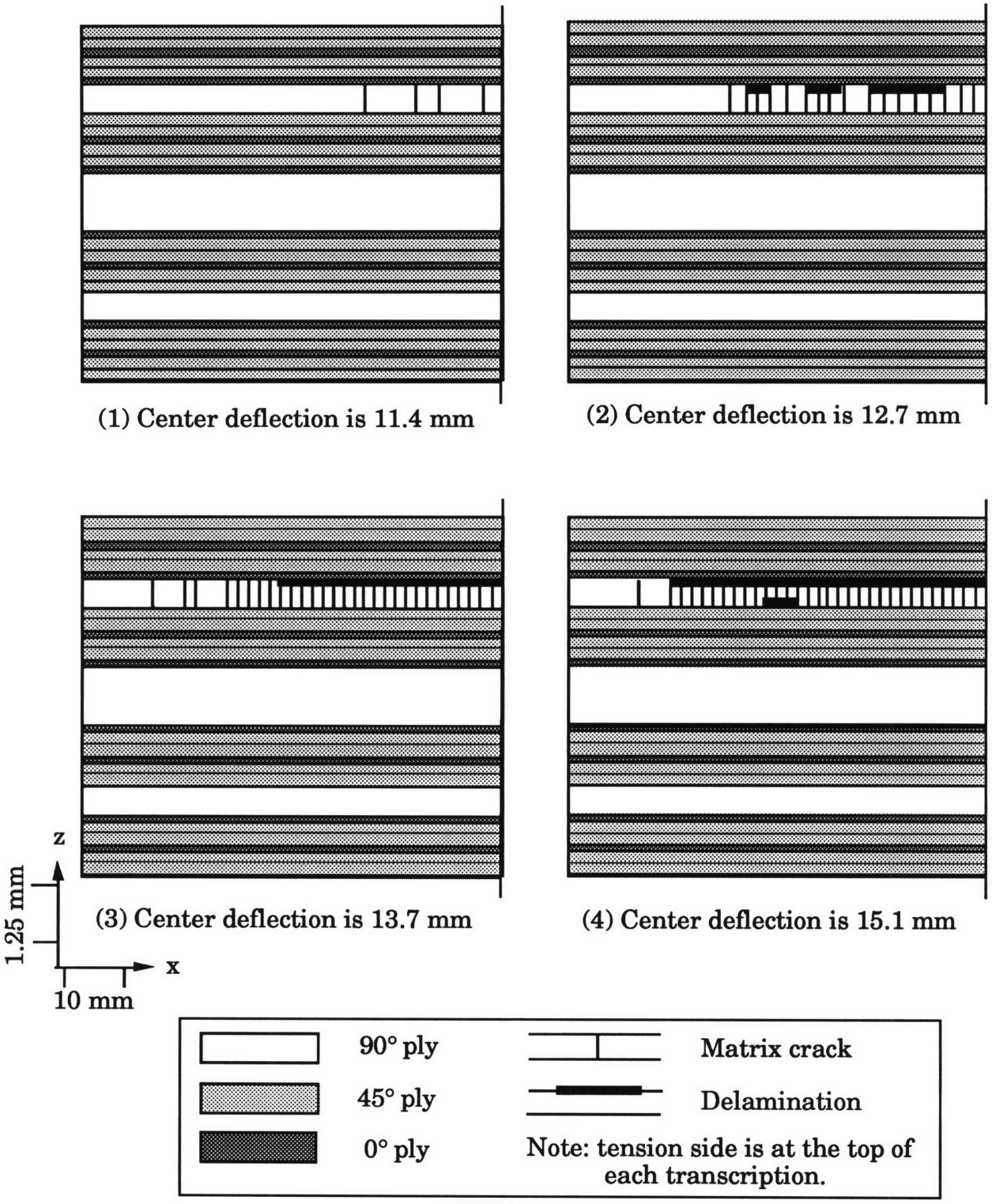

Figure 4.22 Damage history of a typical $[(45_2/-45_2/0)_2/90_5]_{2s}$ specimen statically tested.

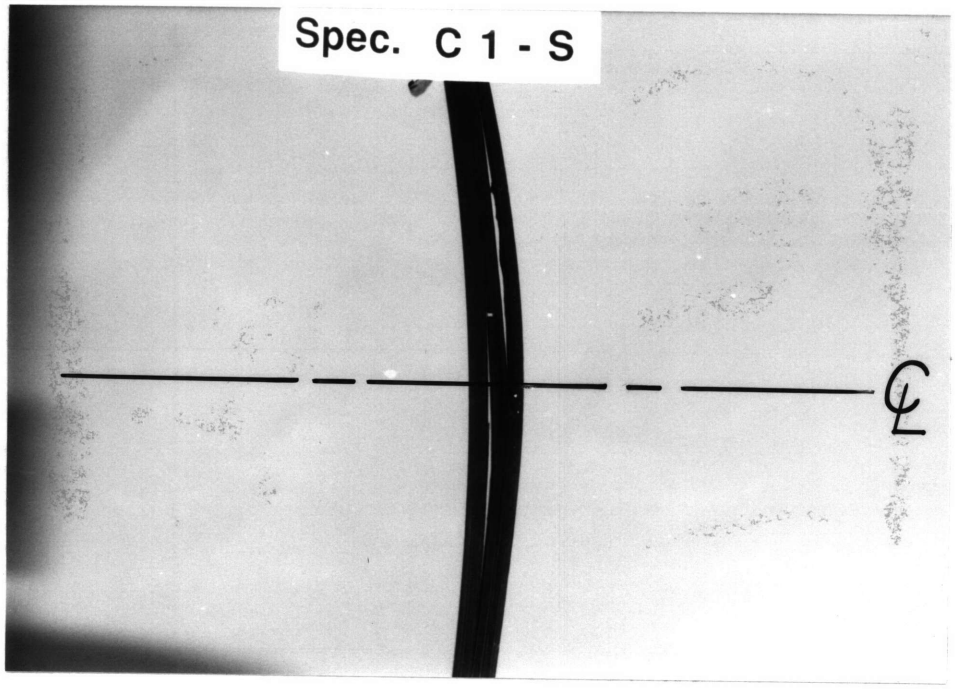

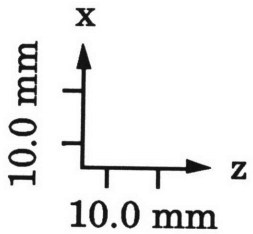

Figure 4.23 Photograph of a typical failed $[(45_2/-45_2/0)_2/90_5]_{2s}$ specimen statically tested.

7% at the fourth characteristic damage state compared to the first measurement of the undamaged specimen although there was a steady decline. The maximum load as well as the buckling load and center deflection at each characteristic damage state for both specimens tested are shown in Table 4.8.

4.3.2 Cyclic Behavior

Ten specimens were tested cyclically to failure. Four specimens were intended to be statically damaged to the first characteristic damage state and then cyclically loaded using the maximum load reached statically as the maximum cyclic load. The initial damage on two of the specimens was slightly more severe than the first state. The other six specimens were statically damaged to the third damage state. Three of the six were cyclically loaded using the maximum load reached statically as the maximum cyclic load. The other three specimens were cyclically loaded using the load equivalent to each specimens' first damage state as the maximum cyclic load. The initial damage state, Southwell buckling load before damage, maximum loads, and the number of cycles to failure for each specimen is shown in Table 4.9.

For the first two specimens initially damaged to the first state, the corresponding damage history is illustrated in Figure 4.24. The first damage state is the state of the specimen after the static loading but before cyclic loading began. Halfway to failure, the second cyclic damage state is defined on the tension side by a crack density of approximately 75% saturation on the central 60 mm portion of the outer tension side 90° ply with discontinuous delaminations beginning to grow. This damage state is further distinguished by the initiation of damage in the form of matrix

Table 4.8 Buckling load and center deflection at each characteristic damage state and maximum load for the $[(45_2/-45_2/0)_2/90_5]_{2s}$ specimens statically tested

Specimen	Characteristic Damage State	Southwell Buckling Load (N)	Center Deflection (mm)	Maximum Load (N)
1	undamaged	11,818	8.5	—
	1	11,680	11.4	—
	2	11,318	12.7	—
	3	11,267	13.7	—
	4	11,093	15.1	—
	failure	—	—	8940
2	undamaged	13,414	6.6	—
	1	13,141	11.4	—
	2	13,088	12.5	—
	3	12,866	14.2	—
	4	12,714	14.7	—
	failure	—	—	9732

Table 4.9 Initial damage state, buckling load, maximum loads, and the number of cycles to failure for each $[(45_2/-45_2/0)_2/90_5]_{2s}$ specimen tested cyclically.

Specimen	Initial Damage State	Southwell Buckling Load (N)	Maximum Static Load (N)	Maximum Cyclic Load (N)	Number of Cycles to Failure
1	1	12,318	8718	8718	608,920
2	1	8701	6805	6805	32,370
3	1+ [a]	12,899	10,140	10,140	53,080
4	1+ [a]	12,806	10,140	10,140	8500
5	3	11,249	8985	8985	1160
6	3	12,508	9652	9652	5000
7	3	10,800	8585	8585	12,190
8	3	11,867	9074	8807	11,810
9	3	9599	8184	7873	28,760
10	3	12,610	10,053	9652	22,370

[a] Initial damage was just beyond the first characteristic damage state.

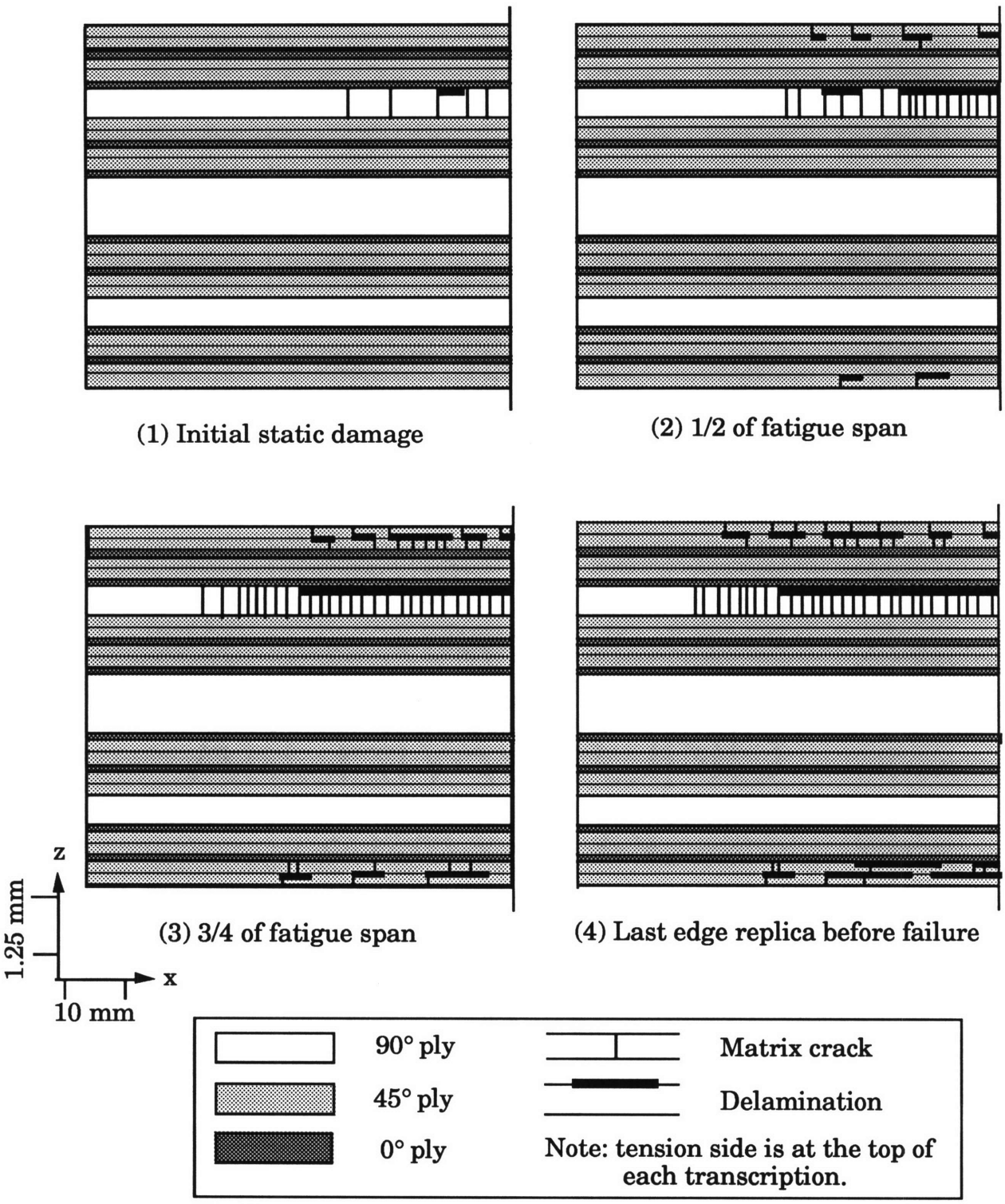

Figure 4.24 Damage history for a typical cyclic $[(45_2/-45_2/0)_2/90_5]_{2s}$ specimen statically damaged up to the first damage state.

cracks and delaminations on the outermost 45° and -45° plies on both the tension and compression sides. These delaminations were not terminated at matrix cracks. By the third cyclic damage state, the tension side 90° ply crack density became saturated in the central 80 mm, dropping to approximately 50% saturation 15 mm to either side of this region. The average crack spacing at saturation was 1.25 mm. The delaminations became continuous across the central 70 mm of the specimen. The damage on the 45° and -45° plies on both sides of the specimen also grew covering about 60 mm of the central portion of the specimen. The fourth cyclic damage state is characterized by the further growth of all damage towards the specimen ends.

Thus, damage growth in the early stages of the test was highlighted by the damage in the tension side 90° ply while the latter half of the test was highlighted by the growth of damage in the 45° and -45° plies on both sides of the specimen. Failure of these specimens occurred on both the tension and compression sides with some easily visible damage on the compression side prior to failure allowing the predictability of failure. A photograph of a failed specimen in shown in Figure 4.25. The entire tension half as well as the outer 45° and -45° effective ply portion of the compression half of the specimens were destroyed.

For the other two specimens specified for initial damage up to the first damage state statically (specimens 3 and 4), the resulting initial damage state was more severe than the previous two but not quite at the second damage state, as shown in the damage history of these two specimens in Figure 4.26. The crack density was higher with larger delaminations than for the damage of specimens 1 and 2 represented in Figure 4.24. The second cyclic damage state consisted of the crack density

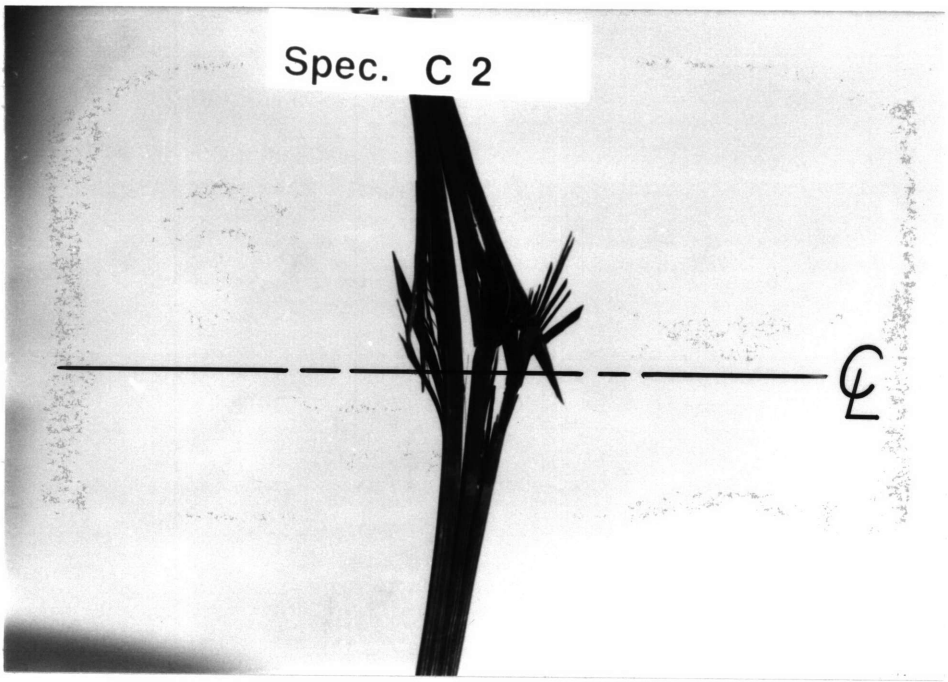

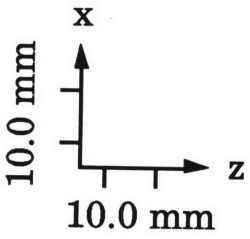

Figure 4.25 Photograph of a typical failed cyclic $[(45_2/-45_2/0)_2/90_5]_{2s}$ specimen statically damaged up to the first damage state.

reaching saturation in the central 70 mm of the tension side 90° ply with a continuous delamination along the 0°/90° interface in this region. Crack density dropped to approximately 50% saturation 10 mm to either side of this region. Again, the average crack spacing at saturation was 1.25 mm. This damage state is also distinguished by the initiation of damage in the form of matrix cracks and short delaminations in the 45° and -45° plies on the tension side only. By the third cyclic damage state, this damage moved closer to the specimen ends, as did the damage in the 90° ply. The fourth cyclic damage state is characterized by the initiation of damage in the 45° and -45° plies on the compression side in the form of cracks and short delaminations. The initiation of compression side damage occurred much closer to failure than in the first two specimens, where compression side damage initiated by the second damage state, concurrent with the initiation of the tension side 45° and -45° ply damage. The damage on the tension side covered approximately 80 mm of the central portion of the specimen by this time.

At failure, the compression side failure was still in the early stages, and failure occurred in the tension half in the form of delaminations along the 90° plies with some 0° ply failure on the tension side. The compression side remained intact. The failure was abrupt with no easily visible signs of damage to predict failure. A photograph of a failed specimen is shown in Figure 4.27. As in the previous laminate, a small difference in initial damage, thus increasing the cyclic load level, can greatly affect the failure of a specimen.

The damage history for the six specimens initially damaged to the third damage state statically (specimens 5 to 10) was similar for all six during most of the cyclic portion of the test. The difference in loading

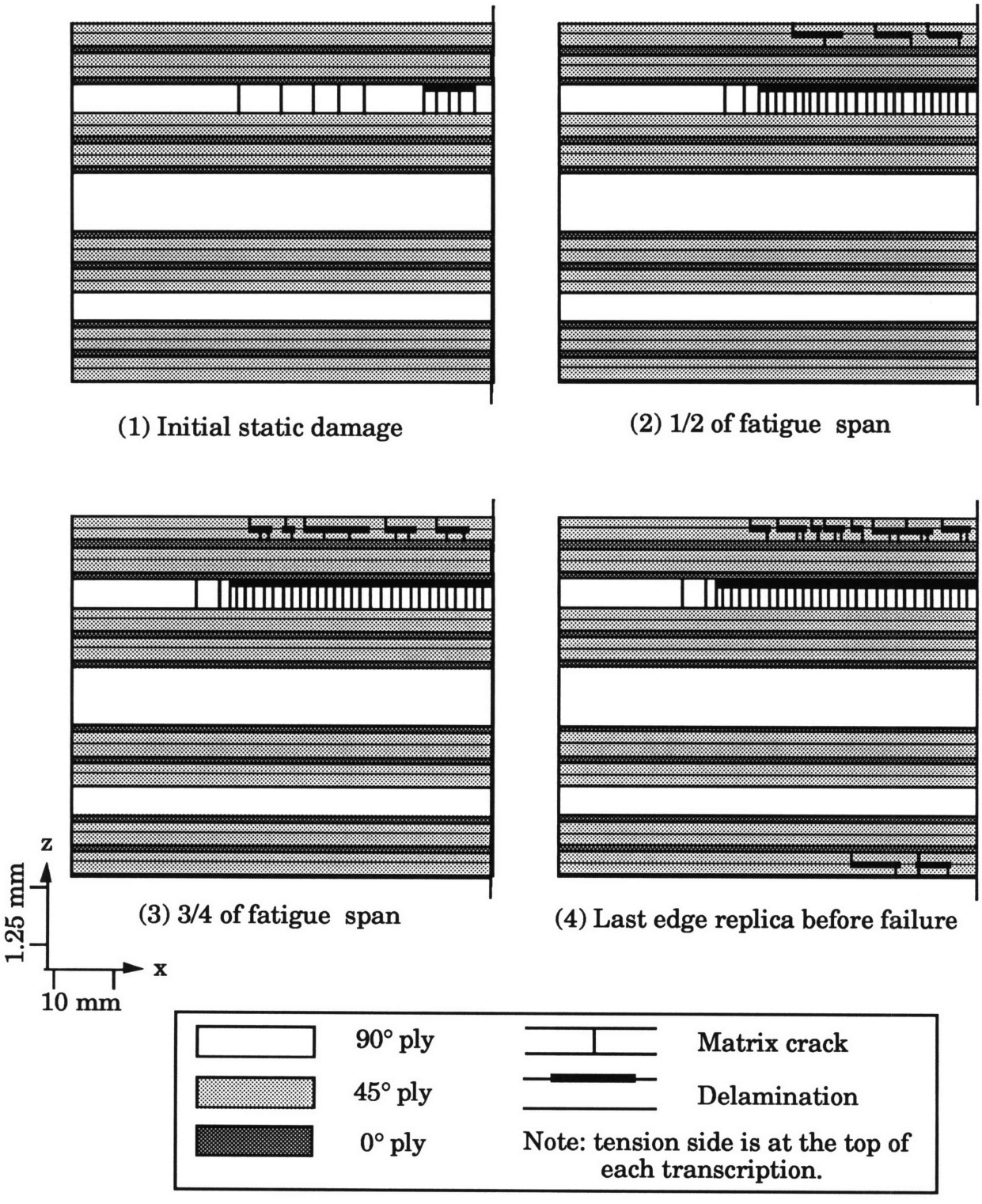

Figure 4.26 Damage history for a typical cyclic $[(45_2/-45_2/0)_2/90_5]_{2s}$ specimen statically damaged just beyond the first damage state.

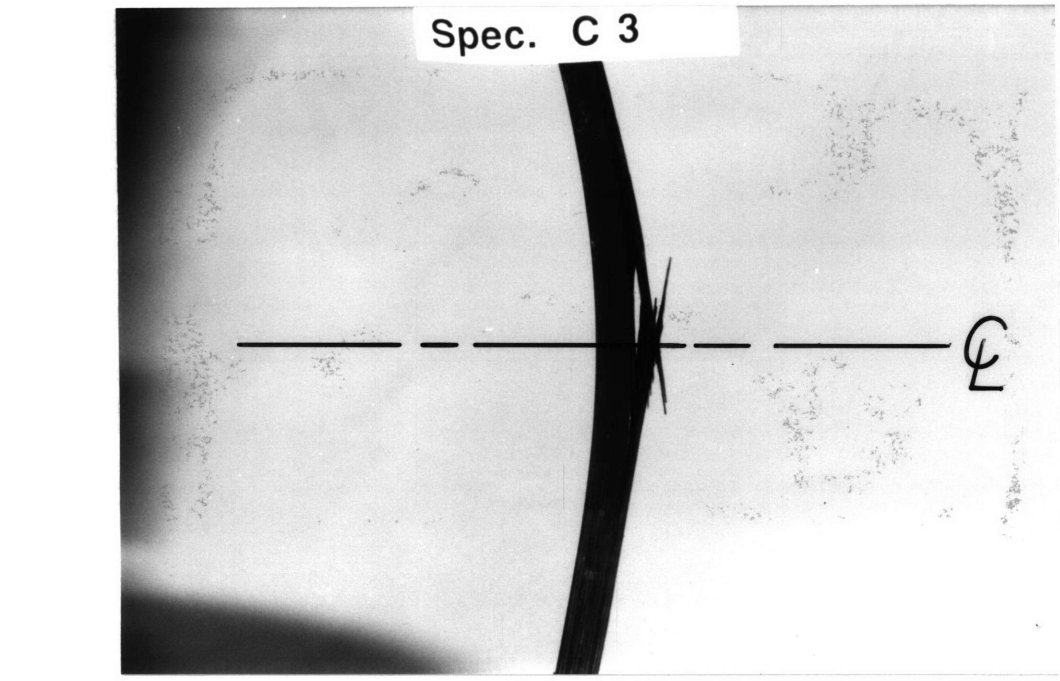

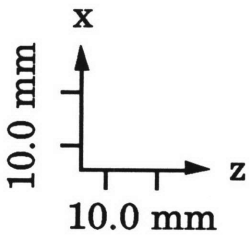

Figure 4.27 Photograph of a typical failed cyclic $[(45_2/-45_2/0)_2/90_5]_{2s}$ specimen statically damaged past the first damage state.

history became evident late in the test. In Figure 4.28, the damage history of specimens 5 to 7, cyclically loaded at the higher cyclic load corresponding to the third characteristic damage state, is illustrated. There is a strong resemblance to specimens 3 and 4 except the first damage state is more advanced in the tension side 90° ply due to the increased static loading. Again, the compression side damage does not initiate until just prior to failure. The crack saturation and continuous delamination in the tension side 90° ply covered 85 mm of the central portion of the specimen. The failure of specimens 5 to 7 was abrupt and in the form of delaminations along the tension side 0°/90° and 45°/-45° interfaces and central 90° plies as shown by the photograph in Figure 4.29. Gross delaminations at the 45°/-45° interfaces and angle ply splits became visible just prior to failure on the tension side.

The damage history of specimens 8 to 10, cyclically loaded at the lower level, is shown in Figure 4.30. The compression side delaminations at the fourth cyclic damage state for these specimens are larger than that for specimens 5 to 7. The crack saturation and continuous delamination on the tension side 90° ply covers approximately 70 mm of the central portion of the specimen. These specimens failed in a similar manner to specimens 1 and 2 as seen in the photograph of Figure 4.31. Failure occurred on both the tension and compression sides with delaminations along 0°/90° interfaces. The lower load level apparently impeded the growth of the tension side damage too close to the specimen ends, allowing the compression side damage to become more prominent late in the test, thus contributing to failure. This is similar to the finding in the literature that a lower fatigue load level influences the interaction and increases the contribution of delaminations leading to failure in notched laminates [32]. The average

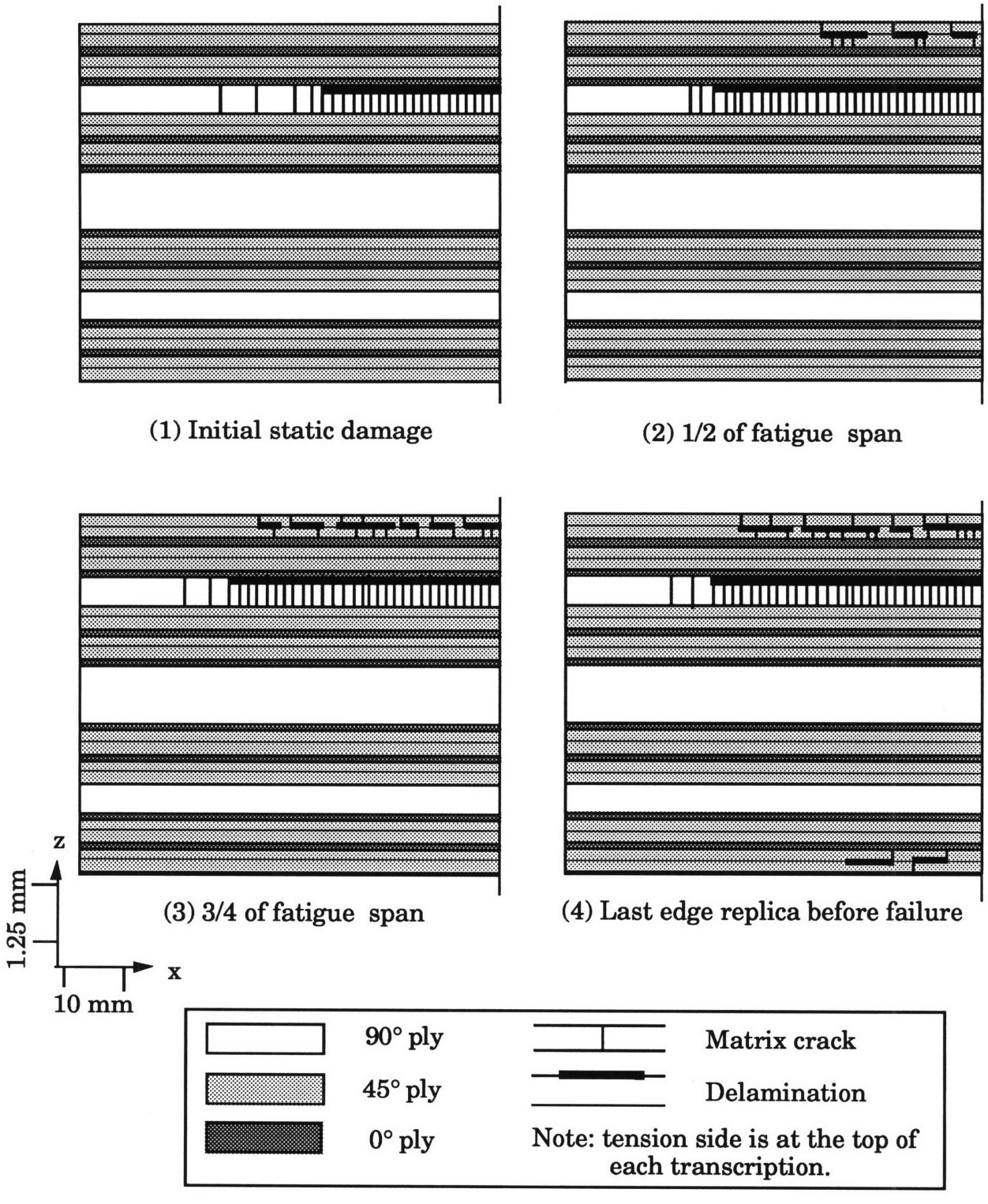

Figure 4.28 Damage history of a typical cyclic $[(45_2/-45_2/0)_2/90_5]_{2s}$ specimen statically damaged to the third damage state with a high cyclic load level.

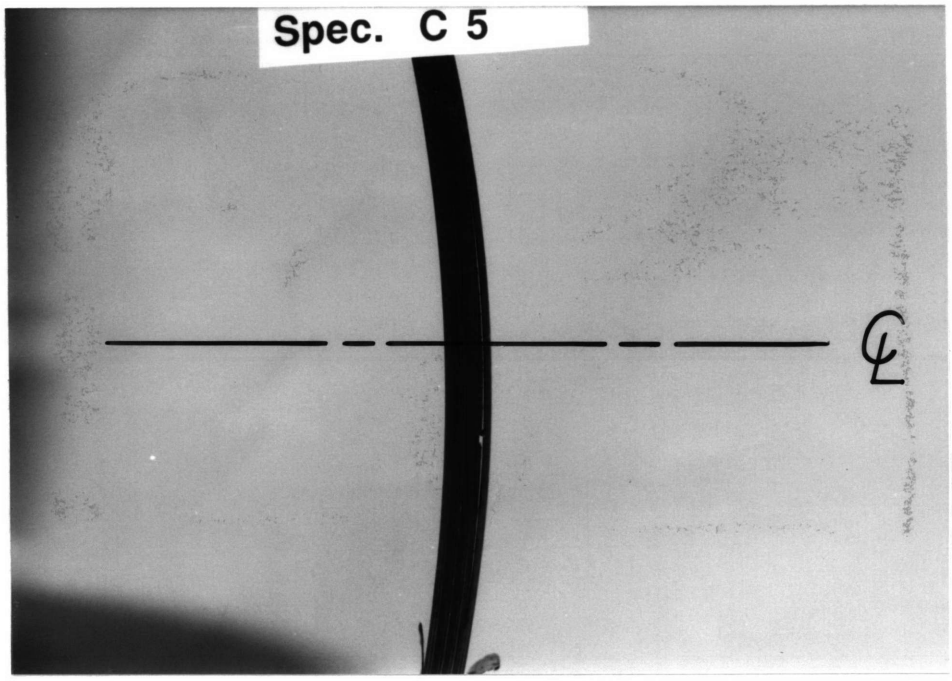

Figure 4.29 Photograph of a typical failed cyclic $[(45_2/-45_2/0)_2/90_5]_{2s}$ specimen statically damaged to the third damage state with a high cyclic load level.

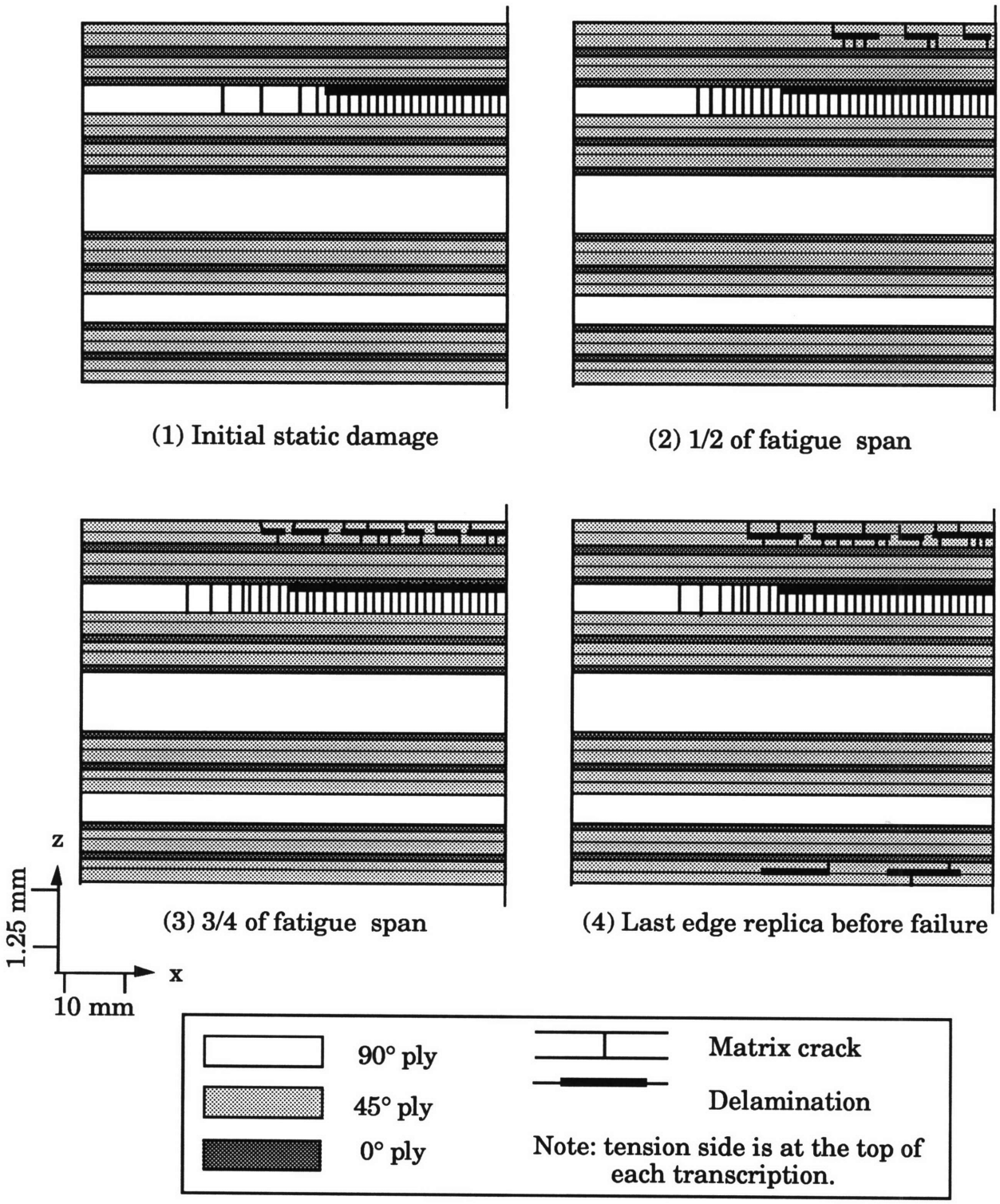

Figure 4.30 Damage history for a typical cyclic $[(45_2/-45_2/0)_2/90_5]_{2s}$ specimen statically damaged to the third damage state with a low cyclic load level.

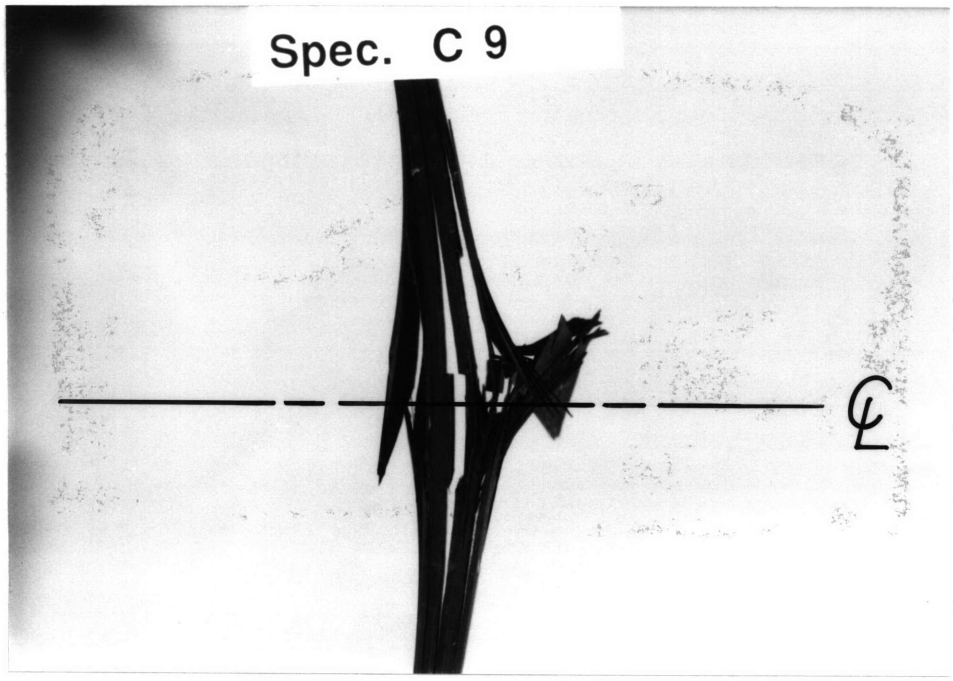

Figure 4.31 Photograph of a typical failed cyclic $[(45_2/-45_2/0)_2/90_5]_{2s}$ specimen statically damaged to the third damage state with a low cyclic load level.

number of cycles to failure for specimens 8 to 10 was greater than for specimens 5 to 7.

For all of the specimens of this laminate type, the stiffness, as measured by Southwell buckling loads, increased slightly at first and then steadily declined with cyclic loading as shown in Figure 4.32. The overall stiffness did not degrade significantly. Specimens 5 and 6 are not plotted because they failed before sufficient stiffness data was taken. The data is presented in tabular form in Appendix A. Stiffness reductions just prior to failure were not captured by the data since there were usually several thousand cycles between the last measurement and ultimate failure making up 5 to 20% of the total cycle time depending on the number of cycles to failure of a particular specimen.

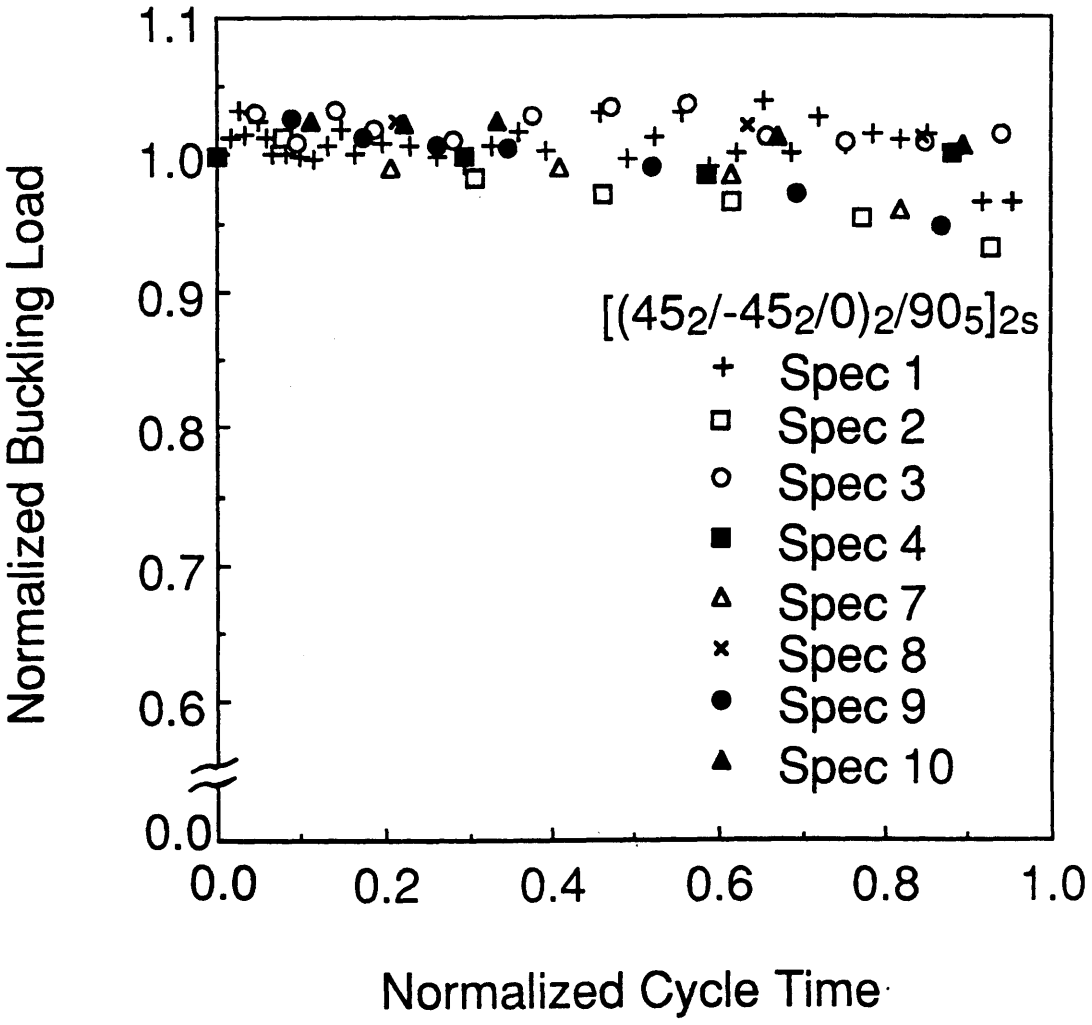

Figure 4.32 Normalized Southwell buckling loads versus normalized cycle time for $[(45_2/-45_2/0)_2/90_5]_{2s}$ specimens.

Chapter 5

DISCUSSION

5.1 $[45_4/-45_4/(0/90)_4]_{2s}$ Laminate Pre-Damage

Damage in the form of matrix cracks was present on most of the specimens of this laminate type prior to testing. As explained in section 4.1, the damage occurred in the 45° and -45° effective plies and was biased toward one side of the specimens with most of the damage occurring in a surface 45° ply. No damage was present in the opposite surface 45° or -45° plies. An example of this damage is shown in Figure 4.1. The damage varied among specimens and even across the width of some specimens, with the replicas of the two edges of a specimen showing different damage.

This occurrence of damage on specimens before any loads were applied is due to the manufacturing process. Using classical laminated plate theory, the ply stresses in ply axes were calculated for this laminate exposed to a cooling of 280°F, based on a 350°F set temperature and a laboratory temperature of 70°F. The material properties used are listed in Table 3.1. The longitudinal, transverse, and shear coefficients of thermal expansion used are -0.2 μstrain/°F, 16.0 μstrain/°F, and 0.0 μstrain/°F respectively. The ply longitudinal, transverse, and shear stresses in ply axes in the 45° and -45° plies are found to be approximately -40 MPa, 40 MPa, and -0.08 MPa respectively. The transverse stress is within 15% of the transverse tensile strength listed for this material in Table 3.1. Because of

the scattered and inconsistent nature of the damage and the high transverse tensile stresses present, the damage in the form of matrix cracks in the 45° and -45° plies is, therefore, likely due to residual cooling stresses.

It is interesting to note that the occurrence of this initial damage varied across the thickness of each specimen. The majority of cracks were biased toward one surface with the opposite surface damage free. This indicates a slight unsymmetry in the laminate during manufacturing which could cause some bending of the laminate. Clamping the laminate to the cutting table during the machining process using a straight bar across the laminate may produce additional stresses if bending occurred. This possible bending, coupled with the high residual cooling stresses and the stresses induced by clamping the laminate to the cutting table can result in matrix failure biased to one side of the laminate.

It is clear from the results that the matrix damage affected the static and cyclic performance of the laminate. Depending on the orientation of the specimens in the jig, which determined whether the damage was biased toward the tension or compression side (once compressive loads were applied), the damage accumulation varied. For the orientation where the damage was biased toward the tensile side of the specimens, most of the initial damage was in this outermost 45° ply where damage would be expected due to compressive loading. Thus, the damage growth was similar to that of a specimen where no initial damage due to manufacturing was detected [38]. The initial damage due to manufacturing did not have adverse effects on the behavior of specimens when orientated toward the tension side.

When the specimens were orientated with the damage due to manufacturing biased toward the compression side, the damage accumulation differed. Just as the presence of tension side matrix damage changes the laminate to a nonsymmetric laminate with a different neutral axis, the presence of compression side matrix damage produces additional changes in the neutral axis, thus changing the behavior from that of the above orientation. The center deflection at each characteristic damage state was lower for the specimens statically tested with the initial damage biased toward the compression side.

The mechanisms governing this compression side damage growth differ from that which occur due to cyclic loading with no initial compression side pre-damage where delaminations initiate and grow independent of matrix cracks. With pre-damage on the compression side, delaminations link the existing matrix cracks and are not independent of them.

Initial matrix damage present on the inner 45° and -45° effective plies does not significantly effect the behavior of the specimens. The 0° plies carry most of the load and the inner ply groups would not be expected to see significant bending stresses. This is consistent with the observation that the damage on the inner 45° and -45° ply groups did not significantly progress with static or cyclic loading.

It is evident from the results that the initial damage due to manufacturing when orientated toward the compression side has a significant effect on the behavior of the specimens statically loaded to failure and cyclically loaded to failure. The potential effects of the manufacturing process need to be considered to avoid the occurrence of pre-damage due to high residual cooling stresses, machining, and non-

symmetries that may develop, or a combination of these. Ignoring these can result in unexpected matrix cracking, adversely effecting the behavior of the structure, unless detected by means of nondestructive testing.

The nature of the pre-damage in these specimens was such that the matrix cracks were slight and usually difficult to detect. Because the cracking damage was scattered, standard nondestructive techniques may not be adequate in detecting the presence of this damage in a structure. The inability to detect pre-damage can allow a structure to exhibit unexpected failure modes, as evidenced by the compression side failure on the static specimens. Significant amounts of pre-damage can result in premature failure, similar to the failure of cyclic specimen 6, which failed after 20 cycles.

5.2 Characteristics of Damage Accumulation

The various damage modes present in the tested specimens initiated under different loading conditions. The tension side damage in the $[45_4/\text{-}45_4/(0/90)_4]_{2s}$ and $[\pm 45/0/90_4]_{4s}$ laminates initiated under static loading, while the cyclic loading initiated compressive side damage and caused both tension and compression side damage to progress. For the $[(45_2/\text{-}45_2/0)_2/90_5]_{2s}$ laminate, damage on the tension side 90° ply was initiated under static loading, while under cyclic loads, damage in the outermost 45° and -45° plies on both the tension and compression sides was initiated with all damage in all plies growing.

The tension side damage on all laminates resulting from static loading initiated where it was expected: at the longitudinal center of the specimens in the outermost effective plies (of at least four ply thicknesses).

This damage was in the form of in-plane matrix cracks. Because of the longitudinal gradient stress field, the crack density varied along the length, becoming saturated in the central 50 to 70 mm region of the specimen first. The pattern of this damage growth under cyclic loading was similar to that under static loading, but usually extended to 80 to 100 mm of the central region of the specimens. Thus, cyclic loading increased the damage area on the tension side. Delamination initiation in these plies was related to the stress concentrations caused by matrix cracks as initiation always occurred at the intersection of a matrix crack and a ply interface. Initially in the form of short, discontinuous delaminations connecting the pre-existing cracks, they eventually joined to form a single continuous delamination over much of the length of the specimen with ends still terminating at a matrix crack. These delaminations always initiated on the outermost interface of the damaged ply where the stresses would be higher due to bending effects.

The damage which initiated due to cyclic loading was on the compression side for the $[45_4/\text{-}45_4/(0/90)_4]_{2s}$ and $[\pm 45/0/90_4]_{4s}$ laminates. Because edge replicas were only taken at intervals of cyclic loading, it was difficult to isolate one damage type (matrix cracks or delaminations) before the other occurred. For the $[45_4/\text{-}45_4/(0/90)_4]_{2s}$ laminate, a couple of replicas showed delaminations along the 45°/-45° interface on the compression side with no matrix cracks present. Generally, delamination growth was independent of matrix cracking and did not stop at crack locations. Crack density increased after the delaminations were formed, but never quite reached the saturation level reached in the static to failure tests. The damage on the compression side of the $[45_4/\text{-}45_4/(0/90)_4]_{2s}$ laminate appears to be initiated by delaminations forming at the 45°/-45° interface, with

matrix cracking occurring in the regions of delaminations. This indicates a different mechanism governing damage initiation and growth due to cyclic gradient stress fields from that of static loading. Cyclic loading, combined with the out-of-plane deflections, can cause voids and inclusions in the interply matrix layer to grow, eventually increasing the out-of-plane stresses enough to cause the matrix interlayer to crack. Thus, a delamination originates, allowing the sublaminate to buckle without any restriction from the rest of the laminate.

The two competing damage modes that occur can be clearly distinguished. Tension side damage initiates as a result of static loading and its growth is controlled by matrix cracks. Compression side damage initiates after cyclic loading and is controlled by the propagation of delaminations which are independent of the in-plane, matrix cracks.

For the $[\pm 45/0/90_4]_{4s}$ laminates, compressive side matrix cracks and delaminations always coexisted in the edge replicas. Generally, delaminations at the 90°/0° interface were independent of matrix cracks while the delaminations at the 0°/-45° interfaces coexisted with matrix cracks in the -45° and 45° plies but did not link them. The growth of the 90°/0° delamination preceded the growth of the 0°/-45° delamination. The former delaminations were thus always larger and moved closest to the specimen ends, indicating a more critical out-of-plane stress at that interface. It was observed, close to failure for one specimen, that small 90°/0° and 0°/-45° delaminations coexisted with what was interpreted as a 0° fiber break. The edge replica revealed a break in the single 0° ply on all successive replicas, indicating damage at the specimen edge in the 0° ply. The 90°/0° and 0°/-45° delaminations appeared to propagate from this point. No matrix cracks in the -45° or 45° plies existed with the initiation of this

damage. In another instance, matrix cracks in the -45° and 45° plies were observed without 90°/0° and 0°/-45° delaminations. These delaminations and a 0° fiber break developed in successive replicas. It is unclear which damage type on the compression side of the $[\pm 45/0/90_4]_{4s}$ laminates occurs first, in-plane or out-of-plane, but the growth of delaminations are clearly not dependent on matrix cracking as evidenced by the 90°/0° delamination growth.

The damage due to cyclic loading for the $[(45_2/-45_2/0)_2/90_5]_{2s}$ laminate appeared on the outermost 45° and -45° plies on both the tension and compression sides. It was impossible to isolate the matrix cracks and delaminations in these plies, but the delaminations never stopped at matrix crack locations on either side. Unlike the damage in the tension side 90° effective ply, delamination growth at the 45°/-45° interfaces was independent of matrix cracking. Once the delamination started propagating, more matrix cracks developed in those regions, mostly in the adjacent -45° ply. Although it is unclear which damage type occurs first, it is clear that a high crack density is not necessary for delamination initiation and growth as in the damage due to static loading. In fact, delamination growth often increased the crack density.

From the damage histories due to cyclic loading of these laminates, it is impossible to develop a simple relationship on the interaction between the initiation of damage types for all of the laminates as can be developed for the damage due to static loading. This interaction is dependent on the laminate type. One consistent result, though, is that the compression side damage which initiated as a result of cyclic loading is delamination controlled and not dependent on matrix cracking. The delaminations propagate away from regions of in-plane damage eventually creating some matrix

cracking. This is in contrast to the matrix crack controlled tension side damage due to static loading.

Each of the three laminates achieved different crack saturation levels in the effective ply groups where delamination growth was dependent on in-plane damage. From the laminate types used in this investigation, the crack density at saturation varies with the effective ply thickness and the ply angle. As shown by the $[\pm 45/0/90_4]_{4s}$ and $[(45_2/-45_2/0)_2/90_5]_{2s}$ laminates, a thicker 90° effective ply (5 versus 4) had an increased crack spacing, decreasing the crack density by one-third. This is the opposite to what would be expected with increasing ply thickness giving an increase in crack density. The different compliances of the two laminates compared here may account for this discrepancy. The 90° effective ply in the $[\pm 45/0/90_4]_{4s}$ laminate is also closer to the side of the specimen than in the $[(45_2/-45_2/0)_2/90_5]_{2s}$ laminate. The crack density also varies with the ply angle, as seen with the $[45_4/-45_4/(0/90)_4]_{2s}$ and $[\pm 45/0/90_4]_{4s}$ laminates. The -45° effective ply (n=4) in the $[45_4/-45_4/(0/90)_4]_{2s}$ laminate exhibited a smaller crack density than the 90° effective ply (n=4) in the $[\pm 45/0/90_4]_{4s}$ laminate by a factor of two. The $[\pm 45/0/90_4]_{4s}$ laminate, exhibiting a higher crack density, is more compliant than the $[45_4/-45_4/(0/90)_4]_{2s}$ laminate.

As seen in chapter four, the stiffness of the specimens, as measured by Southwell buckling loads, generally increased slightly at first and then steadily declined throughout the rest of the test. The degradation was not significant until just prior to failure. The large degradation of stiffness occurring when damage became grossly visible to the naked eye was not captured by the data since measurements were taken at specific intervals. There were usually two to three thousand cycles between the last static test sequence and failure. This degradation, just prior to failure, was large

enough to affect the stroke necessary for the test machine to reach the desired loads. The stiffness did not degrade significantly over most of the cyclic portion because there was little or no fiber breakage in the 0° plies, which carry most of the load in the specimens. Until the delaminations became large enough to split the specimens into effectively two specimens with reduced bending stiffness, the required load-carrying capabilities of the specimens was maintained. Thus, stiffness would be inadequate as a measure of damage or a warning method for failure for structures under bending fields.

5.3 Static versus Cyclic Damage Growth

The work by Wolfe [38] investigated the damage accumulation of thick laminates subjected to a gradient stress field due to static loading. Damage was restricted to the tension side only. In this investigation, the damage accumulation of the same laminates subjected to a cyclic gradient stress field was studied. There are significant differences in the damage histories between the two loading conditions. With cyclic loading, the initiation and growth of compression side damage, non-existent under static loading, became a dominant factor in the failure. Compression side damage, in the form of delaminations leading to sublaminate buckling, degraded the load-carrying capability of the specimens significantly just prior to failure. Stiffness reduction was observed once the delaminations became grossly visible to the naked eye, just prior to the failure of the specimens.

The initiation of compression side damage adversely affected the behavior of the laminates for most of the conditions tested. One possible

reason for this damage could be the shear stress due to the bending of the specimen. This shear stress would not be expected to be significant in the outer plies though, far from the neutral axis. The mechanisms under which this damage initiates are more likely related to the repeated loading with out-of-plane deflections. With cyclic loading, sublaminate buckling can occur as a result of existing defects growing in the matrix interply layer. After cyclic loading, these defects become significant, creating out-of-plane stresses large enough to initiate cracking in the matrix interlayer not present under static loading.

Thus, the damage initiation, damage accumulation, and failure modes of specimens under cyclic loading differ from that under static conditions. Cyclic loading revealed critical damage modes not found with static loading. Thus, performing static tests on a structure will not necessarily expose all possible damage modes. Laminates cyclically loaded at load levels below which damage occurs under static loading may still exhibit damage due to cyclic gradient stress fields.

5.4 Cyclic Load Level Effects on Damage Growth and Failure

The cyclic tests of the $[\pm 45/0/90_4]_{4s}$ and $[(45_2/-45_2/0)_2/90_5]_{2s}$ laminates demonstrate the effects of initial damage level, hence the maximum cyclic load level, on the damage growth and failure of these laminates. As explained in chapter four, the $[\pm 45/0/90_4]_{4s}$ specimens were statically damaged to two different damage states before cyclic loading at the maximum loads reached statically for each specimen. The $[(45_2/-45_2/0)_2/90_5]_{2s}$ specimens were statically damaged to two different

damage states. The specimens damaged to the higher state were cyclically loaded at two different maximum load levels.

The tension side damage growth of the $[\pm 45/0/90_4]_{4s}$ specimens statically damaged to a higher state was similar to that of the specimens statically damaged to the first state. The initiation of the compression side damage occurred much closer to failure, though, when normalizing cycle time. As explained in section 4.2.2, of the six specimens statically damaged to the higher state, three of the specimens had initial damage slightly more severe. The three with the less severe initial damage failed in the same manner as the specimens statically damaged to the lower level. The initiation of the compression side damage occurred at approximately the same number of cycles as in the specimens damaged to the lower state, but failure occurred at a lower number of cycles. Failure occurred on both the tension and compression sides. For the three specimens with the more severe damage at the higher state, failure occurred on the tension side only, at a much lower number of cycles. Compression side damage still initiated, although at a much lower number of cycles than all of the previous specimens. Increasing the cyclic load level does not change the damage modes initiated, but changes their interaction with the effect of reducing the number of cycles to failure.

It is interesting to note that for the latter three specimens, when the tension side damage dominated failure, the initiation of compression side damage occurred at relatively the same time with respect to the total number of cycles to failure as the former three specimens, despite the much lower number of cycles to failure. The severity of the initial damage on the latter three specimens, increasing the maximum cyclic loads, was apparently large enough so that the tension side damage progressed closer

to the specimen ends before compression side damage became a factor, causing strictly tension side failure. For the three specimens statically damaged to the less severe higher state, compression side damage initiated late in the fatigue portion of the test, but the cyclic loads were such to keep the tension side damage from growing too close to the specimen ends before the compression side damage became critical so that compression side damage was a factor in failure. The relative growth of these two competing modes of damage, tension side and compression side damage, is dependent on the initial damage state and the cyclic load level. Cyclic loading at higher load levels can result in a different behavior than at lower levels because of a change in the dominance of various damage modes in cyclic gradient stress fields.

The behavior of the $[(45_2/-45_2/0)_2/90_5]_{2s}$ specimens demonstrate similar dependence on load level. For the two specimens statically damaged to the first state, damage in the 45° and -45° plies initiated early in the fatigue portion of the test. Failure occurred on both the tension and compression sides. For the two specimens with more severe damage but not quite at the second damage state, the compression side 45° and -45° ply damage initiated close to failure. Failure occurred on the tension side only before compression side damage could become dominant. The slight increase in initial damage and the increase in the cyclic load level was enough to change the relative growth of the tension and compression side damage modes and hence the failure mode.

The three specimens statically damaged to the third damage state and cyclically loaded at the higher load level behaved similar to the two specimens damaged just past the first damage state, demonstrating tension side failure. The three specimens initially damaged to the higher

state but cyclically loaded at the lower load level had similar damage accumulation up to failure as the former three, although the tension side damage did not grow as close to the specimen ends late in the test. Failure resembled the first two specimens initially damaged to the first state because the tension side damage grew slowly with the lower cyclic load, allowing the compression side damage to become critical once it initiated. The higher initial damage state accelerated tension side damage progression at first, but the lower maximum cyclic load reduced the dominance of this damage mode. These tests demonstrate the influence loading history has on the damage progression and failure of these laminates. Varying the cyclic load level changes the dominance of the competing damage modes. Cyclic loading at higher load levels doesn't necessarily reveal all of the critical damage modes that may occur in composite structures under real conditions.

5.5 Implications on Structural Certification

Evaluating the behavior of large structures under cyclic loads can be very expensive and time consuming. Taking measures to reduce certification time can be significant in economic terms. As a result, some philosophies of structural certification maintain that composite structures are insensitive to cyclic loading, exhibiting all of the critical failure modes during static testing. Load enhancement factors are also used to reduce testing time.

This investigation shows that cyclic testing under gradient stress fields exposes damage modes not experienced during static testing. Compression side delaminations and matrix cracks in the

$[45_4/-45_4/(0/90)_4]_{2s}$ and $[\pm45/0/90_4]_{4s}$ laminates as well as delaminations and cracking in the outermost compression and tension side 45° and -45° effective plies in the $[(45_2/-45_2/0)_2/90_5]_{2s}$ laminate are due to cyclic loading and are not seen with static loading to failure. One explanation for these damage modes occurring could be a growth of voids, which increase the out-of-plane stresses, creating matrix interply cracking and leading to sublaminate buckling. Hence, matrix sensitive failure modes are sensitive to cyclic loading. If the laminates tested were evaluated based on the static testing performed by Wolfe [38], their expected behavior under repeated bending would be quite different from that seen in this work. Certifying structures on the basis of possessing adequate static strength can overestimate their life range. Structures expected to endure gradient stress fields in a real environment should be evaluated on their behavior under these same conditions.

Evaluating the behavior of structures under real conditions requires testing using carefully simulated load spectra. Load enhancement factors, used to reduce testing time, will not always reveal the same behavior as would be seen in the field. As shown in this investigation, varying the cyclic load level changes the dominance of the various damage modes, affecting the behavior of the structure. Increasing the cyclic load level in the $[\pm45/0/90_4]_{4s}$ and $[(45_2/-45_2/0)_2/90_5]_{2s}$ laminates changed the relative growth of the damage modes such that the compression side damage was not critical. Thus, the effect of using a higher load level on these laminates to speed up testing time would be to mask out the importance of this compression side damage for lower cyclic load levels, giving a much different failure mode in the laboratory than what would actually occur. Depending on the relationship between the load enhancement factor and

the life enhancement factor, there is the definite potential of overestimating the cyclic lifetime at the lower load level of interest. When certifying composite structures for fatigue, the affects of load history and load levels should be carefully studied so that the tests correctly simulate the real conditions.

Chapter 6

CONCLUSIONS AND RECOMMENDATIONS

A test program to study damage accumulation in simply-supported graphite/epoxy beam-columns subjected to static and cyclic gradient stress fields was developed and carried out. The mechanisms of damage initiation, damage progression, and failure were studied, and the damage accumulation histories of three layups were compiled. From this work, the following conclusions have been drawn:

1. Damage in the form of matrix cracks, present in the 45° and -45° ply groups on some of the $[45_4/\text{-}45_4/(0/90)_4]_{2s}$ specimens prior to testing, was due to residual manufacturing stresses. This damage was varied among specimens and was biased toward one surface, with the opposite surface 45° and -45° ply groups being free of damage.

2. The initial damage due to manufacturing had a significant effect on the static and cyclic behavior of the $[45_4/\text{-}45_4/(0/90)_4]_{2s}$ specimens only when it was biased toward the compression side. The mechanisms of compression side damage initiation and growth under cyclic loading differed when this pre-damage was present than from when it was biased toward the tension side.

3. The effects of the manufacturing process need to be considered to account for the potential occurrence of pre-damage in the desired

layup since nondestructive techniques may not detect slight initial matrix cracking.

4. For the three specimen types studied, the damage due to static loading initiated at the longitudinal center of the specimen in the outermost tension side effective plies of at least four ply thicknesses. This damage accumulated similarly under cyclic loading as in static loading, with delaminations initiating at stress concentrations at the intersection of matrix cracks with a ply interface.

5. For the three laminates studied, the two modes of damage, tension side damage which initiated under static loading and compression side damage which initiated under cyclic loading, each propagate toward the specimen ends until one or both modes become critical enough to cause ultimate failure.

6. The tension side damage which initiated under static loading is matrix crack controlled while the compression side damage which initiated under cyclic loading is delamination controlled and propagates independently of matrix cracks, leading to sublaminate buckling.

7. For the layups studied, crack density is affected by effective ply thickness, ply orientation, neighboring ply, and overall compliance of the layup.

8. The stiffness of most of the specimens of all three layups increased slightly at first with cyclic loading, then steadily declined throughout the rest of the test. However, stiffness degradation was not significant

and would be inadequate as a measure of damage or a warning method for impending failure.

9. Cyclic loading reveals critical damage modes not found with static loading and, hence, should be used when ascertaining all possible damage modes.

10. Increasing the cyclic load levels in the $[(45_2/\text{-}45_2/0)_2/90_5]_{2s}$ and $[\pm 45/0/90_4]_{4s}$ and specimens eventually changes the relative growth of the two damage modes, thus increasing the dominance of the tension side damage and effectively reducing the dominance of the compression side damage. The failure mode changes from both a compression and tension side failure to only tension side failure.

11. Higher cyclic load levels to reduce testing time should not be used during certification to avoid hiding critical damage modes, giving an incorrect failure mode and potentially overestimating or underestimating cyclic lifetime.

12. Truncating low load levels of a load spectrum during certification can alter the behavior of the structure, as low cyclic loads can allow damage modes not otherwise considered significant to become critical.

The following recommendations for further work are made based on the results of this work:

1. Cyclic tests at load levels below which damage occurs statically should be performed on these specimen types to determine if a threshold exists for the initiation of the damage due to cyclic gradient stress fields.

2. Damage accumulation should be studied in buckled plates of the same laminate types statically and cyclically to examine the progression of damage in the transverse direction as well as longitudinally.

3. The effect of placing film adhesive at the critical interfaces to suppress the initiation and growth of delaminations [42] in these specimen types under static and cyclic loading should be assessed.

4. The causes for the initiation and progression of the compression side delaminations (independent of matrix cracking) due to cyclic loading should be studied.

5. The effect of varying the eccentricity with which load is applied, thus varying the through-the-thickness gradient stress field, on the damage initiation and progression of specimens of the same layups, should be investigated.

6. The effect, on the initiation and progression of the damage modes, of varying the load spectra should be determined for gradient stress fields.

REFERENCES

1. Awerbuch, J. & Hahn, H. T., "Fatigue and Proof-Testing of Unidirectional Graphite/Epoxy Composites," *Fatigue of Filamentary Composite Materials, ASTM STP 636*, 1977, pp. 248-266.

2. Hahn, H. T. & Kim, R. Y., "Proof Testing of Composite Materials," *Journal of Composite Materials*, Vol. 9, July 1975, pp. 297-311.

3. Chou, P. C. & Wang, A. S. D., "Statistical Analysis of Fatigue of Composite Materials," AFML-TR-78-96, Interim Technical Report, July 1978.

4. Ramani, S. V. & Williams, D. P., "Notched and Unnotched Fatigue Behavior of Angle-Ply Graphite/Epoxy Composites," *Fatigue of Filamentary Composite Materials, ASTM STP 636*, 1977, pp. 27-46.

5. Reifsnider, K. L., Stinchcomb, W. W. & O'Brien, T. K., "Frequency Effects on a Stiffness-Based Fatigue Failure Criterion in Flawed Composite Specimens," *Fatigue of Filamentary Composite Materials, ASTM STP 636*, 1977, pp. 171-184.

6. Ryder, J. T. & Walker, E. K., "Ascertainment of the Effect of Compressive Loading on the Fatigue Lifetime of Graphite/Epoxy Laminates for Structural Applications," Air Force Materials Laboratory Final Report AFML-TR-76-241, Wright-Patterson Air Force Base, Ohio, December 1976.

7. Rosenfeld, M. S. & Huang, S. L., "Fatigue Characteristics of Graphite/Epoxy Laminates Under Compressive Loadings," *Proceedings of the AIAA/ASME 18th Structures, Structural Dynamics, and Materials Conference*, April 1977, pp. 423-427.

8. Stinchcomb, W. W., "Nondestructive Evaluation of Damage Accumulation Processes in Composite Laminates," *Composites Science & Technology*, Vol. 25, No. 2, 1986, pp. 103-118.

9. Talreja, R., "Damage Models for Fatigue of Composite Materials," *Fatigue and Creep of Composite Materials*, Proceedings of the RISØ International Symposium on Metallurgy and Materials Science, September 1982, pp. 137-153.

10. Graves, M. J., "The Effects of Compression-Compression Fatigue on Balanced Graphite/Epoxy Laminates With Holes," TELAC Report 79-1, Massachusetts Institute of Technology, February 1979.

11. Mar, J. W., Graves, M. J. & Maass, D. P., "Effects of Compression-Compression Fatigue on Balanced Graphite/Epoxy Laminates with Holes," *Journal of Aircraft*, Vol. 18, No. 9, September 1981, pp. 744-747.

12. Daken, H. H. & Mar, J. M., "Splitting Initiation and Propagation in Notched Unidirectional Graphite/Epoxy Composites Under Tension-Tension Cyclic Loading," *Composite Structures*, Vol. 14, 1985, pp. 111-133.

13. Mar, J. M., "Fracture, Longevity, and Damage Tolerance of Graphite/Epoxy Filamentary Composite Material," *Journal of Aircraft*, Vol. 21, No. 1, January 1984, pp. 77-83.

14. Fanucci, J. P. & Mar, J. W., "Fatigue Damage in Thin Composite Laminates Using Out-of-Plane Moire Interferometry," *Journal of Composite Materials*, Vol. 16, March 1982, pp. 94-102.

15. Reifsnider, K. L., Henneke, E. G. & Stinchcomb, W. W., "Defect-Property Relationships in Composite Materials," AFML-TR-76-81, Part IV. Air Force Materials Laboratory, June 1979.

16. Ye, L., "Role of Matrix Resin in Delamination Onset and Growth in Composite Laminates," *Composites Science & Technology*, Vol. 33, No. 4, 1988, pp. 257-277.

17. O'Brien, T. K., "Interlaminar Fracture of Composites," NASA-TM 85768, June 1984.

18. Hwang, W. & Han, K. S., "Interlaminar Fracture Behavior and Fiber Bridging of Glass-Epoxy Composite Under Mode I Static and Cyclic Loadings," *Journal of Composite Materials*, Vol. 23, April 1989, pp. 396-430.

19. Hojo, M., Tanaka, K., Gustafson, C. G. & Hayashi, R., "Effect of Stress Ratio on Near-threshold Propagation of Delamination Fatigue Cracks in Unidirectional CFRP," *Composites Science & Technology*, Vol. 29, No. 4, 1987, pp. 273-292.

20. Gustafson, C. G. & Hojo, M., "Delamination Fatigue Crack Growth in Unidirectional Graphite/Epoxy Laminates," *Journal of Reinforced Plastics and Composites*, Vol. 6, January 1987, pp. 36-52.

21. Trethewey, Jr., B. R., Gillespie, Jr., J. W. & Carlsson, L. A., "Mode II Cyclic Delamination Growth," *Journal of Composite Materials*, Vol. 22, May 1988, pp. 459-483.

22. Ye, L., "On Fatigue Damage Accumulation and Material degradation in Composite Materials," *Composites Science & Technology*, Vol. 36, No. 4, 1989, pp. 339-350.

23. Aboudi, J., "Micromechanics Prediction of Fatigue Failure of Composite Materials," *Journal of Reinforced Plastics and Composites*, Vol. 8, March 1989, pp. 150-166.

24. Harris, C. E., Allen, D. H. & Lo, D. C., "A Mechanics Framework for a Progressive Failure Methodology for Laminated Composites," *Proceedings of the American Society of Composites Fourth Technical Conference*, October 1989, pp. 767-781.

25. Rotem, A. & Nelson, H. G., "Failure of a Laminated Composite Under Tension-Compression Fatigue Loading," *Composites Science & Technology*, Vol. 36, No. 1, 1989, pp. 45-62.

26. Talreja, R., "A Continuum Mechanics Characterization of Damage in Composite Materials," *Fatigue of Composite Materials*, pp. 83-111.

27. Hwang, W. & Han, K. S., "Cumulative Damage Models and Multi-Stress Fatigue Life Prediction," *Journal of Composites Materials*, Vol. 20, March 1986, pp. 125-151.

28. O'Brien, T. K., "Towards a Damage Tolerance Philosophy for Composite Materials and Structures," NASA Technical Memorandum 100548, Langley Research Center, March 1988.

29. Rotem, A., "Stiffness Change of a Graphite/Epoxy Laminate Under Reverse Fatigue Loading," *Journal of Composites Technology & Research*, Vol. 11, No. 2, Summer 1989, pp. 59-64.

30. Maier, G., Ott, H., Protzner, A. & Protz, B., "Damage Development in Carbon Fibre-Reinforced Polimides in Fatigue Loading as a Function of Stress Ratio," *Composites*, Vol. 17, No. 2, April 1986, pp. 111-120.

31. Saunders, D. S. & Van Blaricum, T. J., "Effect of Load Duration on the Fatigue Behavior of Graphite/Epoxy Laminates Containing Delaminations," *Composites*, Vol. 19, No. 7, May 1988, pp. 217-228.

32. Razvan, A., Bakis, C. E., Wagneiz, L. & Reifsnider, K. L., "Influence of Cyclic Load Amplitude on Damage Accumulation and Fracture of Composite Laminates," *Journal of Composites Technology & Research*, Vol. 10, No. 1, Spring 1988, pp. 3-10.

33. Poursartip, A., Ashby, M. F. & Beaumont, P. W. R., "The Fatigue Damage Mechanics of a Carbon Fibre Composite Laminate: I - Development of the Model," *Composites Science & Technology*, Vol. 25, No. 3, 1986, pp. 193-218.

34. Lifshitz, J. M., "Deformational Behavior of a Unidirectional Graphite/Epoxy Composite Under Compressive Fatigue," *Journal of Composites Technology & Research*, Vol. 11, No. 3, Fall 1988, pp. 99-105.

35. Talreja, R., "Transverse Cracking and Stiffness Reduction in Composite Laminates," *Journal of Composite Materials*, Vol. 19, July 1985, pp. 355-375.

36. Whitworth, H. A., "Modeling Stiffness Reduction of Graphite/Epoxy Composite Laminates," *Journal of Composite Materials*, Vol. 21, April 1987, pp. 362-372.

37. Hwang, W. & Han, K. S., "Fatigue of Composites - Fatigue Modulus Concept and Life Prediction," *Journal of Composite Materials*, Vol. 20, March 1986, pp. 154-165.

38. Wolfe, C., "Damage Accumulation of Graphite/Epoxy Laminates in a Gradient Stress Field," S. M. Thesis, Department of Aeronautics and Astronautics, Massachusetts Institute of Technology, 1989.

39. Flaggs, D. L. & Kural, M. H., "Experimental Determination of the In Situ Transverse Lamina Strength in Graphite/Epoxy Laminates," *Journal of Composite Materials*, Vol. 16, March 1982, pp. 103-116.

40. Lagace, P. A., Brewer, J. C. & Varnerin, C. F., "TELAC Manufacturing Course Notes," TELAC Report 88-4, Massachusetts Institute of Technology, 1988.

41. Brewer, J. C., "The Effect of Ply Thickness on the Free Edge Delamination of Graphite/Epoxy Laminates," TELAC Report 85-9, Massachusetts Institute of Technology, 1985.

42. Bhat, N. V., "Delamination Suppression in Graphite/Epoxy Compostites Via Efficient Use of Film Adhesive Layers," TELAC Report 89-14, Massachusetts Institute of Technology, 1989.

APPENDIX A

The average thickness and average width for each specimen are listed in this appendix. The average thickness is calculated from nine measurements and the average width is calculated from three measurements. Measurement locations are shown in Figure 3.6.

Table A.1 Average thickness and width for the $[45_4/-45_4/(0/90)_4]_{2s}$ specimens.

Specimen [a]	Average Thickness (mm)	Average Width (mm)
S1	8.91	37.88
S2	9.07	37.93
S3	8.98	37.78
S4	9.10	37.71
1	9.05	37.89
2	8.79	37.87
3	8.86	37.87
4	8.66	37.89
5	9.02	37.80
6	9.14	37.89
7	9.04	37.89
Average	8.96 (1.6%)[b]	37.85 (0.2%)[b]

[a] Specimens S1 to S4 are static specimens. Specimens 1 to 7 are cyclic specimens.

[b] Coefficient of variation

Table A.2 Average thickness and width for the $[(45_2/-45_2/0)_2/90_5]_{2s}$ specimens.

Specimen [a]	Average Thickness (mm)	Average Width (mm)
S1	8.24	38.49
S2	8.63	37.50
1	8.53	37.92
2	7.97	37.11
3	8.47	37.45
4	8.38	37.44
5	8.29	38.05
6	8.50	37.52
7	8.11	37.54
8	8.29	36.79
9	8.03	37.57
10	8.61	36.06
Average	8.32 (3.0%)[b]	37.70 (1.5%)[b]

[a] Specimens S1 and S2 are static specimens. Specimens 1 to 10 are cyclic specimens.

[b] Coefficient of variation

Table A.3 Average thickness and width for the $[\pm 45/0/90_4]_{4s}$ specimens.

Specimen [a]	Average Thickness (mm)	Average Width (mm)
S1	7.46	37.90
S2	7.45	36.95
1	7.71	37.14
2	7.45	38.95
3	7.35	37.48
4	7.70	37.44
5	7.83	37.18
6	7.69	37.67
7	7.56	37.55
8	7.76	37.53
9	7.72	37.49
10	7.52	37.97
Average	7.60 (1.9%)[b]	37.60 (1.3%)[b]

[a] Specimens S1 and S2 are static specimens. Specimens 1 to 10 are cyclic specimens.

[b] Coefficient of variation

APPENDIX B

The Southwell buckling load data at various cycle times for nearly all the specimens are listed in this appendix. This data is plotted in Figures 4.12, 4.21, and 4.32. Not all of the specimens cyclically tested are listed because specimen failure may have occurred before sufficient data could be obtained.

Table B.1 Southwell buckling load[a] at each static test interval for the $[45_4/-45_4/(0/90)_4]_{2s}$ specimens tested cyclically.

No. of Cycles	Specimen 1	Specimen 3	Specimen 4	Specimen 5	Specimen 7
0	18,170	16,971	16,253	18,637	18,328
2500	17,568	17,121	16,426	19,935	19,074
5000	17,555	16,950	15,926	19,139	19,569
7500	17,089	16,644		19,351	19,052
10,000		16,354		19,105	19,134
15,000				19,454	19,182
25,000				18,622	18,802
30,000				18,045	18,068

[a] All loads in Newtons

Table B.2 Southwell buckling load[a] at each static test interval for $[\pm 45/0/(90)_4]_{4s}$ specimens 1 to 4 tested cyclically.

No. of Cycles	Specimen 1	Specimen 2	Specimen 3	Specimen 4
0	9339	8860	7702	9847
2500	9048	8294	7827	9830
5000	9361	8545	7697	9875
7500	9709	8685	7715	9806
10,000	9125	8579	8133	9826
15,000	9283	8255	7718	9847
20,000	9201	8542	7661	9817
25,000	9016	8742	7777	9763
30,000	9434	8667	7514	9812
35,000	9308	8338	7487	9708
40,000	9049	8734	7360	9389
45,000	9201	8230	7422	9226
50,000	9001	8082		
55,000	9143	8428		
60,000	8834			

[a] All loads in Newtons

Table B.3 Southwell buckling load[a] at each static test interval for $[\pm 45/0/(90)_4]_{4s}$ specimens 5 to 9 tested cyclically.

No. of Cycles	Specimen 5	Specimen 6	Specimen 7	Specimen 8	Specimen 9
0	9946	9506	9097	9952	9908
2500	10,158	9457	9132	9962	9927
5000	10,212	9474	9064	9756	9919
7500	10,195	9570	9046	9986	9924
10,000	10,112	9536	8972	9888	
15,000	10,073	9405	9001		
20,000	10,131	9451	8952		
25,000	10,047	9363			
30,000	10,080	9405			
35,000	9991	9331			
40,000	9870	9332			
45,000		9307			

[a] All loads in Newtons

Table B.4 Southwell buckling load[a] at each static test interval for $[(45_2/-45_2/0)_2/90_5]_{2s}$ specimens 1 to 4 tested cyclically.

No. of Cycles	Specimen 1	Specimen 2	Specimen 3	Specimen 4
0	13,109	8712	12,893	12,824
2500	13,220	8793	13,292	12,801
5000	13,195	8803	13,007	12,639
7500	12,978	8825	13,317	12,828
10,000	13,276	8572	13,134	
15,000	12,843	8470	13,041	
20,000	13,093	8413	13,268	
25,000	12,878	8306	13,339	
30,000	13,069	8119	13,365	
35,000	13,008		13,049	
40,000	12,841		13,014	
50,000	12,702		13,083	
60,000	12,700			
70,000	12,663			
80,000	12,649			
90,000	12,769			
100,000	12,921			
200,000	12,606			
300,000	13,073			
400,000	12,687			
500,000	12,872			
600,000	12,230			

[a] All loads in Newtons

Table B.5 Southwell buckling load[a] at each static test interval for $[(45_2/-45_2/0)_2/90_5]_{2s}$ specimens 7 to 10 tested cyclically.

No. of Cycles	Specimen 7	Specimen 8	Specimen 9	Specimen 10
0	10,543	11,428	9625	12,930
2500	10,450	11,704	9884	13,249
5000	10,440	11,699	9740	13,227
7500	10,377	11,675	9686	13,255
10,000	10,118	11,572	9674	13,095
15,000			9539	13,010
20,000			9341	
25,000			9125	

[a] All loads in Newtons